Fluid structure interaction of violent wave events

A study into the influence of structure properties on breaking wave impacts

Master thesis

Fallon Scholte

Delft University of Technolog

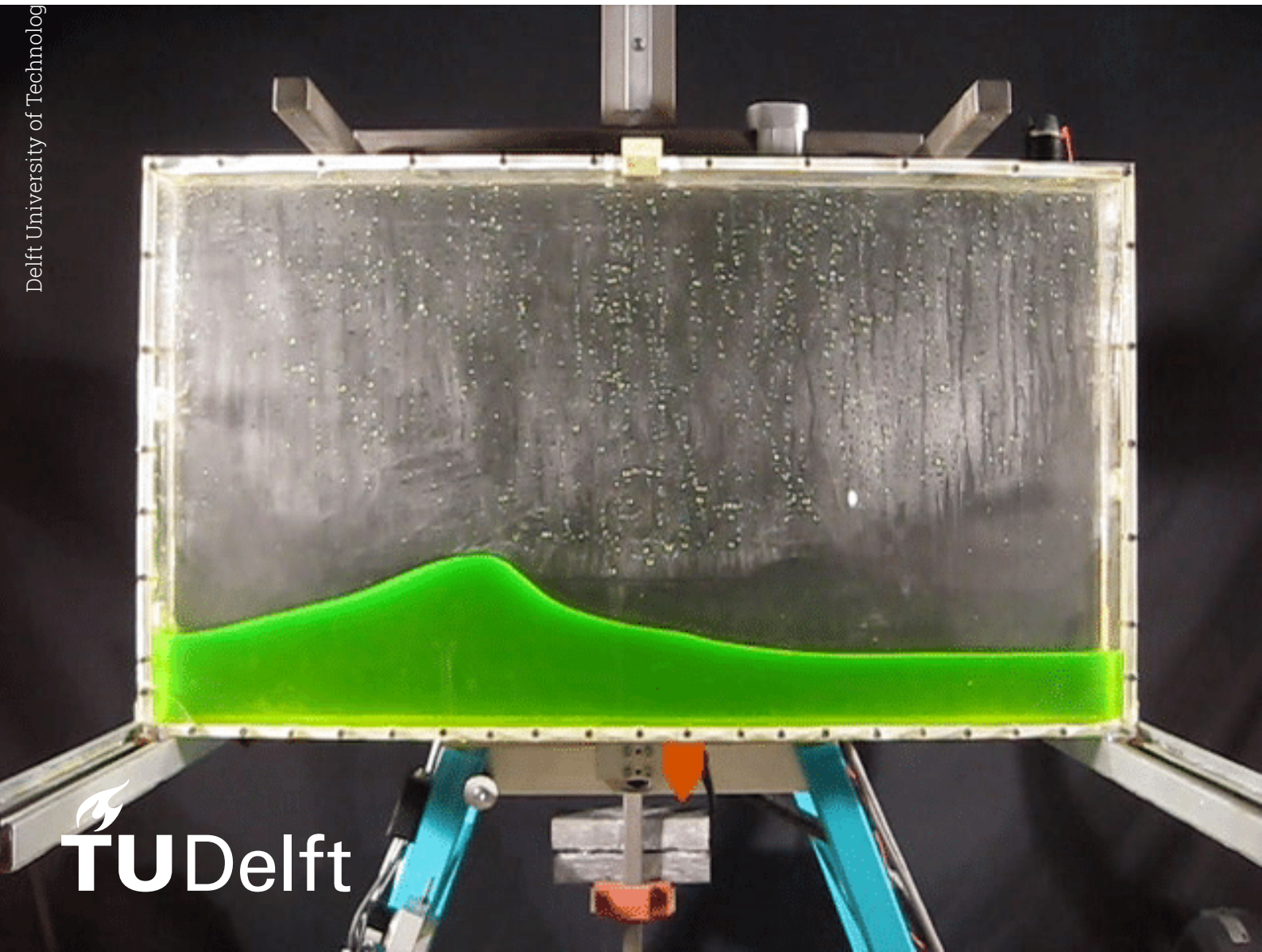

TU Delft

Fluid structure interaction of violent wave events

A study into the influence of structure properties on breaking wave impacts

by

Fallon Scholte

Student Name	Student Number
Fallon Scholte	4555155

This thesis MT.24/25.005.M. is classified as confidential in accordance with the general conditions for projects performed by the TUDelft.
Date of exam: 02-10-2024

Thesis committee:	Dr. ir. P.R. Wellens
	Dr. ir. H.J. de Koning Gans
	MSc A.D. Boon
Project Duration:	September, 2023 - October, 2024
Faculty:	Faculty of Mechanical Engineering, Delft

Cover: [7] Sloshing wave in tank.

TU Delft

Preface

This report is written to obtain my masters degree Maritime Technology, with a specialization in Ship Hydromechanics at the TU Delft. For my thesis I was determined to find a assignment in the field of Ship Hydrodynamics, as I found the courses of this field the most interesting during my master. When I contacted Peter Wellens he suggested a subject that involved fluid-structure interaction for large wave impacts. I was enthusiastic to take on this challenge. This report is written primarily for those interested in research in the field of fluid-structure interaction. Also readers interested in my thesis process can find insight in this report. *I want to thank Peter Wellens for offering me the opportunity to work on this project and providing me with guidance during the process. It was great to work with Peter as he was always very helpful and made effort to guide me through this process. I also want to thank the employees of the MT Towing Tank of the TU Delft. They have provided me with their supervision and help with the preparations of my experiments, but also with conducting my experiments in the sloshing rig. I want to thank Anna Boon and Henk de Koning Gans for being part of my thesis committee and for contributing to my final grading. Lastly I want to thank my fellow students. During the academic year and during the summer holiday we have worked on our thesis projects together. They have even helped me with my experiments in the sloshing rig.*

Fallon Scholte
Delft, September 2024

Summary

This study investigates the effect of dynamic properties of a structure on the magnitude of impacts loads of breaking waves. A literature review in the field of violent wave impact on flexible structures is done. From this review, it is concluded that the hydro flexibility of structures have great impact on the fluid-structure interaction. In earlier studies, it is found that models of constructions in breaking waves are not accurate yet, using knowledge that is available up until now. There are studies that show suggestions of influence on the structures own properties. However, no extensive research had been done in this field. That is why the main objective of this study is to research if the natural frequency of a construction is of influence on the impact force of violent waves.

To answer the research question, a model is made and an experiment is carried out. The model consists of two parts, first a pendulum is used to represent a simplified structure to interact with a breaking wave. Using the model, a simulation of pendulums with different natural frequencies is done. The pendulums interact with the same wave each time. The second part of the model consists of a beam that is impacted by a breaking wave. Simulations are carried out where beams with different natural frequencies are impacted by the same wave.

To verify the model and further elaborate on the research question, an experiment is done. This experiment is done in the Sloshing rig at the faculty of Mechanical Engineering at the TU Delft. During the experiment, four different plates with different natural frequencies are used. They are exposed to the same wave impact each time. The model and the experiment results are compared and used to form a conclusion.

It is concluded that wave impacts are of higher magnitude on structures with a higher natural frequency. The difference between the measured and predicted forces indicates that the fluid- structure interaction of these plates lead to this difference. This can be explained by the different fluid- structure interaction for plates with different natural frequencies. If velocities of the plates with higher natural frequencies are higher, the Morison component of the impact force becomes larger. Therefore these impacts can become higher than for other structures. As the natural frequency of the plate increases, the results show relatively higher measured deflections as well.

Contents

1

Introduction

Vessels that operate on sea and offshore structures will encounter extreme water events during their life time. These extreme water events are for example slamming, green water events and sloshing. Slamming can happen when ship is operating in heavy weather and waves. The motions of a ship can become very large, this can cause a part of the ship to drop from air into water. In these type of conditions, waves can flow onto the deck of a ship. This is called a green water event. Incidents involving green water and slamming have caused accidents that led to ship damage and crew injuries. When having a better understanding of the behaviour of structures under green water circumstances, more safety measures can be taken. This can prevent hazardous events during ship operations.

An other challenge in shipping that includes extreme wave events is sloshing in fuel tanks. In order to reduce harmful emissions in shipping, the industry must find alternatives for traditional fuels. LNG is a fuel that results in less CO2 and NOx emissions. LNG can be transported safely in LNG carriers. However using LNG as fuel will bring new challenges. In smaller scale tanks, different physical phenomena are dominant. During sailing, the fuel in a fuel tank moves. Often the dynamics of the ship causes the fuel in the tank to form sloshing. This means the fluid forms breaking waves with large impact inside of the fuel tank. Due to the construction of the tanks at low temperature and the need of a cargo containment system, the impact forces of the breaking waves are important to predict. Tank failure and leakage can form hazardous situations for crew and shipping safety.

For all these types of impacts, a lot of research questions are still remaining. In earlier research, hydro elasticity is found to be of great influence on impact of extreme water events. It turns out, fluid structure interaction is important to take into account. In section 1.1, an overview of previous research on this topic will be given. In section 1.2 a gap in existing knowledge will be determined and in section 1.3, the main objectives of this study will be presented.

1.1. Research background

The types of waves that can be present in fuel tanks include breaking waves. This process is called sloshing. The impact of breaking waves is a research field where still a few questions are remaining. The first research in this field was possible starting in the 1930's, using piezo-electric probes. These are a type of pressure measuring device. In these early experiments, the pressures measured at the impact of a breaking wave where a lot higher than expected. They exceeded values expected from the wave energy. [21] The pressure peaks are dependant on the wave characteristics such as speed, height and steepness. For breaking waves, the pressures also heavily depends on the stage of breaking when the waves hit the wall. When the wave hits the wall at the point that it just starts overturning, the largest impact pressures can be found. Once the wave has formed a jet and air pocket the total impact decreases. When the wave is completely broken, there is a lot of air mixture present and the impact is lower. However in more recent research, contradicting phenomena have been observed. The largest

peak pressures are observed when a breaking wave shows a large air pocket. [20]. If large air bubbles have a larger oscillation period than the impact, the impact can be prolonged and the impulse increases. In past researches, great variability is shown in pressures of violent wave impact [21], [14]. At flip trough impacts points, the pressure peaks were highest. Especially for these type of wave impacts, identical waves show a lot of scatter in their pressure data. When the total pressure is integrated over time, the impact values show consistency. To conclude, breaking wave impact on rigid walls is studied quite well in the past. The impacts show different pressures at different stages of wave breaking.

[11] Investigates hydro elasticity for slamming impacts. Hydro elasticity means the deforming of structures when impacted by surrounding fluid. In the slamming process, two phases are identified. First the structural inertia phase where the structure hits the water surface. Secondly a subsequent free vibration phase occurs. At slamming impacts, large peak pressures occur. However, these peak pressures are not important to the maximum bending stress. It is found that bending stress is dependant on the drop velocity of the vessel. The maximum stresses occur in the time after a fourth of the largest natural period of the impacted structure. [19] investigated the hydro elastic response of a multihull vessel with slamming on the deck in head waves. This study also found that the maximum stresses are dependant on the fall velocity. The stresses do not show dependency on the exact place of impact on the structure. The study also concludes that the elasticity of the structure strongly influences the stresses in the wet deck. [3] investigates the behaviour of a flexible LNG tank system when impacted by breaking waves (sloshing). In the study, experimental data is used from the Sloshel project. This data includes the impact pressures on rigid walls. The study conducts FE calculations to take into account the hydro elasticity in order to calculate the structural responses. Three different impact types are identified. One where the impact duration is shorter than the natural frequencies, one where the time scale is the same and one where the impact duration is longer than the natural frequencies. For breaking waves holds, the higher the pressures, the smaller the impact area and duration. During breaking wave impact, different load characteristics occur. Impacts from breaking waves with air pockets involve oscillating loads. During the impact, different deformation modes are alternating in the structure.The interaction between structural responses and the loads is very complex. Small local modes are often excited earlier than the global modes. This leads to complex combinations of local and global deformations. It is concluded that local loads are not filtered by the structure. They can influence the structure beyond their impact area. The question remains if these local loads can be neglected or how they should be taken into account. [27] conducted an experimental study on the use of baffles in tanks where sloshing is present. They measured the pressures on tank walls and baffles. Mounting a baffle in the tank alters the natural frequency on the tank structure. The maximum impact pressure on the tank wall altered with different natural frequencies caused by the configurations of the baffles. The study concludes that the effectiveness of the baffles depends on the relation between the natural frequency of the construction and the frequency of the waves, but also on the configuration and location of the baffles.

[10] looked into the hydro elastic behaviour of an elastic thin beam in regular waves.The theory based on separating diffraction and radiation and coupled equations between hydrodynamic pressures and deflection are used. The paper concludes that the two theories are in line with each other and that the hydro elasticity plays a big role in the motion of the beam. [18] studied the impact of breaking waves on a plate. The plate is modeled using Euler-Bernoulli beam equations. The static deflection is compared to dynamic deflection. When the maximum impact pressure is below 18 times the dimensionless impact pressure, there is a correlations between these two deflection approaches. With a dynamic magnification factor, the dynamic deflections can be calculated based on static theory. However, the dynamic magnification factors are dependant on the ratio between the duration of the impact pressure and the natural period of the plate t_1/T_1. When this ratio increases to above 1, the dynamic response motion will increase to much larger deflections. [17] carried out an experiment including breaking waves impacting a flexible wall. The main interest of this paper was what type of fluid structure interaction would occur. Data on pressure distribution, deflections of a wall with different thicknesses and kinematics of the flow are gathered. The data showed high interaction between fluid and structures. The experimental data is used to validate computational models. The paper presents a structural model based on the Euler Bernoulli equations. However, they conclude that the model is not accurate yet and more work is needed to fully couple the structure responses to the pressures of the impact fluid.

[4] studied the behaviour of a pendulum in focused breaking waves. In this research, different stages of breaking waves are used to move a pendulum. The pendulum is tested in two levels of height. This

is done by generating waves that breaks at a known position. In this position a pendulum is placed. The front velocity, front angle and surface elevation is different for each wave. For these waves in different stages, the excitation of the pendulum is measured. The first stage wave shows no breaking. For this wave the results are as expected. For waves that are broken further, the results are not as expected. A stronger correlation was expected between the angle of the pendulum and the wave characteristics; front velocity, front angle and surface elevation. Why this correlation is absent is not clear. The study points out that the scaling effects of violent wave impacts are difficult to scale. When using Froude scaling, for example surface tension, compressability of liquid and gas and mass and stiffness of structures is not scaled are not scaled correctly. The unpredictability of breaking waves is also a factor that plays a role. Due to extreme wave events being rare and extrapolating them is not easy. Due to this, every extreme wave impact is different.

To conclude, for rigid walls, the breaking wave impact forces are well researched in literature. It has become clear that flexibility of structures influences maximal stresses. However, motion of flexible structures in breaking waves are not investigated often. The models used in literature do not fully represent the actual responses of the structures that are found in experiments. It is not clear yet what phenomena are still missing, or still have to be taken into account for these type of calculations. It is seen that different types of impact forces influence different parts of the structure in different ways. But no extensive research is this field has been done.

1.2. Problem statement

As stated in section 1.1 little research in hydro elastic interaction in breaking waves is done. In studies that are carried out, importance of fluid-structure interaction is determined. However, questions about the exact fluid-structure interaction are still remaining. Studies have found a lack of relation between pressure distribution of a breaking wave and the response of the structure. Other studies have compared experiments with a modelled violent wave impact. These studies found that the models are not accurate enough yet, using well known methods. Multiple studies point out that scaling the effects of violent wave impacts is difficult.

To conclude, the research gap in this field lies in the effect of the structural properties of a material on the hydrodynamic impact of breaking waves. In previous research, the characteristics of a structure are not taken into account. There are no studies done in the past that discover what the structure itself and its modal motions contribute to the interaction with fluid. In this research, the influence of the natural frequencies and mode shapes of the structure will be investigated. This will be a first step to examine the structural characteristics in fluid structure interaction involving breaking waves. If these characteristics turn out to be important, insight in what phenomena have to be taken into account in future models is gained.

1.3. Main research question

The research gap that is established in section 1.2, is that it is unknown what phenomena can play a role in fluid-structure interactions with breaking waves. This study attempts to gain insight into the structural phenomena that play a role in this type of fluid-structure interaction. In past literature, the structural characteristics of the material itself is not taken into account yet. This study will focus on the natural frequencies and mode shapes of structures that are experiencing extreme wave impacts. This leads us to the main research question:

How is the fluid structure-interaction of a structure in focused breaking waves related to the natural frequencies and mode shapes of a structure?

1.3.1. Objectives literature study

As a first step, literature study will be carried out. The main objective of the literature study is to gain insight in how excising models of breaking waves interacting with a pendulum or a beam are build up. First the dynamics and kinematics of a wave are explained to gain insight in their behaviour. Non dimensional numbers that are important to take into account are determined. After that, detailed modeling equations are gathered.

1.3.2. Objectives computational model

The main objective of the computational model is to predict the findings in the physical experiment. This is important in order to make decisions about the measuring techniques in the tank experiments. Secondly, the model is also important to use for predictions on the conclusions that will be found with the tank experiments. A hypothetical experiment will be carried out using the model, in order to already form an idea of that the outcome will be. The model will also help to analyse the results from the tank experiments. It will take into account the differences in the testing structures used in the sloshing tank. More about this can be read in chapter 3.

1.3.3. Objectives physical experiment

The main objective of the experiment is to answer the main research question. In addition, the experiments are used to help understand if the model makes correct calculations.

1.4. Outline report

This report consists of seven chapters. In chapter 2, the used knowledge from literature is presented and explained. Chapter 3 is about the experiments in the sloshing tank. In this chapter, the details of the experiments are explained. This will also contribute to understanding what the computational model will represent. In chapter 4, the model will be verified by comparing its outcomes to known situations and previous research outcomes. Chapter 5 and 7 will present the results of the experiments of the model and the tank experiments. Lastly, in chapter 9, the conclusions that can be drawn from the model and experiments are presented.

2 Literature

In this chapter, important knowledge from earlier research is gathered. First, the wave and impact types important for this study are explained in section 2.1. In section 2.2, impact from waves on rigid walls is discussed. In section 2.4 Modeling equations regarding the modeling of waves that are used in the model of this study are listed and explained. In section 2.5 and 2.6 the modeling equations regarding the fluid-structure interaction of the pendulum and the plate are explained.

2.1. Wave types

In this study, breaking waves are of interest. Regular waves are a type of wave that follows a sinus shape and has a constant amplitude, wave period and wavelength. Potential theory is applicable to these type of waves. When multiple waves meet, their amplitude will sum up. When a wave becomes large or moves towards shallow water, the wave will become a breaking wave. The characteristics of the wave changing with changing water depth is called the shoaling effect [15]. As seen in figure 2.1, when a wave enters shallow water, the velocity of the wave increases tremendously. In section 2.4.1, more about the modeling of this phenomenon is described.

In maritime engineering, breaking waves are involved at a view types of impact events. These events are slamming, green water events and sloshing. Slamming is an event where a structure like a ship drops from air into a water surface rapidly. A green water event is defined as an event where water slams on deck due to big waves or ship motions. At sloshing, a fluid in a tank forms breaking waves and impacts the structure of the tank [4]. These types of impact events are also referred to as violent wave events. In these type of events, fluid structure interaction is important. In this study, sloshing is of interest. However, slamming and green water are impact types that can be considered when trying

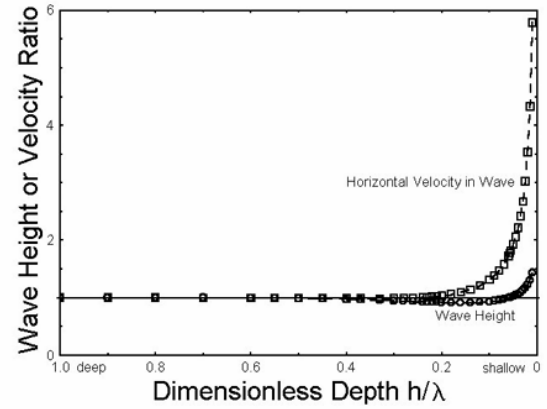

Figure 2.1: Shoaling effect [15].

to answer questions regarding sloshing.

[12] concludes that in slamming, maximum pressure impact can not predict maximum stress in the material. This is because at higher velocities and pressures, the hydro elasticity plays a big role. The importance of hydro elasticity also becomes larger when the value of the highest natural period of the material increases.

[22] has done numerical research regarding sloshing tanks using baffles. Baffles are structures places in the fuel tanks, in order to reduce the motions of the fluid. With this method the impact of the fluid on the tanks can be reduced. The structural response of the baffles are investigated in different configurations. The study concludes that the hydro elasticity of the baffles are of great importance. When taking hydro elasticity into account displacement and force amplitudes turn out around ten times higher compared to evaluations without hydro elasticity. This can be explained by the occurring resonance of the structure with the waves in the fluid. [7] studied the behaviour of sloshing fuel tanks. They investigated the energy dissipation process of the tank and fluid. A numerical study is done beforehand. Later an experiment is carried out. The study concludes that the motions of the fluid includes complex and nonlinear behaviour. For larger amplitude roll motions, wave breaking and violent fluid structure interactions are present. The experiments show that the fluid motions are damping the roll motion of the tank for small motion amplitudes and waves. At large motion amplitudes, breaking waves occur. This leads to larger steady state roll motions of the tank.

In wave interaction problems, the Keulegan-Carpenter (KC) number is often important. This number describes the relation between the excursion length of the fluid particles and the length of the structure that is placed in the flow. The KC number is described in equation 2.1. Here u is the velocity of the fluid, T is the wave period and D is the diameter of the cylinder [16]. The number represents the importance of inertia forces versus drag forces. For KC numbers over the value of 2, impact is often determined using the Morison equation.

$$KC = \frac{uT}{D} \tag{2.1}$$

2.2. Waves rigid wall impact

For regular waves, the wall impact is influenced by the structure of the wall, the water depth, the seabed and the shape of the wave [21]. For steeper waves, second order terms start to play a role in the pressure impact of the waves. This is due to asymmetry between wave crests and troughs. This asymmetry can also be present in deep water. As seen in figure 2.2, the impact pressures on a wall become asymmetrical. A higher pressure peak can even generate an upward jet of water along the wall. The pressure peaks contain a few times the energy that would be estimated using the wave height, $\rho g h$. In conclusion the shape of the wave just before the wave impact influences the wave impact.

2.2.1. Breaking waves

[9] have researched the velocity field of breaking waves experimentally. When a wave is breaking, the wave crest curls over the wave, creating a jet type of motion. This is called a plunging breaking wave. These types of wave have a lot of turbulence. The waves show the highest velocities in the top area near the surface. The development of a breaking wave can be described as a few stages. First the jet forming stage. After the wave has developed a jet, an air pocket can be trapped in the wave. In the last breaking stage, the air will mix with the water and will form a turbulent mixture.

[21] looks into the impact forces of a breaking wave. The study has found that the largest water speeds are present in the overturning crest of the wave, as the overturning of the wave crest results in a jet of water. The air pocket stage will lead to less impact. A pressure diagram of a breaking wave impact on a wall over time is given in figure 2.3. In these type of measurements, large variations are present. This is due to turbulence in the breaking wave, but also because the pressure distribution of the water is very sensitive to the shape of the wave. The pressure peak is inertia dominated as the timescale is way to short for gravitational effects to play a role. The pressure peaks that are found have such high quantities that they cannot be explained by traditional wave theories.

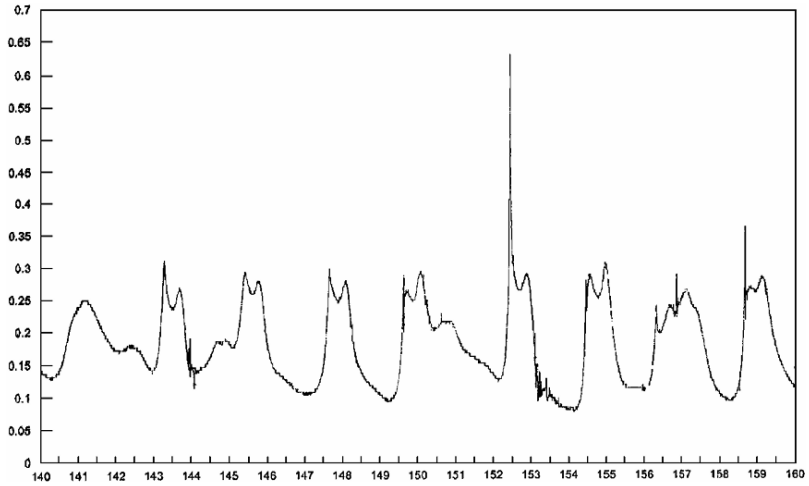

Figure 2 A record of pressure versus time for waves at a wall in a wave flume (courtesy of W. Allsop, H.R. Wallingford).

Figure 2.2: Pressure at a rigid wall of steep non-breaking waves [21].

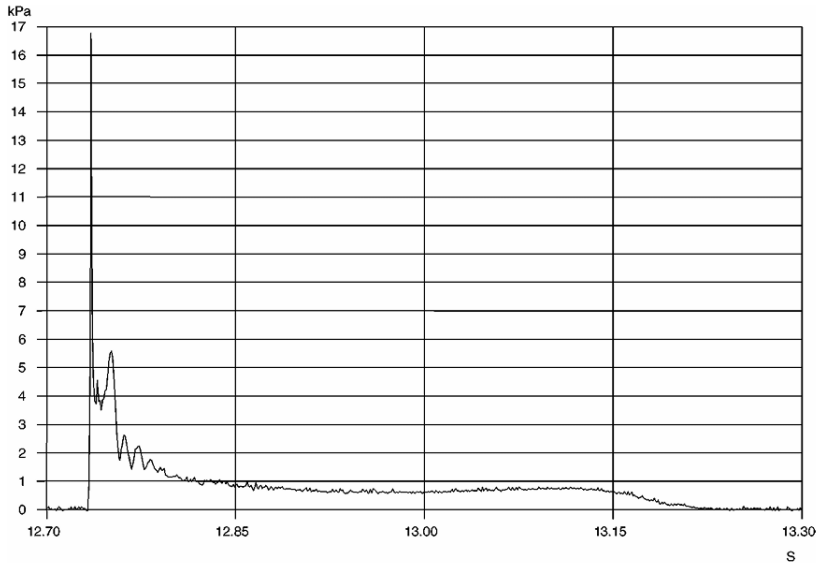

Figure 3 Pressure measurements from the impact of one wave in a Plymouth University laboratory flume (courtesy of M. Walkden, Bristol University).

Figure 2.3: Pressure impact at a rigid wall of a breaking wave [21].

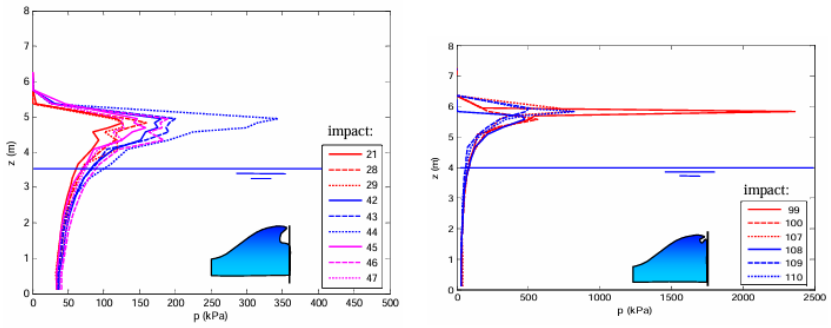

Figure 12. Instantaneous vertical pressure profiles at maximum force for air pocket (left) and flip through impacts.

Figure 2.4: [14]

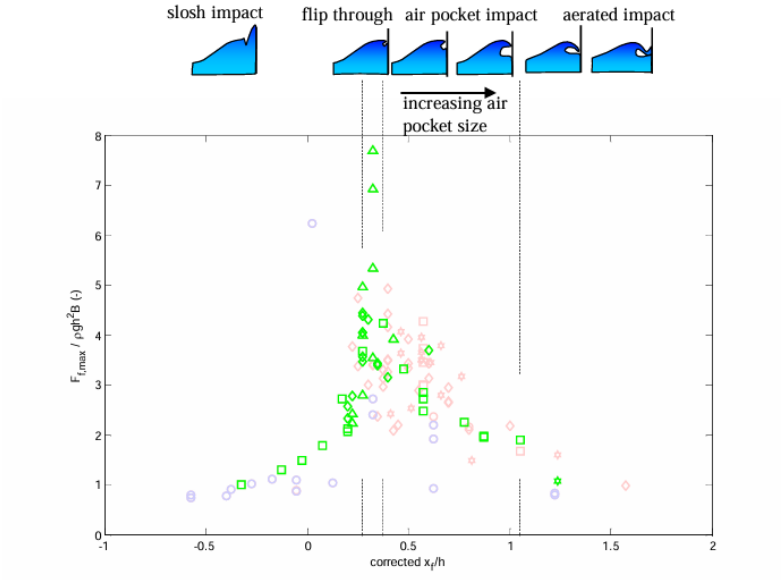

Figure 15. Variation of dimensionless force with focal point.

Figure 2.5: [14]

In the study [14], experiments are done. The impact pressures of a focused breaking wave are measured over the height of a rigid wall, using different water depths. Different breaking stages of the wave are investigated, including the flip through, air pocket and and aerated phase. In figure 2.4 a pressure distribution in z direction is shown for an air pocket type of impact, and a flip through type of impact. The pressure peaks are high especially at the flip trough impact. A high position above the mean water level of the largest peak is visible.

In figure 2.5 an overview of impact forces is given for each stage of the breaking wave. The forces are high especially at the flip trough impact. The study concludes that the flip trough impact only happens at very specific focal points. They create the biggest pressure peaks. The air pocket stage also creates large pressure impacts. The impact forces peak at high locations in z direction.

To conclude, impact forces of a breaking wave differ with wave types and stage of breaking of a wave. In breaking waves, impact pressures can exceed the pressures that would be estimated with hydrostatic pressure by 10 to 100 times. The most extreme velocities occur at the flip trough stage. [20] investigates the flip trough stage of the wave further. This is the stage where the top of the wave starts overturning and forms a jet. When the wave hits a wall at this stage some interesting dynamics occur. In figure 2.7 the velocities of the fluid are visible. The are three stages, first the wave advancement. In this stage the

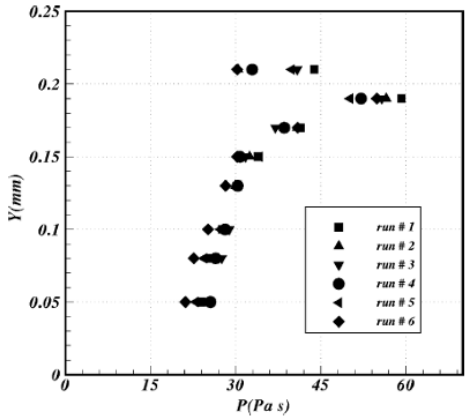

Figure 2.6: Experimental vertical distribution of pressure impulse of breaking wave.

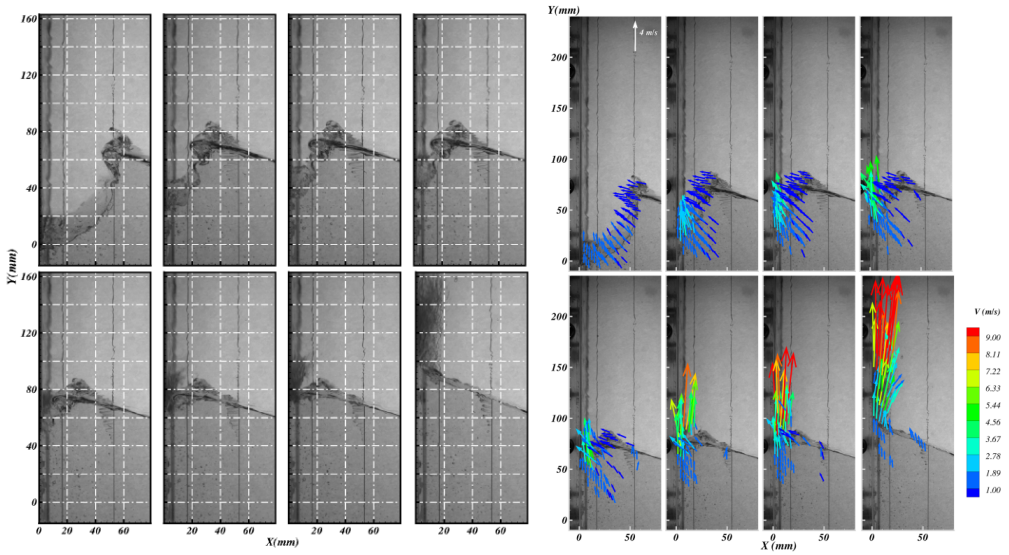

Figure 2.7: The water surface development of a wave turning over at a wall(left).The velocities of the fluid in a breaking wave hitting a wall with flip trough effect.(right) [20]

wave approaches the wall and the through of the waves increases height. During focusing the through and the front move toward each other and this causes a big acceleration of the fluid. Finally at the flip-through phase, the flow forms a jet upwards at the wall. During the focusing stage, accelerations of 1500g are observed. The impact of the breaking waves over time is similar to the one found in [21]. The pressure has a distribution over the height, shown in figure 2.6. The main impact lies above the still water line. The variations over the different experiments are large.

To investigate this breaking wave impact further, a pressure impulse model is applied. The model, originally from [8] is extended with a trapped air implementation. The model is able to predict pressure impulse quite well with an error around 10 to 25%. However, the pressure peak is difficult to predict.

2.3. Added mass influence natural frequencies

Every structure has a natural frequency. This is a frequency in which an item will vibrate after a force is exerted on it. [24] performed a study on the influence of the surrounding fluid of a structure, on the natural frequencies, using a carbon nanotube (CNT). They have found that these natural frequencies of structures are influenced by their surrounding fluid. When the velocity of the fluid increases, the natural frequency of the structure will also increase. The viscosity of the fluid also has an influence. When the fluid velocities are high, the viscosity has a big influence. Larger viscosity's lead to an increase

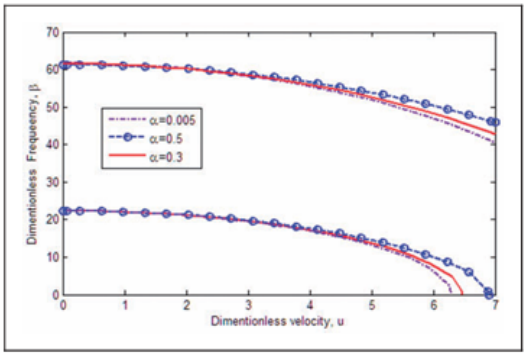

Figure 2.8: [24] Dimensionless natural frequencies with varying dimensionless velocity and viscosity of the fluid.

of the natural frequencies of a system. However, when velocity of the fluid is low, the viscosity barely influences the natural frequency. This relation is illustrated in figure 2.8.

In general cases, natural frequencies are determined when assuming the structure is surrounded by air. In the case of this study, structures are (partially) submerged in water at some moments in time.

2.4. Modeling waves

In this section the method used to model the waves is presented. In section 2.4.1 the modeling of regular waves is shown. In section 2.4.2, it is explained how the breaking waves characteristics are calculated in the model of this study.

2.4.1. Modeling regular waves

To model regular gravity waves the wave potential is used 2.2 [15]. This potential describes the wave and can be used to calculate its velocity. By calculating the derivative of the wave potential to x 2.3, the velocity in x direction is found at any desired location and time. This also holds for the derivative to z, to find the velocity in z direction 2.4.

$$\Phi_w = \frac{\zeta_a g}{\omega} \frac{\cosh k(h+z)}{\cosh kh} \sin(kx - \omega t) \tag{2.2}$$

$$\frac{\partial \Phi_w}{\partial x} = \frac{\zeta_a g k}{\omega} \frac{\cosh k(h+z)}{\cosh kh} \cos(kx - \omega t) = u \tag{2.3}$$

$$\frac{\partial \Phi_w}{\partial z} = \frac{\zeta_a g k}{\omega} \frac{\sinh k(h+z)}{\cosh kh} \sin(kx - \omega t) = w \tag{2.4}$$

To find the accelerations in both directions, the derivative of these equations with respect to time are calculated. This results in 2.5 and 2.6.

$$\frac{\partial}{\partial t}\left(\frac{\partial \Phi_w}{\partial x}\right) = \zeta_a g k \frac{\cosh k(h+z)}{\cosh kh} \sin(kx - \omega t) = \dot{u} \tag{2.5}$$

$$\frac{\partial}{\partial t}\left(\frac{\partial \Phi_w}{\partial z}\right) = -\zeta_a g k \frac{\sinh k(h+z)}{\cosh kh} \cos(kx - \omega t) = \dot{w} \tag{2.6}$$

2.4.2. Modeling breaking waves

In this model, a measurement of the breaking waves is used. The surface elevation is measured at the wave gauge. Based on this information, the wave is transformed to its Fourier components. Every wave component is then modeled as a monochromatic wave. The components are used in linear wave theory to determine the velocities and accelerations at the tube. The Fourier distribution is calculated using equation 2.7. For this study, this part of the model is used directly from the model of [6].

$$\hat{f}(\xi) = \int_{-\infty}^{\infty} f(x)\, e^{-2\pi i \xi x}\, dx. \tag{2.7}$$

To calculate the desired wave data, the following data is gathered from every separate monochromatic wave: angular frequency, amplitude, phase and wave number. Using this information, the velocities and wave heights are calculated. First this is done every wave component separately using equation 2.8 to 2.13.

$$wp = k_w \cdot x + \omega \cdot t + \text{phase} \tag{2.8}$$

$$h = a \cdot \cos(wp) \tag{2.9}$$

$$ys = \min(h, y) \tag{2.10}$$

$$vf = \frac{\cosh(k_w \cdot (ys + h_0))}{\sinh(k_w \cdot h_0)} \tag{2.11}$$

$$u = a \cdot \omega \cdot vf \cdot \cos(wp) \tag{2.12}$$

$$dudt = a \cdot \omega^2 \cdot vf \cdot \sin(wp) \tag{2.13}$$

To calculate the wave height, velocity and accelerations of the total wave, the values found for the wave components are summed.

2.5. Reduced order model

In this section the equations used for the reduced order models of the pendulum and plate are presented and explained.

2.5.1. Hydro elasticity

Hydro elasticity is a way to describe the interaction of water impact on a structure. The hydrodynamic impact pressures are exerted on the structure. The structural response is taken into account by considering the velocity of the deformation. This way the impact load often turns out smaller [2]. Two types of modeling are possible. Strong formulation uses a coupled equation of the governing equations of the fluid domain and the governing equations of the structural domain. This is complicated and very case specific. The weak formulation solves the problem step by step. The impact is first established on a rigid structure. From here, the structure response is calculated and taken into account. The first impact calculation can turn out way to high leading to instabilities in the calculation. In this study hydro elasticity is applied in the calculations of the pendulum using the weak formulation. In the calculations of the plate, this implementation will become complex. The model is chosen to take into account the impact of the fluid, but the motion of the plate does not influence the impact. This simplification will influence the result of the model. This is why experiments are carries out later on.

2.5.2. Modeling waves pendulum interaction

To model the movement of the pendulum in a breaking waves there are five stages. Rest, water entry, submerged vibration, water exit and free vibration. For problems with sloshing and a moving structure, a two-way coupled model is needed. This means the impact influences the motion, and the motion is coupled back to influence the impact. In this type of problem, the submerged part of the structure is a function of time. This influences the added mass and drag over time.
For the model a few assumptions are made. The pendulum only has one degree of freedom. Only the tube part undergoes a force from the moving water. This force is constant over the width of the tank.
The motion of the pendulum is described by equation 2.14. I is the moment of inertia, c the damping coefficient and k the restoring force coefficient. M is the external moment and theta is the position of the pendulum.

$$I\ddot{\theta} + c\dot{\theta} + k\sin\theta = M \tag{2.14}$$

$$I = mL^2 \tag{2.15}$$

The external moment M is modeled by taking the force of the water times the arm of the pendulum. This is described in equation 2.16. The arm of the pendulum is describes as L.

$$M = \beta F_m L \cos\theta \tag{2.16}$$

The force on the tube is determined by equation 2.17. The force depends on the velocity u and acceleration a, relative to the water. V and A represent the volume and frontal area of the tube. C_m and C_d represent the added mass coefficient and drag coefficient.

$$F_m = \rho(C_m V a + \frac{1}{2} C_d A|u|u) \tag{2.17}$$

In this equation V represents the submerged volume of the pendulum. The acceleration a in this equation represents the relative acceleration of the pendulum with respect to the wave speed. The speed u is the also the relative speed of the pendulum with respect to the wave velocity.

The buoyancy and the drag of the air is not included in the model. [6] has concluded that these factors do not influence the outcome of the model significantly. Entry and exit phenomena of the water are not taken into account in this model.

2.6. Modeling waves plate interaction

In this section the modeling of the plate is explained further. For simplification, the plate is modelled as a beam. This is considered an acceptable simplification because the load on the plate will be constant in y-direction.

2.6.1. Euler-Bernoulli beam theory

For this model the plate will be modelled in 2D, using the Euler-Bernoulli beam theory [1]. The equation that describes the deflection of the beam is shown in 2.18. In this equation, μ represents the mass per unit length and EI represents the flexural rigidity. The deflection of the beam in meters is represented by w. In the case of this research, the plate is homogeneous. This means the equation can be simplified to 2.19.

$$\frac{\partial^2}{\partial x^2}\left(EI\frac{\partial^2 w}{\partial x^2}\right) = -\mu\frac{\partial^2 w}{\partial t^2} + q(x,t) \tag{2.18}$$

$$EI\frac{\partial^4 w}{\partial x^4} = -\mu\frac{\partial^2 w}{\partial t^2} + q(x,t) \tag{2.19}$$

Free vibration

For a free vibrating beam, $q(x,t) = 0$. The resulting equation is as in 2.20. This partial differential equation can be solved using separation of variables. Resulting in the general standard solution 2.22. This equation describes the normal mode of the beam. In this equation ω_n is the natural frequency of the vibration of the beam. There are infinite natural frequencies that all describe a mode of the beam. The constants A_n can be solved sing boundary conditions. $T(t)$ is described in equation 2.23. The total solution is the sum of all the modes 2.24.

$$EI\frac{\partial^4 w}{\partial x^4} + \mu\frac{\partial^2 w}{\partial t^2} = 0 \tag{2.20}$$

$$w(x,t) = W(x)T(t) \tag{2.21}$$

$$W(x) = A_1\cosh(\beta x) + A_2\sinh(\beta x) + A_3\cos(\beta x) + A_4\sin(\beta x), \quad \text{with} \quad \beta_n = \frac{\mu\omega_n^2}{EI} \tag{2.22}$$

$$T(t) = A\cos(\omega t) + B\sin(\omega t) \tag{2.23}$$

$$w(x,t) = \sum_{n=1}^{\infty} w(x,t) \tag{2.24}$$

In this research the beam is clamped, free. This is well known as a cantilevered beam. The boundary conditions for this configuration are listed in 2.25. The moment of inertia of the beam is shown in 2.26. To approach the solution of this equation, we first look into the free vibration of the beam. This means there is no external load on the beam $q(x,t) = 0$. The standard form of the solution is shown in equation 2.28 [23]. Here, ω_n represents the natural frequency of the beam. Each solution using a natural frequency is called a mode. To approximate the solution, the first few modes are taken into account. For each mode the solution is calculated. Each $w_i(x,t)$ with corresponding ω_n forms a solution.

$$w(0) = 0, \quad w'(0) = 0, \quad w''(l) = 0, \quad w'''(l) = 0 \tag{2.25}$$

$$I = \frac{bH^3}{12} \tag{2.26}$$

$$W_n(x) = C_n \left[\sin(\beta_n x) - \sinh(\beta_n x) - \alpha_n(\cos(\beta_n x) - \cosh(\beta_n x))\right] \tag{2.27}$$

$$\text{with} \quad \alpha_n = \left(\frac{\sin(\beta_n l) + \sinh(\beta_n l)}{\cos(\beta_n l) + \cosh(\beta_n l)}\right) \tag{2.28}$$

Forced vibration

When a beam is influenced by en external force, the motion is called a forced vibration. This is the case in this study. The solution $w(x,t)$ is assumed as 2.29. When filling this in in equation 2.19, this results in 2.30.

$$w(x,t) = \sum_{n=1}^{\infty} W(x)q(t) \tag{2.29}$$

$$EI \sum_{n=1}^{\infty} \frac{d^4 W_n(x)}{dx^4} q_n(t) + \mu \sum_{n=1}^{\infty} W_n(x) \frac{d^2 q_n(t)}{dt^2} = f(x,t) \tag{2.30}$$

$W_n(x)$ is the characteristic function of the beam and satisfies equation 2.31. When this equation is filled in in equation 2.30, this results in 2.32.

$$EI \frac{d^4 W_n(x)}{dx^4} - \omega_n^2 \mu W_n(x) = 0 \tag{2.31}$$

$$\sum_{n=1}^{\infty} \omega_n^2 W_n(x) q_n(t) + \sum_{n=1}^{\infty} W_n(x) \frac{d^2 q_n(t)}{dt^2} = \frac{1}{\mu} f(x,t) \tag{2.32}$$

Equation 2.32 is multiplied by $W_n(x)$ and there is integrated from 0 to l over the length of the beam x. This results in equation 2.33. In this equation, $Q_n(t)$ and b are defined in equation 2.34 and 2.35.

$$\frac{d^2 q_n(t)}{dt^2} + \omega_n^2 q_n(t) = \frac{1}{\rho\mu} Q_n(t) \tag{2.33}$$

$$Q_n(t) = \int_0^l f(x,t) W_n(x)\, dx \tag{2.34}$$

$$b = \int_0^l W_n(x)^2\, dx \tag{2.35}$$

The total term $q_n(t)$ is defined by 2.36. The first two terms represent the free vibration of the beam. The third term represents the steady state vibration that results from the force. In [17], similar model is used. This paper concludes that the model is not completely correct. This is why experiments will be carried out.

$$q_n(t) = A_n cos(\omega_n t) + B_n sin(\omega_n t) + \frac{1}{\mu b \omega_n} \int Q_n(\tau) sin(\omega_n (t - \tau)) d\tau \tag{2.36}$$

2.6.2. External force

The external force on the plate is determined by two phenomena. First is the Morison force that the flow exerts over the structure. This is calculated in the same way as in the reduced order model discussed is section 2.5.2. A new phenomena that is important in this part of the model in the slamming impact. This is done by integrating the pressure of the water over the length of the wall. The water pressure is defined as 2.37 [2]. At the same time the deformation and velocity of the wall must be taken into account.

$$P_1 + \frac{1}{2}\rho v_1^2 + \rho g h_1 = P_2 + \frac{1}{2}\rho v_2^2 + \rho g h_2 \tag{2.37}$$

$$\Delta p = \frac{1}{2}\rho \Delta v_1^2 \tag{2.38}$$

$$EI\frac{\partial^4 w}{\partial x^4} + \mu\frac{\partial^2 w}{\partial t^2} = f(x,t) \tag{2.39}$$

$$f(x,t) = \frac{1}{2}\rho v_{wave}^2 A_{wet} + \frac{1}{2}\rho C_d A_{wet}\left(v_{wave} - \frac{\partial w}{\partial t}\right) + \rho C_m V_{wet}\left(\dot{v}_{water} - \frac{\partial^2 w}{\partial t^2}\right) \tag{2.40}$$

In this model, the velocity of the plate itself will be neglected. This assumption will influence the results. However, in this case the calculation is meant to predict what will happen in the experiment. Taking into account the velocity and acceleration will make the partial differential equation of the beam 2.39, very complicated to solve. That is why, for now, we accept the simplification. This results in equation 2.41.

$$f(x,t) = \frac{1}{2}\rho v_{wave}^2 A_{wet} + \frac{1}{2}\rho C_d A_{wet}\left(v_{wave}\right) + \rho C_m V_{wet}\left(\dot{v}_{water}\right) \tag{2.41}$$

2.6.3. Load distribution

As seen in section 2.4.2, the velocities and accelerations are constructed using experimental data. From this information, the load over the height z of the plate is defined in a load distribution, using the method described in section 2.6.2. To be able to use this load distribution in calculating the deflections of the plate, a Fourier decomposition of the load is made [26]. This means the load is decomposed in a sum of a constant load, and multiple sines and cosines 2.42.

$$F(t,z) = a_0 + \sum_{n=1}^{\infty}\left(a_n cos(n\omega t) + b_n sin(n\omega t)\right) \tag{2.42}$$

The coefficients of the components a_0, a_n, b_n are calculated using equation 2.43 to 2.45. This coefficients represent how much of this component is presents in the distributed load.

$$a_0 = \frac{1}{L}\int_0^T F(t,z)\,dz \tag{2.43}$$

$$a_n = \frac{2}{L}\int_0^T F(t,z)cos(n\omega t)\,dz \tag{2.44}$$

$$b_n = \frac{2}{L}\int_0^T F(t,z)sin(n\omega t)\,dz \tag{2.45}$$

2.7. Integration and stability pendulum model

For this model a differential equation is solved numerically. First we focus on the model of the pendulum. To solve this multiple methods are available. These methods have different stability regions regarding the time step. A small time step will generally lead to more accurate results, but this will also lead to a long computational time.

2.7.1. Euler forward

For this problem the forward Euler method is first tried. This is the most simple integration method. The value of the next time step is gained as in equation 2.46.[25] To use this method, the stability region must be acceptable.

$$y_{n+1} = y_n + (t_{n+1} - t_n) f(t_n, y_n) \tag{2.46}$$

This model is formed by a second-order initial-value problem. To consider the stability, the problem is transformed to a system of first order differential equations. Equation 2.14 is transformed, leading to 2.48.

$$y_1' = y_2 \tag{2.47}$$

$$y_2' = -\frac{c}{I} y_2 - \frac{k}{I} y_1 + \frac{M}{I} \tag{2.48}$$

This leads to the system 2.49 to 2.51.

$$A = \begin{pmatrix} 0 & 1 \\ -\frac{k}{I} & -\frac{c}{I} \end{pmatrix} \tag{2.49}$$

$$y = \begin{pmatrix} y_1 \\ y_2 \end{pmatrix} \tag{2.50}$$

$$g = \begin{pmatrix} 0 \\ \frac{M}{I} \end{pmatrix} \tag{2.51}$$

The stability region of Euler forward is established using the eigenvalues of the system.

$$\text{If } |1 + \lambda_j \Delta t| < 1, \text{ stability} \tag{2.52}$$

This does not hold for this system, meaning this method is not applicable.

2.7.2. Runge Kutta 4

This method has a larger stability region than the Euler forward method. The integration scheme is as described in equation 2.53 to 2.57.

$$y_{n+1} = y_n + \frac{1}{6}(k_1 + 2k_2 + 2k_3 + k_4) \tag{2.53}$$

$$k_1 = \Delta t f(t_n, y_n) \tag{2.54}$$

$$k_2 = \Delta t f\left(t_n + \frac{1}{2}\Delta t, y_n + \frac{1}{2}k_1\right) \tag{2.55}$$

$$k_3 = \Delta t f\left(t_n + \frac{1}{2}\Delta t, y_n + \frac{1}{2}k_2\right) \tag{2.56}$$

$$k_4 = \Delta t f\left(t_n + \Delta t, y_n + k_3\right) \tag{2.57}$$

The RK4 method is stable when equation 2.58 is satisfied.

$$-1 \leq 1 + x + \frac{1}{2}x^2 + \frac{1}{6}x^3 + \frac{1}{24}x^4 \leq -1, \text{ where } x = \lambda \Delta t \tag{2.58}$$

3

Sloshing tank experiments

In this chapter, the experiments that will be done in the Sloshing Rig of the faculty Mechanical engineering at the TU Delft will be explained. The results will be discussed in chapter 7. The model discussed in chapter 5, will be a simplified computational model of the situation in the tank. This chapter will therefore also give insight in the setup of the model.

3.1. Setup experiment

The aim of the experiment is to gain insight in the structural responses of a flexible material in breaking waves. In this case the material is stainless steel. Structures with varying natural frequencies will be used to gain insight in the influence of the structures own characteristics on the response motion.

The experiments will consist of testing steel plates with different natural frequencies. In the experiment, four stages of wave breaking will be tested. These wave stages are illustrated in figure 3.1 [5]. The different wave types will be generated by using different focus points in x direction. The experiment will be done four times with the four different plates described in section 3.1.1.

3.1.1. Set up

For this experiment the Sloshing rig of the TU Delft is used. By moving the tank in x direction, waves will be generated. This generated wave will break at the desired location. This is explained in more detail in section 3.1.2. At the desired location, the structure is placed so that the clearance to the water level is at the desired value. After wave impact, the wave will dissolve over time. This set up is shown schematically in figure 3.2. To clarify the configurations, a similar figure including the different configurations is shown in figure 3.3

We now look further into the structures that are placed in the breaking waves. In this experiment, it is important that the parameter of interest is varied. It is important that by doing this, all other variables are kept constant. The variable of interest is the natural frequency of the structure. A few aspects are important to take in to account when changing the natural frequency. The natural frequency for a plate clamped - free is described in equation 3.1. When the length or thickness of the plate is changed, the natural frequency is changed. However, this will also influence the total weight of the plate, the wet area and the moment of inertia of the plate. In order to handle these effects, the following set up for the structures is designed.
For the plate, four different thicknesses are used to vary the natural frequency. The clearance between the water level and the plate will always stay constant. Changing the thickness does mean that the stiffness of the plate will vary, this influences the displacement. This effect will be accounted for in the data analysis. The width of the plate is kept the same over all tests and the plate is almost as wide as the tank in order to reduce 3D effects. A schematic image is shown is figure 3.4 and 3.5.

The structure is installed so that the force and the moment on the plate can be measured. The force on

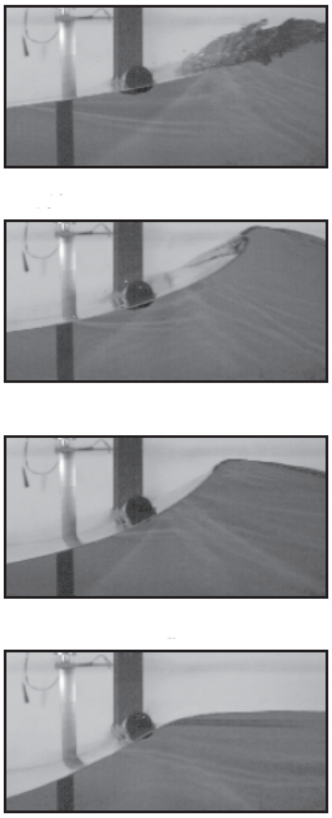

Figure 3.1: Four stages of breaking waves

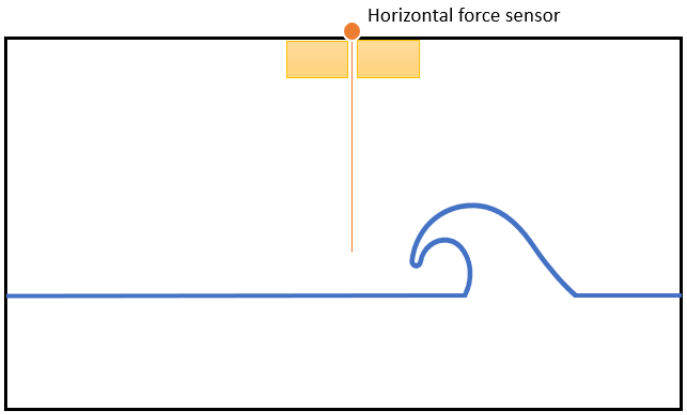

Figure 3.2: Experiment with plate, schematically.

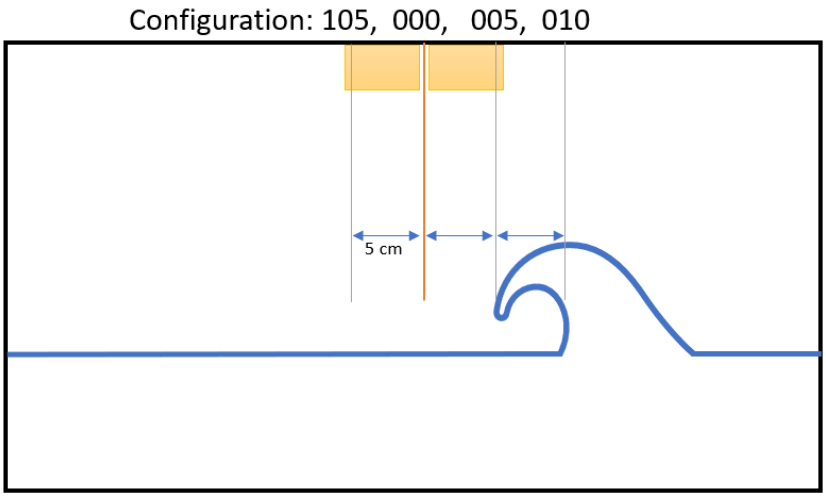

Figure 3.3: Experiment with plate, showing the positions of the plate in different configurations.

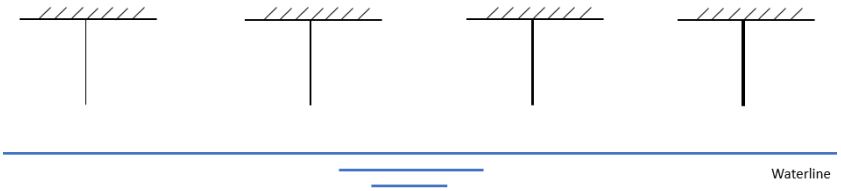

Figure 3.4: Set up experiment with plate, side view of the different plates

the plate is measured in x direction. The installation is shown schematically in figure 3.6. In this image the placement of the wave probes is shown as well. Also the dimensions of the plate inside the tank are indicated. In figure 3.7, the placement of the camera is shown. The camera is placed here due to the limited space, caused by the frame that moves the rig. With a mirror, the frame will be visible as indicated. Lastly, the force measurement set up is show in more detail in figure 3.8.

$$\omega_n = \beta_n^2 \sqrt{\frac{EI}{\mu}} \tag{3.1}$$

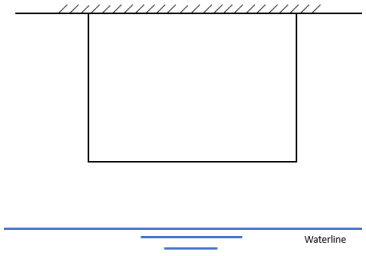

Figure 3.5: Set up plate, frontal view

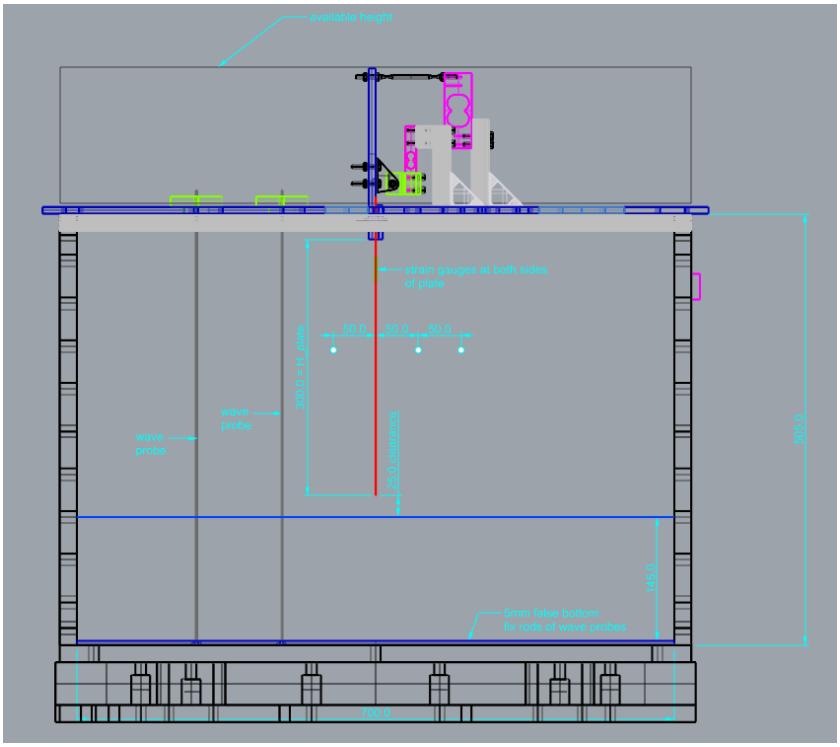

Figure 3.6: Set up of the rig for the experiment

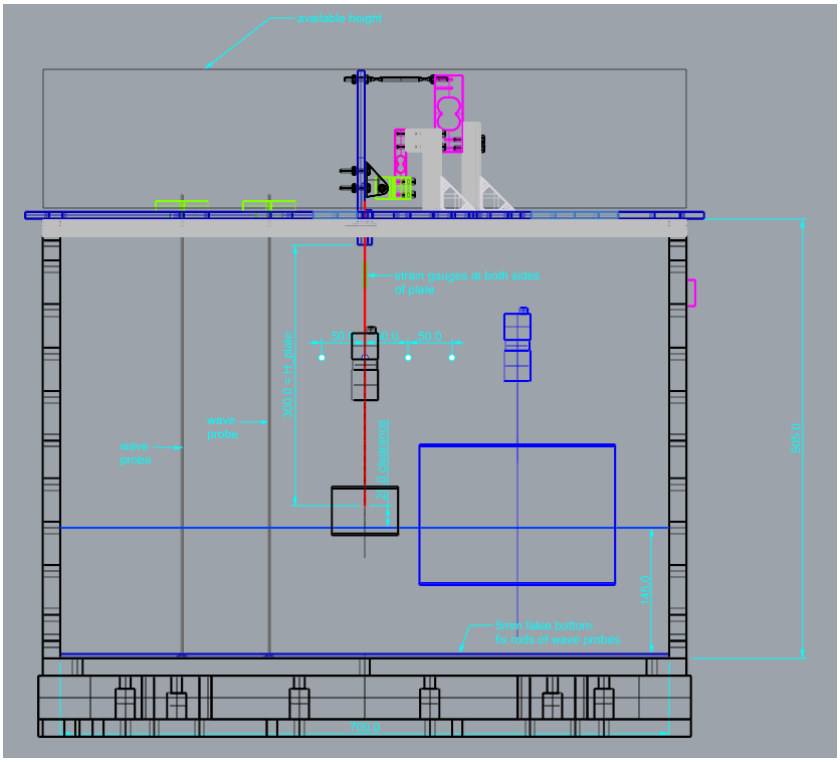

Figure 3.7: Set up of the rig with cameras

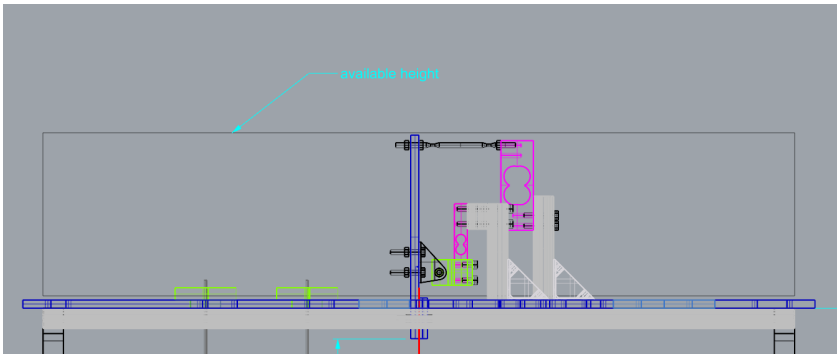

Figure 3.8: Set up of the force measurement system

3.1.2. Wave generation

The waves used in this experiment will be generated using a motion of the tank in x direction. Each run, the motion of the tank will be identical. The aim is for the wave to be identical as well in each run. For each wave type that is tested, the breaking stage differs at the location of the structure. This is done by placing the structure at a different locations in x-direction.

The wave will break on the same location each time. The four structure locations will be at $-0.05m$, $0.00m, 0.05m$ and $0.10m$ oriented from the midpoint of the tank. The breaking process of the wave will take some time and space to develop. In order to make the wave break at the desired location, the tank is moved in a sinusoidal motion in x direction. This movement in the experiment will be the same as in the simulation in ComFLOW. This ComFLOW simulation is described in table 3.3. Due to the size of the wave with respect to the water depth, the wave will break. The process of the breaking wave as designed in ComFLOW is illustrated in figure 3.9. The exact breaking process can be different in different runs, even for the same waves. This is why the wave heights will be measured at the experiment. In this experiment, it is the intention to make the same wave every time. Only the focus point differs, this results in different characteristics at the location of the structure. To keep an overview of which wave configuration is which, the different structure -wave positions are given in table 3.1. In this table the clearance represents the distance in z-direction between the bottom of the structure and the still water surface. x_f represents the distance in x-direction between the breaking location of the wave and the structure

Table 3.1: Locations of the plate in breaking waves

Configuration	clearance z (m)	x_f (m)
000	0.025	0.0
005	0.025	0.05
010	0.025	0.10
105	0.025	-0.05

3.1.3. Measuring

To analyse the desired phenomena in this experiment, the rise time and quantity of the horizontal impact force will be measured. The rise time means the time period in with the force on the plate increases from zero to its maximum value. This rise time of the wave force is measured because there must be looked in to the natural period of the structure relative to the rise time of the force in order to make useful comparisons between the different plates.

In addition, the deflection and frequency of the motion of the plate will be measured with a camera. The camera will film the impact process. From these images the deflections over time can be measured. Lastly, it is important to measure the wave. The wave must behave the same each time the test runs. To make sure this is the case, the wave is measured each time. This is done using wave probes.

3.2. Experiment and waves simulation

To create the desired wave in the sloshing tank, a 2D simulation in ComFLOW is done. To conduct this simulation, a geometry representing the the sloshing rig and a plate is made. The dimensions of the geometry can be found in table 3.2. The additional information of the simulation can be found in table 3.3.

Table 3.2: Input geometry ComFLOW

	x	y	z
Slosh rig	0.0, 0.7	0.0, 0.2	0.0, 0.496
Beam	0.34, 0.35	0.0, 0.2	0.170, 0.496

Table 3.3: Input data ComFLOW

Water level	0.145 m
Motion x frequency	0.6 s^{-1}
Motion x amplitude	0.055 m
Runtime simulation	3 s

The simulation output is viewed in Paraview. The wave is showing the correct breaking location. This is illustrated in three time snapshots in figure 3.9.

The forces on the plate are also evaluated in ComFLOW. The force on the plate is plotted over time in figure 3.10. In reality, the motion of the slosh tank will be stopped after the first impact of the wave on the beam. The water will continue to move, but these impacts are not of interest. In figure 3.10, the forces on the beam, calculated by ComFLOW are shown. They are shown for the configurations 000, 005, 010 and 105. In ComFLOW, only a rigid beam is used to predict the forces.

In figure 3.11 the pressure on the beam is plotted. The x axis represents the length of the beam. For clarity of the image, not the whole length is plotted. The different lines represent different moments in time. This is plotted for configuration 000.

In figure 3.12, the pressure is plotted over time. Here, the different line represents the different points on the height of the beam. This is plotted for configuration 000.

3.3. Planning experiments

During the experiments, each plate will be tested using different wave breaking stages. This is done to investigate if the effects are the same at different load distributions. In table 3.4, an overview of all the test configurations is given.

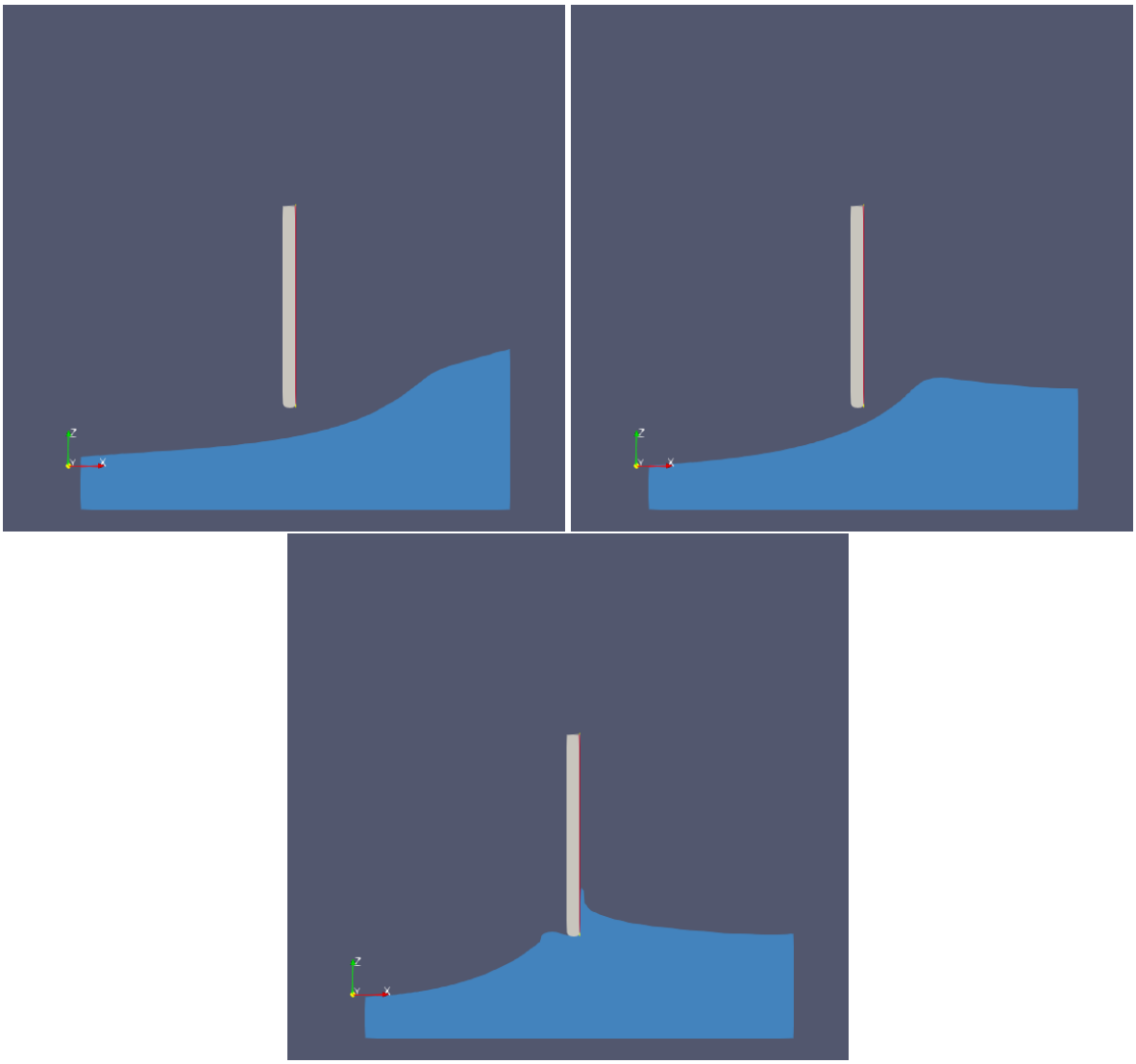

Figure 3.9: Predicted wave impact ComFLOW, three different time points

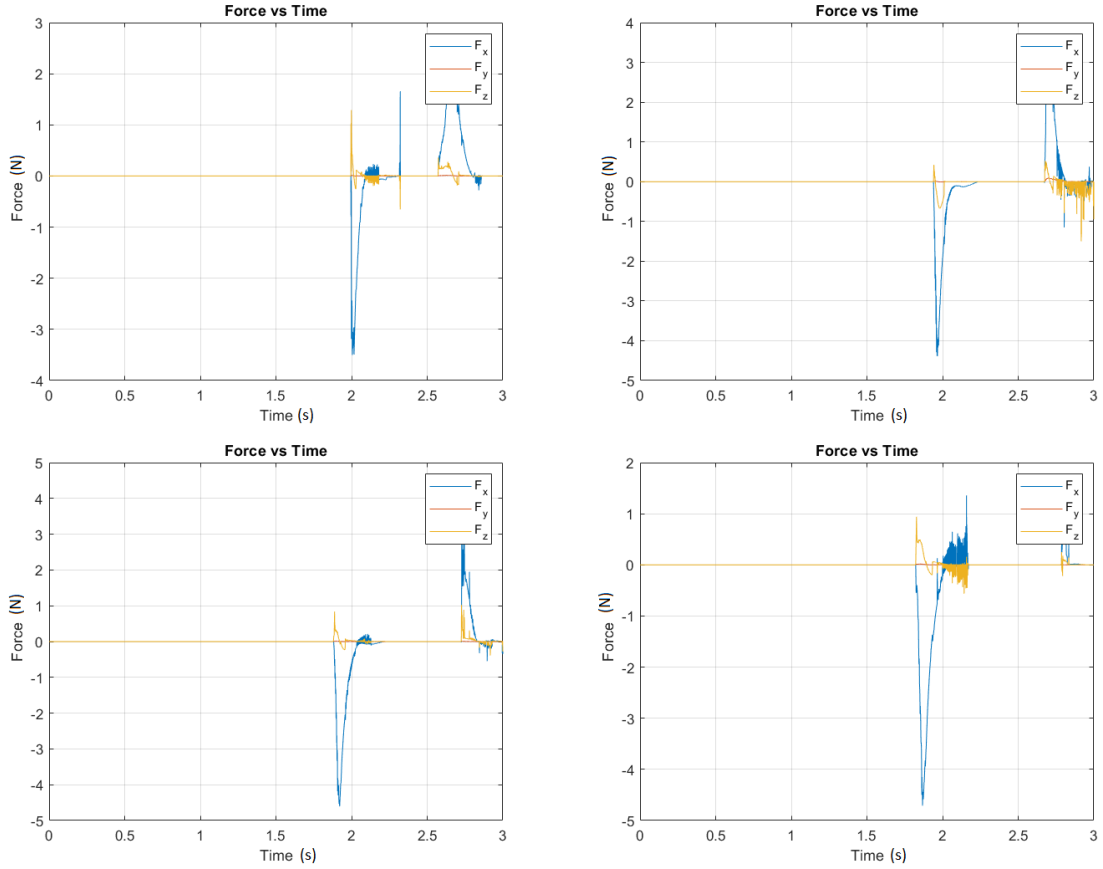

Figure 3.10: Predicted force by ComFLOW on the plate over time.
Top left: configuration 105.
Top right: configuration 000.
Bottom left: configuration 005 .
Bottom right: configuration 010

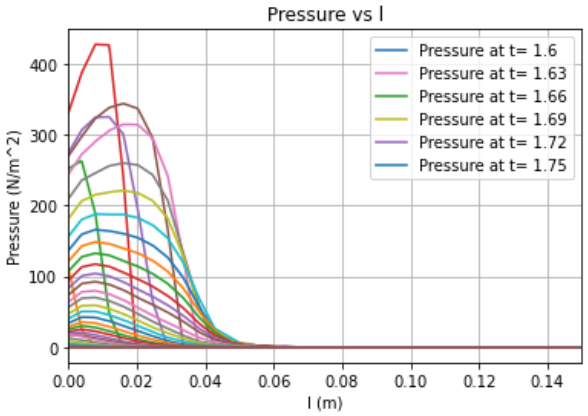

Figure 3.11: Predicted pressures on the plate over length

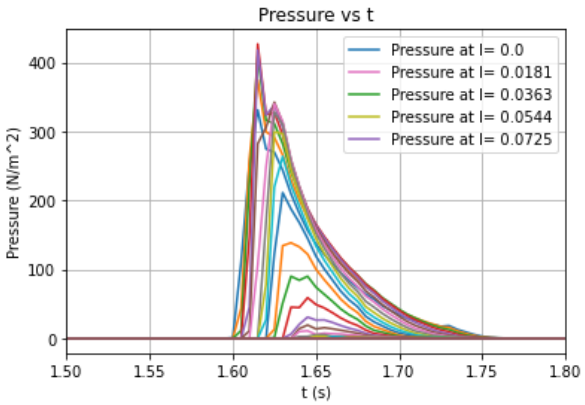

Figure 3.12: Predicted pressures on the plate over time, at different heights

Table 3.4: Timetable Plate tests

Test	configuration	repetitions
Plate 1	000	3
Plate 1	005	3
Plate 1	010	3
Plate 1	105	3
Plate 2	000	3
Plate 2	005	3
Plate 2	010	3
Plate 2	105	3
Plate 3	000	3
Plate 3	005	3
Plate 3	010	3
Plate 3	105	3
Plate 3	000	3
Plate 3	005	3
Plate 3	010	3
Plate 3	105	3

4

Previous experiments and model verification

In this chapter, a short description of the experiments of [5] and [6] is given. In section 4.1, the model used for the pendulum is verified using the findings of [5]. In section 4.2, the model of the beam is verified using reference simulations.

4.1. Pendulum model

In previous research [5], a pendulum is used to represent a structure in waves in a simplified manner. The pendulum is a simplification of a structure that experiences a transition from dry to wet, then vibrates in a wet condition. After that the pendulum experiences a transition from wet to dry, and a vibration in dry condition occurs. This means the pendulum will experience added mass and added damping, due to the surrounding water. In this section, the model of this study is compared to the results of [5].
The model is based on the equations described in section 2.5.2. The equations are discretized to use in a numerical calculation using equation 4.1 to 4.4.

$$I\ddot{\theta} + c\dot{\theta} + k\sin\theta = M \tag{4.1}$$

$$\ddot{\theta} = \frac{M - c\dot{\theta} - k\sin\theta}{I} \tag{4.2}$$

$$\dot{\theta}^{n+1} = \dot{\theta}^{n} + dt\left(\ddot{\theta}^{n}\right) \tag{4.3}$$

$$\dot{\theta}^{n+1} = \dot{\theta}^{n} + dt\left(\frac{M - c\dot{\theta} - k\sin\theta}{I}\right) \tag{4.4}$$

4.1.1. Pendulum in monochromatic waves

To validate the model that calculates the motion of the pendulum, the model of this study is used to recreate the findings of [5]. The motion of the pendulum is calculated using the reduced order model as in chapter 2.5.2. For this experiment the center of the pendulum is 1 cm above the mean free surface. The pendulum has a radius of 2.5 cm. The length of the pendulum is 1.05 m and the width is 1.5 m. The natural period of the pendulum T= 2.06. Parameters that are relevant are $k = 31.7$ Nm/rad, $I = 2.17$ kg m2, $c = 0.205$ ms/rad. $C_d = 2, C_m = 1$. The natural period of the pendulum is $T = 2.06$ s
The waves used in this experiment are of length $\lambda = 1, 3, 5$ and $7m$. with an amplitude of 45 mm,54 mm, 50 mm, and 45 mm respectively. At t=0, the wave height is 0 at the location of the pendulum. The wave for $\lambda = 7$ is plotted in figure 4.1.

In figure 4.2, the responses of the pendulum in all wavelengths are shown. The motions are in agreements with the data of [5]. The motions calculated by this study are shown in figure 4.3. Besides the

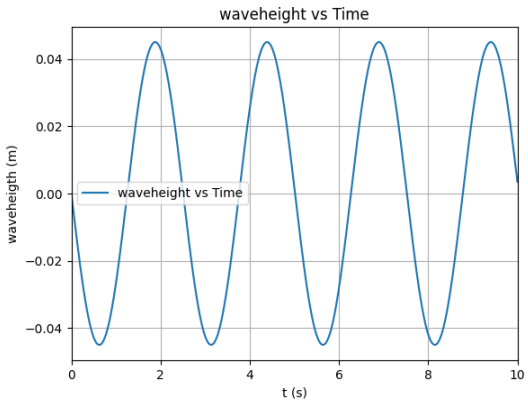

Figure 4.1: Wave height over time of waves $\lambda = 7m$

verification of the model, a few things can already be learnt from these experiments. For $\lambda = 7$, $T_{wave} =$ 2.51 s. This is higher than the natural period of the pendulum. As seen in the results, a different frequency motion shows in the motion of the pendulum. For $\lambda = 5$, $T_{wave} =$ 1.94s. For this motion the amplitude is increasing due to the waves. This means for a wave period (almost) equal to the one of the pendulum is causing resonance. For the waves of 3m, the wave period is 1.41s. This means that the waves are out of phase with the pendulum and the response decreases a bit over time. For the smallest waves of 1m length, the wave period is 0.80 s. The motion of the pendulum shifts to the positive angle.

4.1.2. Pendulum in breaking waves

The pendulum is now exposed to a breaking wave. This is done similar to the experiments in [6]. The modelled wave and pendulum is identical to the one in the previous study. In this experiment, the modelled wave is the same each time. Only the location of the pendulum is varied. The pendulum is located at four different x locations. On each of these locations the pendulum is varied at two different z locations. The locations in x direction make sure that the pendulum undergoes different stages of wave breaking, as the breaking of the wave develops over time and distance. The locations of the pendulum are shown in table 4.1. The clearance indicates the distance between the mean water surface and the bottom of the pendulum. The x_{pen} is at 0 m when the breaking process of the wave starts exactly at the location on the pendulum. At $x_{pen} = -1.5m$ the wave is the most furthered in breaking when meeting the pendulum.

Configuration	clearance (m)	x_{pen} (m)
500	0.05	0.0
505	0.05	-0.5
510	0.05	-1.0
515	0.05	-1.5
605	0.1	-0.5
610	0.1	-1.0
615	0.1	-1.5

Table 4.1: Locations of the pendulum in breaking waves

The velocities and wave elevation at the desired points are measured in an experiment [6]. This data will be used to calculate the expected motions of the pendulum. To illustrate, in figure 4.4, the wave elevation and velocity at $x = -0.5$m are shown. It must be taken into account that the Fourier reconstructions of the wave shape do not result in a highly accurate model of the wave. Also at the configurations 510 and 520, the wave has a lot of air- water mixing. This results is less accurate measurements of the wave gauges.

The motion of the pendulum is calculated using the reduced order model as in chapter 2.5.2. The

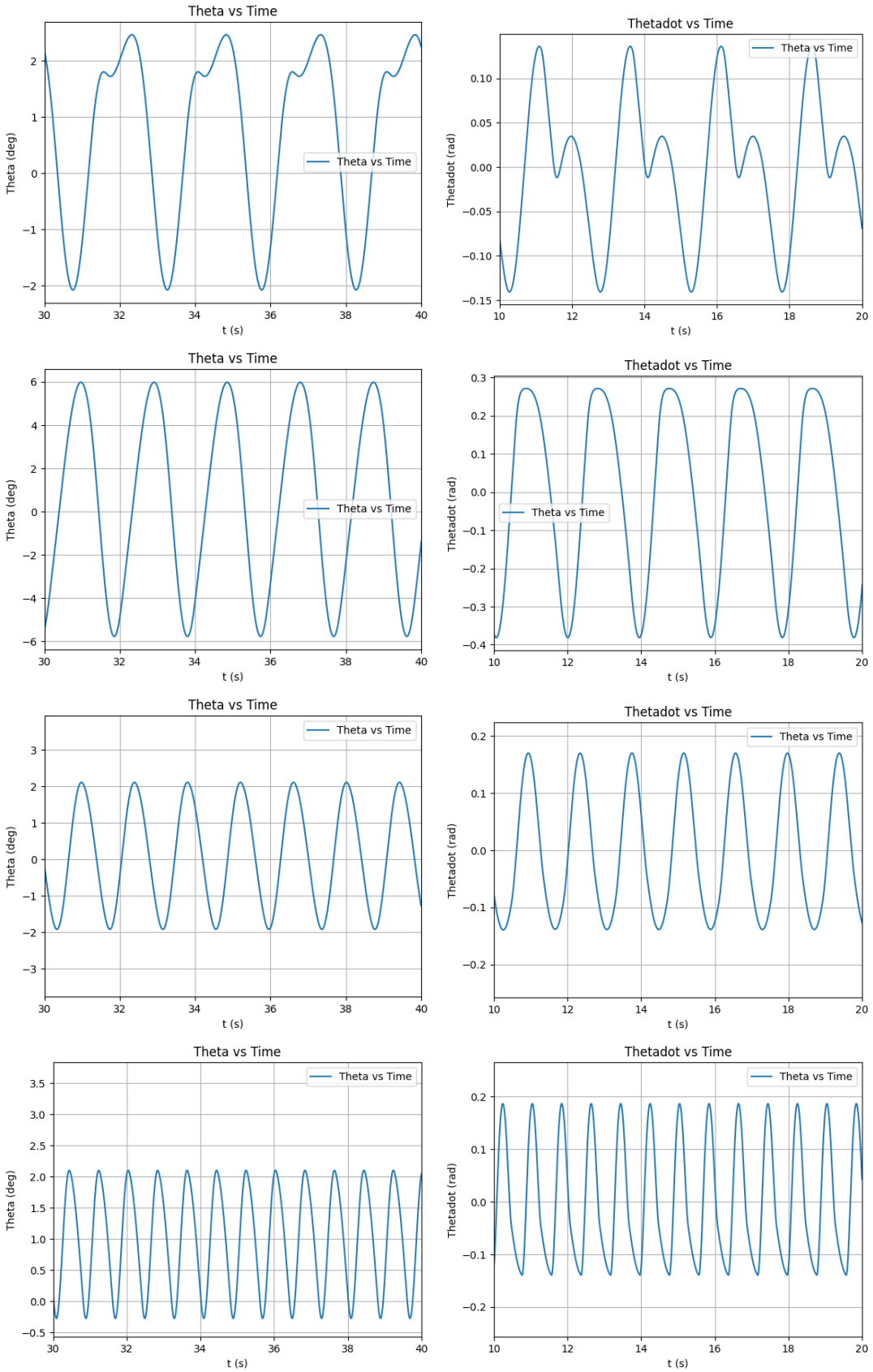

Figure 4.2: Theta (left column) and theta dot (right column) vs time with pendulum in surface of different waves. Top row: $\lambda = 7$, second row: $\lambda = 5$, third row: $\lambda = 3$, fourth row: $\lambda = 1$

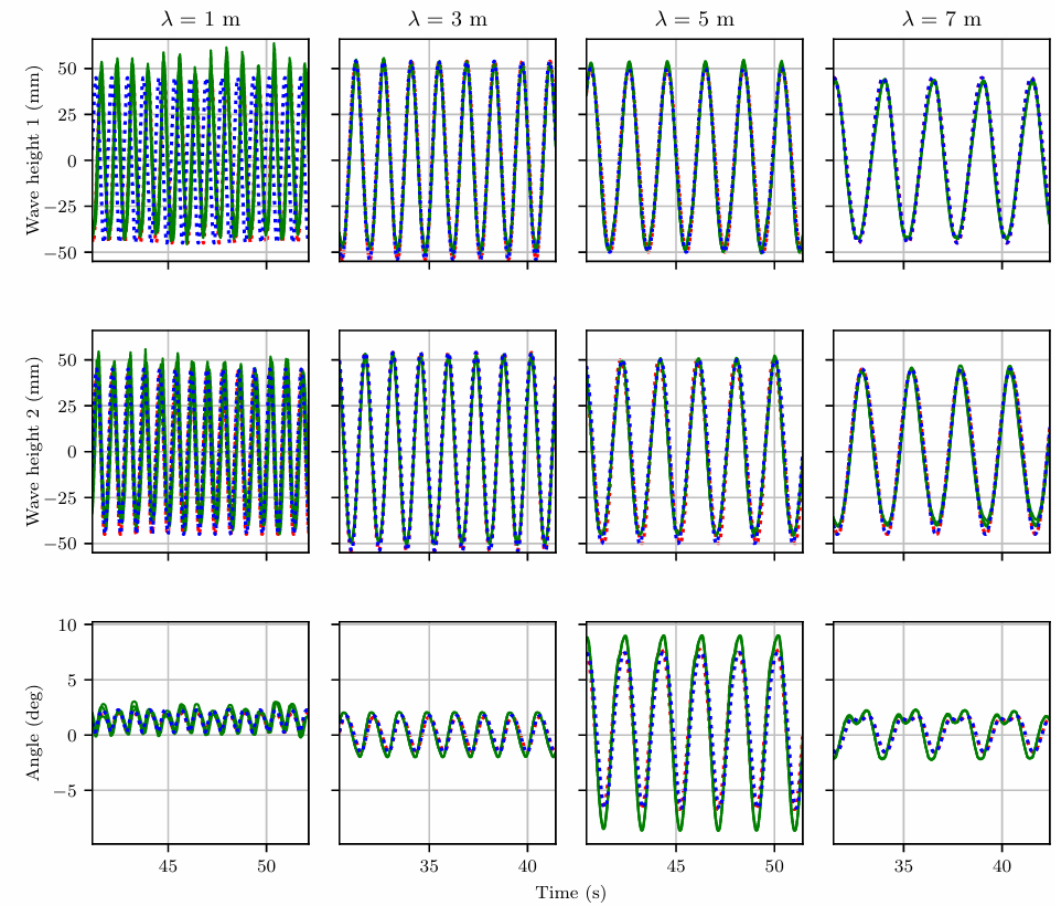

Figure 4.3: On the top two row, the wave elevations of 2 wauge gauges are plotted. On the bottom row, the response motion of the pendulum is shown. Results of the study [5]

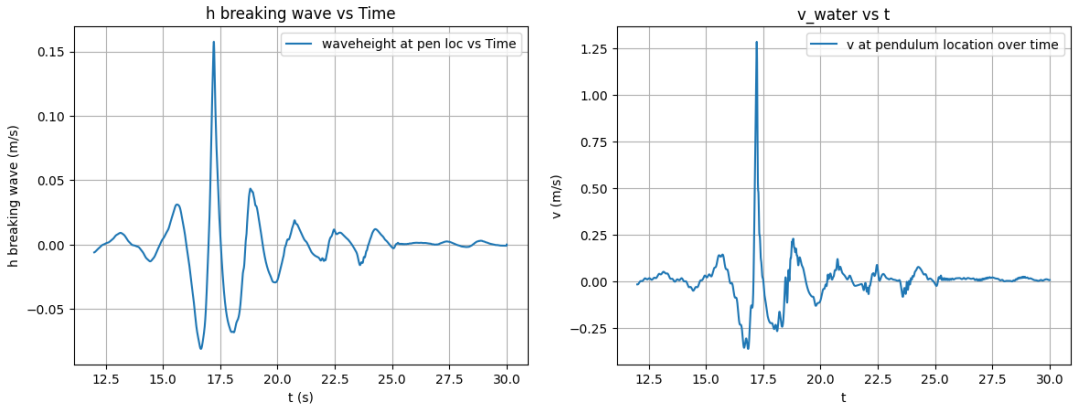

Figure 4.4: Wave elevation and water velocity at location x=-0.5m.
left: Wave elevation, right :Velocity

resulting motions are plotted in figure 4.5. The motions are in agreement with the findings of [6]. The results of this previous study are shown in figure 4.7. However, the study also shows that the model results have an error at the configurations that include air- water mixing. This is due to the inaccuracy of the measurements as stated before.

From this experiments, a few things can be learnt. The more wave breaking is developed, the higher the velocities are in the crest of the wave. This can lead to larger impacts on the pendulum. However, a further stage of wave breaking also comes with more air- water mixture. The air can lead to a decrease of the impact. When surface elevation of the wave is larger, the pendulum travels a longer road while submerged. In this case, the pendulum can be impacted by a force in the negative direction as well. This is due to the different velocity directions inside the breaking wave. This can lead to lower response angles than expected. At the higher clearance position, the pendulum is impacted by a higher part of the wave, with higher velocities. The pendulum is however impacted over a shorter amount of time, possibly leading to lower total impact.

As seen in the figures, the highest response angle is found at configuration 510 and 505. The response at 515 being lower can be explained by the less accurate measurements of the wave velocity at highly developed breaking waves. It is also possible that the counteracting force is relatively higher at configuration 515.

At the high clearance responses, the further the wave is broken, the lower the response of the pendulum. In experiments [5], it turns out the reduced order model overestimates the response for configuration 505, 510, 600 and 605.

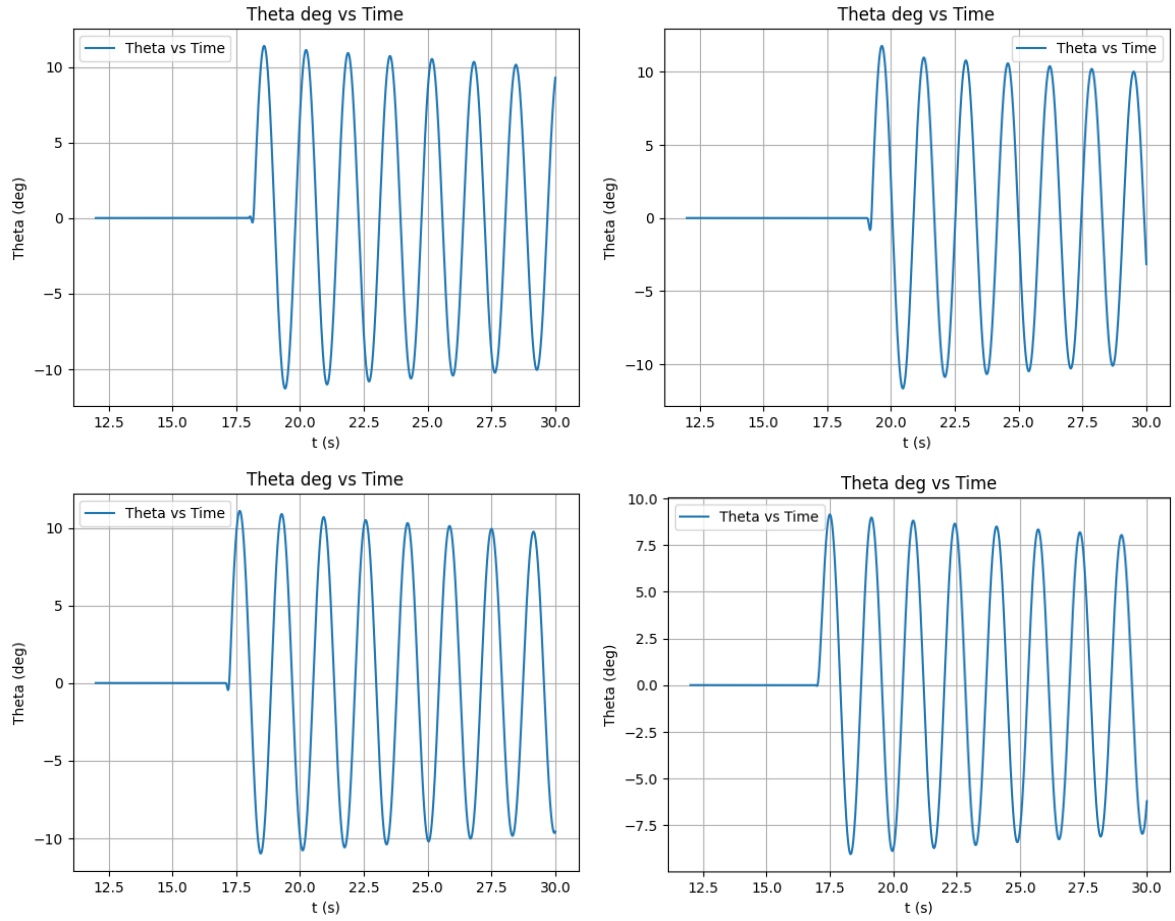

Figure 4.5: Resulting pendulum motion for low clearance configuration.
Top left: configuration 515. Top right: configuration 510. Bottom left: configuration 505. Bottom right: configuration 500.

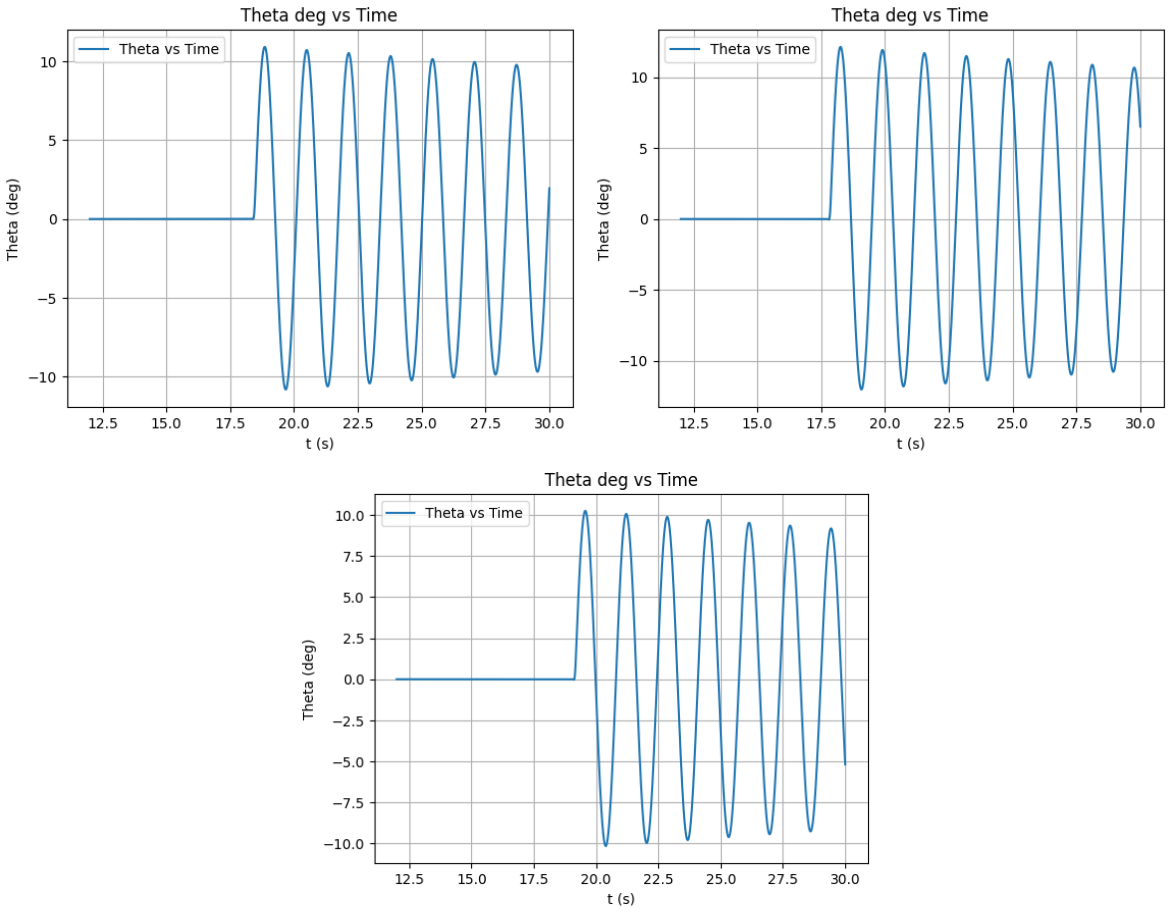

Figure 4.6: Resulting pendulum motion for high clearance configuration.
Top left: configuration 605. Top right: configuration 610. Bottom: configuration 615.

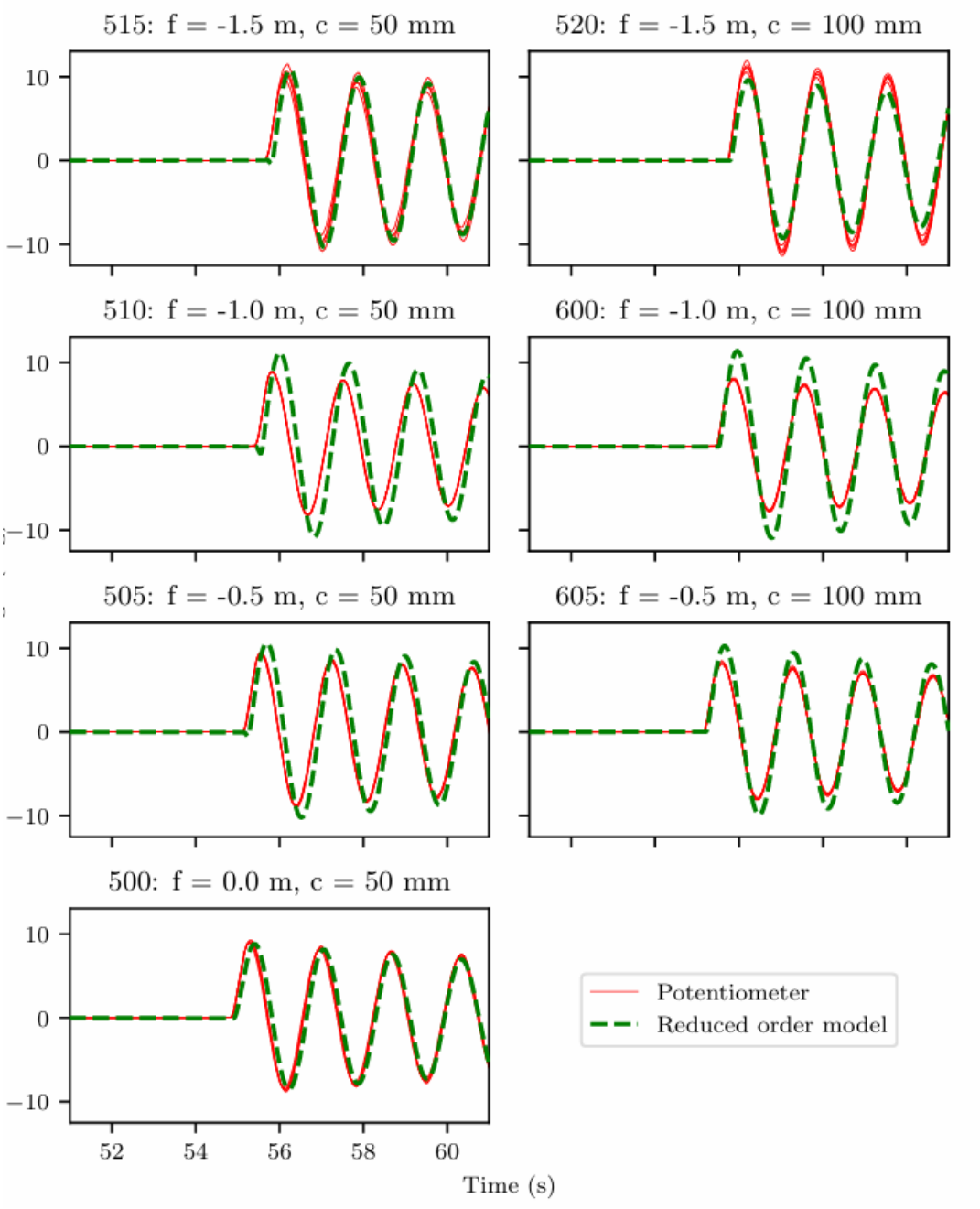

Figure 4.7: Response motion of pendulum in breaking waves, model and experiment. Findings of the study [6].

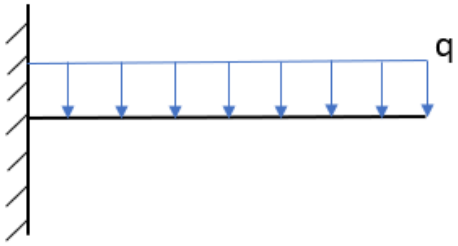

Figure 4.8: Schematic cantilevered beam

4.2. Beam model

In this section we look further into the model of the beam experiencing an impact of a breaking wave. The breaking wave is identical to the one used for the pendulum models. The beam is modelled using the equations described in section 2.6. The equations are discretized for numerical calculations using the method described in equation 4.5 to 4.11.

$$\frac{d^2 q_n(t)}{dt^2} + \omega_n^2 q_n(t) = \frac{1}{\rho\mu} Q_n(t) \tag{4.5}$$

$$\frac{dv}{dt} = \frac{1}{\rho\mu} Q_n(t) - \omega_n^2 q_n(t) \tag{4.6}$$

$$v = \frac{dq}{dt} \tag{4.7}$$

$$\frac{v^{n+1} - v^n}{dt} = \frac{1}{\rho\mu} Q_n(t) - \omega_n^2 q^n \tag{4.8}$$

$$\frac{q^{n+1} - q^n}{dt} = v^n \tag{4.9}$$

$$v^{n+1} = \frac{dt}{\rho\mu} Q_n(t) - \omega_n^2 q^n * dt + v^n \tag{4.10}$$

$$q^{n+1} = v^n * dt + q^n \tag{4.11}$$

4.2.1. Known distributed load

To verify the model, a theoretical beam in a known situation is tested. Assume a beam with length $l = 0.85$ and a thickness $th = 0.005$. The value of E is 10^6. For this test, a distributed load is applied on the beam. The load is constant over the length of the beam. The load increases slowly over time, until it reaches $2N/m$. The beam is a cantilevered beam, with a distributed load that is constant over length, but not over time. The schematic image of the beam with load is given in figure 4.8. The development of the beam over time is illustrated in figure 4.9.

In the situation of a cantilevered beam, with a constant distributed load, a well known equation 4.12 can be used [13]. This results in $w = 25.6$m.

$$w = \frac{ql^4}{8EI} \tag{4.12}$$

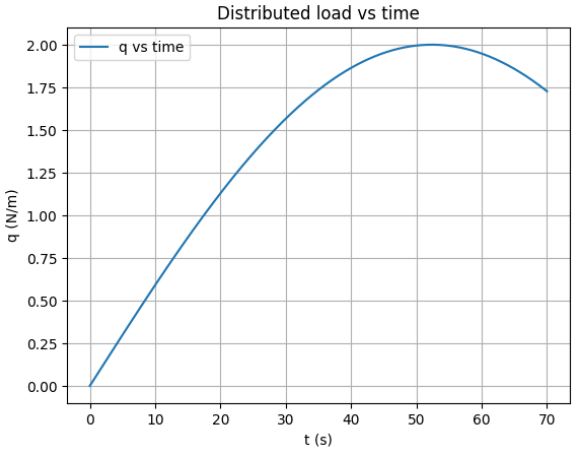

Figure 4.9: Distributed load on the beam over time

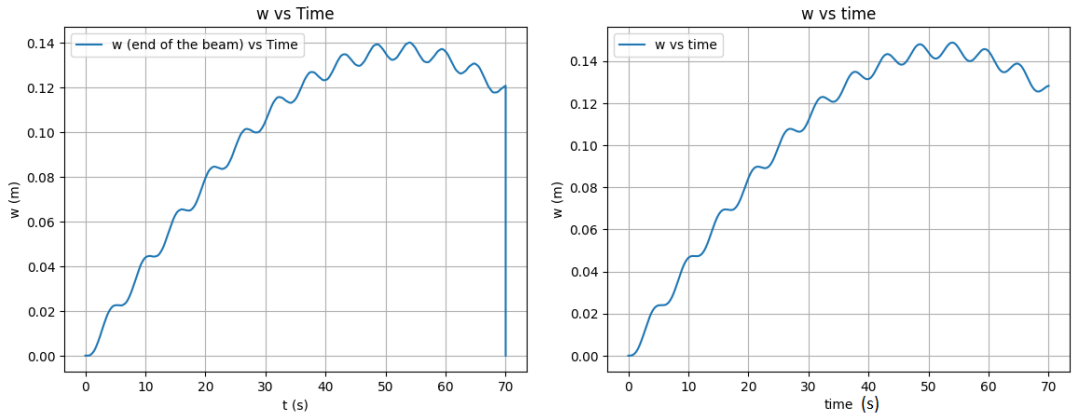

Figure 4.10: Deflection w of the beam, test situation. Left: using numerical method. Right: using Duhamels integral

The model is tested, using the load given in figure 4.9. This is done using the numerical method presented in section 2.6 and 2.7. The result of w is given in figure 4.10 a.

The simulation is conducted a second time using an analytic method. This method uses the Duhamel integral 4.13. As seen in figure 4.10 b, the results of the deflection w over time show strong agreement with the results of the numerical method. This indicates that the model gives desirable results.

$$q_n(t) = A_n cos(\omega_n t) + B_n sin(\omega_n t) + \frac{1}{\mu b \omega_n} \int_0^t Q_n(\tau) \sin(\omega_n (t-\tau))\, d\tau \tag{4.13}$$

4.2.2. Breaking wave load

Now that the model gives the desired results in the situation that is described, the beam must be applied to the situation of the wave impact. The wave impact is not constant over the height of the beam. The load distribution of the beam in the wave is shown in figure 5.6. In order to take this load into account, a Fourier transform of the load in z direction is used. This is done as described in section 2.6.3.

4.2.3. Deflections over length

If modelled correctly, the beam should move according to its natural mode shapes. These are the mode shapes that correspond with the cantilevered beam. These mode shapes are known. These modes lead to the movement shapes plotted in figure 4.11 [28].

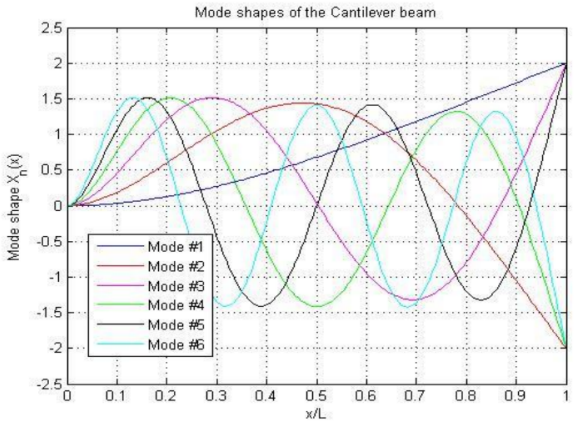

Figure 4.11: Shapes of cantilevered beam [28]

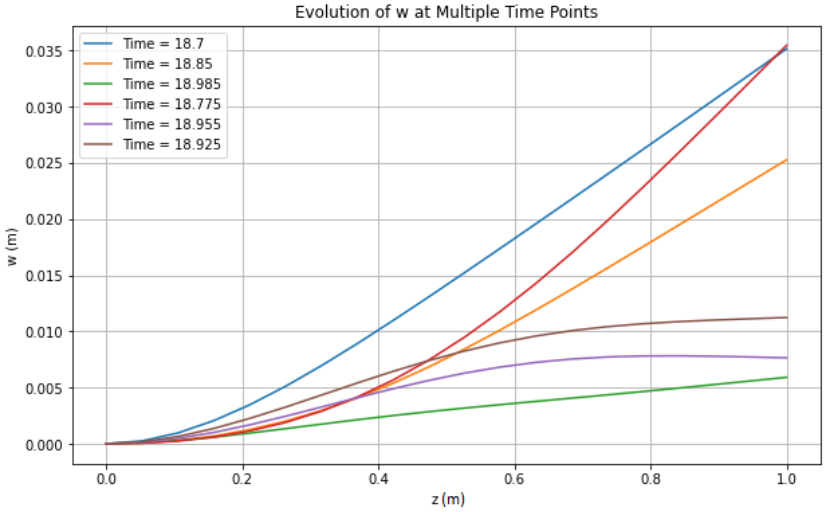

Figure 4.12: Shape of the beam at different points in time.

We will now look into the beam model using the load of the breaking wave. At configuration 505, the beam shows the deflections over the length of the beam, shown in figure 4.12. In the figure, the shapes can be spotted form different modes. This results are as desired from the model.

5

Results model experiments

Previous to the experiments in the tank, an experiment is carried out using the model described in section 2.5. This model experiments are important for multiple reasons. The results of the model will predict what happens during the experiments in the tank. This is important to choose the correct measuring devises and gain insight in the feasibility of the results. Secondly, the model and the experiments will be used jointly to form conclusions and answers on the research questions.

5.1. Pendulum model

First, an experiment with pendulums of different natural frequencies is used. The same model of the pendulum is used as in chapter 4. Also, for this modeling experiments, the same waves and configurations are used as described in chapter 4. In table 5.1, the used variations of the pendulum are shown. The point of this experiment is to see if the rise time of the force and the natural frequency of the pendulum has influence on its motion. Note that only the effective length is varied. The actual length of the pendulum stays the same, leading to the same interaction location with the water each time. This length is 0.6 m. The effective length means, in this experiment, the length used to calculate the response motion of the pendulum. The experiment is done three times using 3 wave impact moments, configuration 505, 515 and 605. These configurations are chosen because their results turn out more accurate when compared to the experiment in [6]. The impact forces at the location of the pendulum are plotted in figure 5.2.

Table 5.1: Effective lengths pendulum

Test	Effective length pendulum (m)	Total mass (kg)
1	0.46	9.86
2	0.48	9.86
3	0.51	9.86
4	0.53	9.86

5.1.1. Configuration 505

In figure 5.3, the deflections of the pendulums with different effective lengths are shown. They undergo the wave impact at configuration 505. The load on the pendulum over time is plotted in figure 5.2. In table 5.2, the maximum deflections and kinetic energy of the pendulum motion are listed.

5.1.2. Configuration 515

In figure 5.4, the deflections of the pendulums with different effective lengths are shown. They undergo the wave impact at configuration 515. The load on the pendulum over time is plotted in figure 5.2b. In table 5.3, the maximum deflections and kinetic energy of the pendulum are listed.

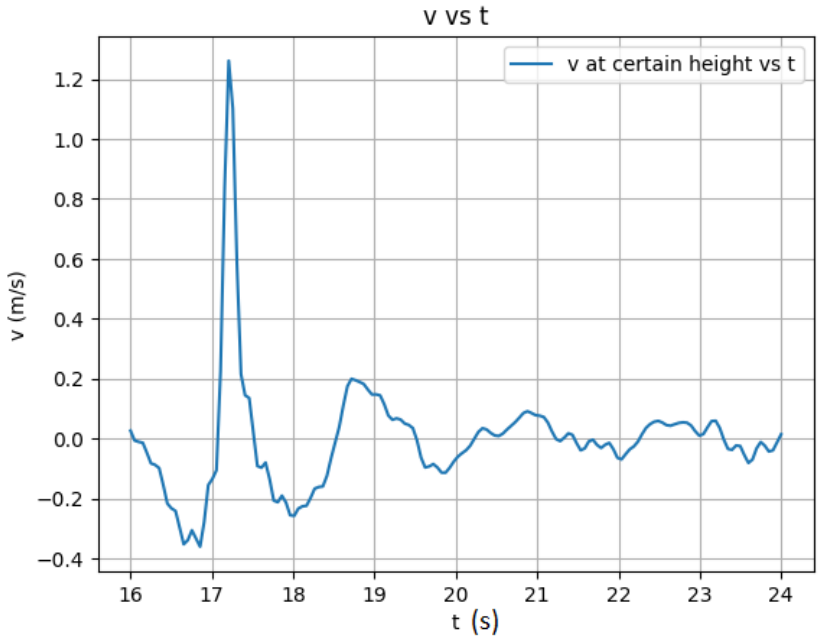

Figure 5.1: Velocity of the water at starting location of the pendulum over time, configuration 505

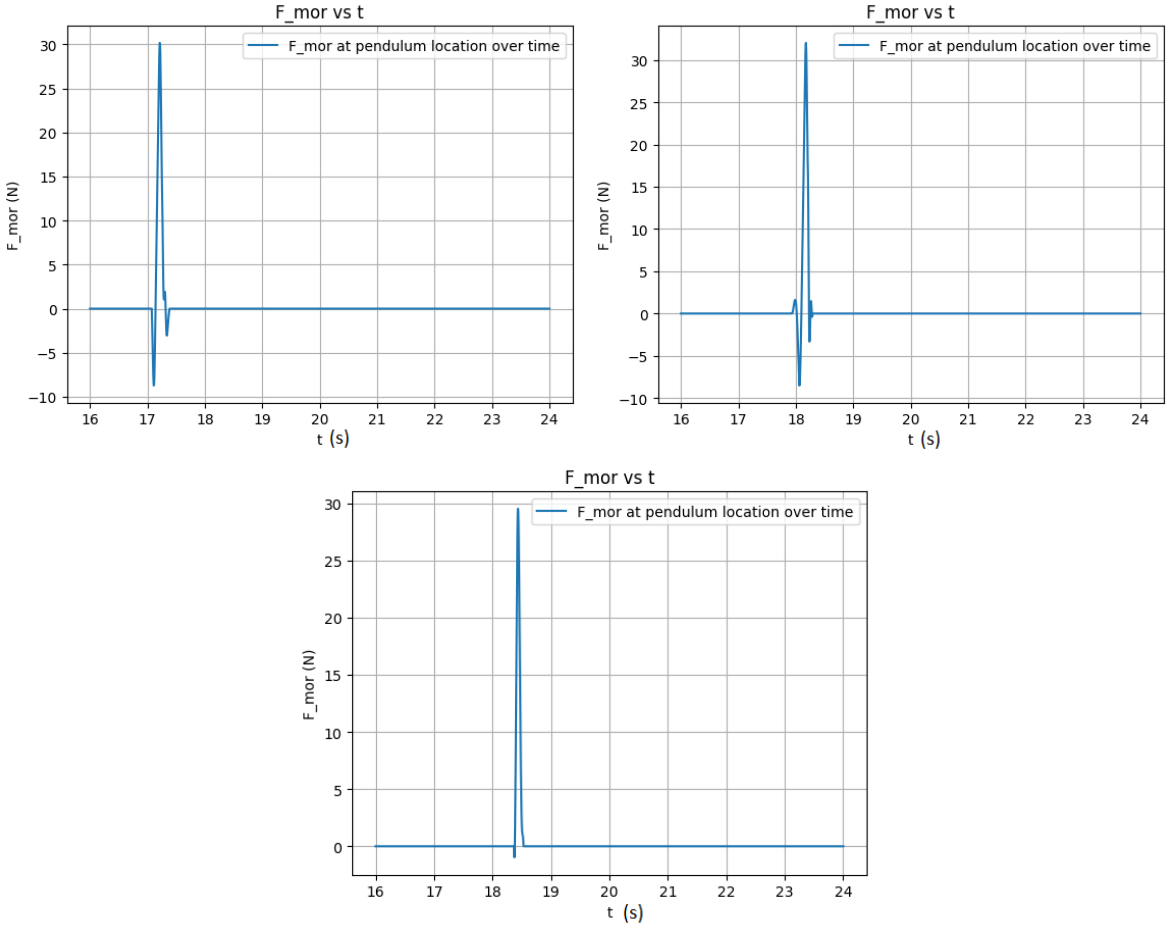

Figure 5.2: Impact load at pendulum over time.
Top left: configuration 505
Top right: configuration 515
Bottom: configuration 605

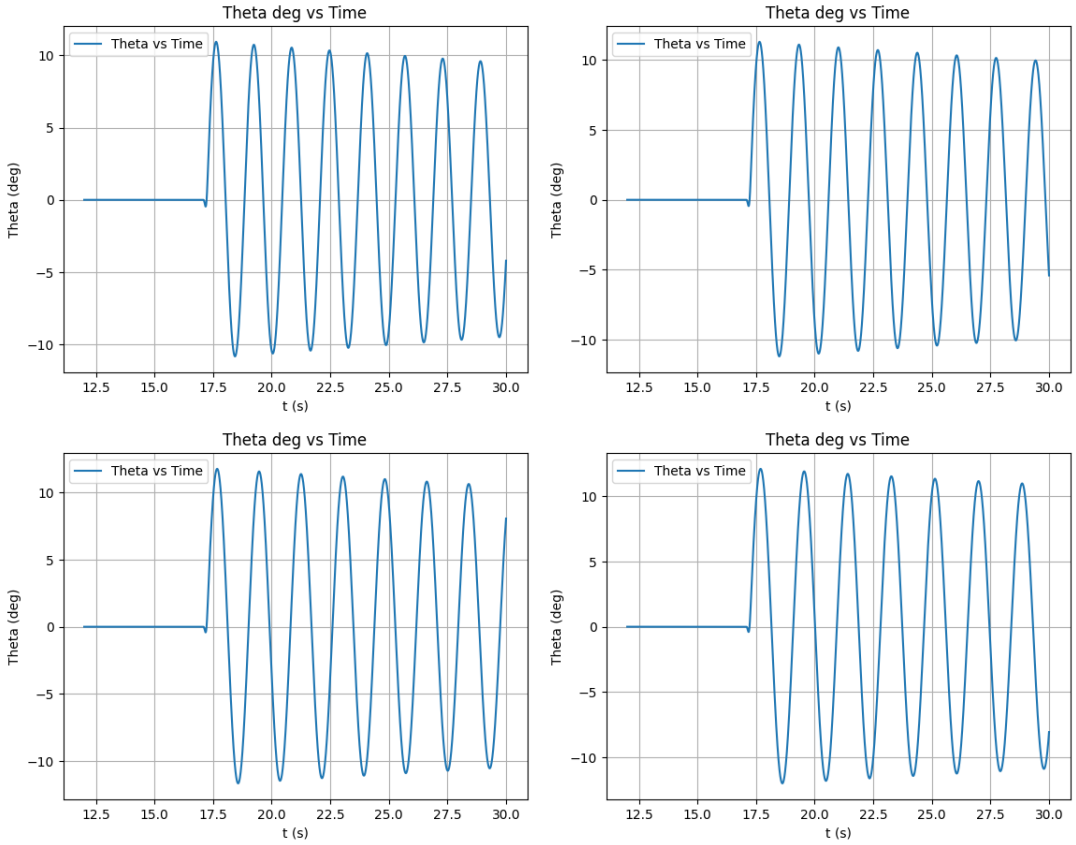

Figure 5.3: Deflections of pendulums with different effective lengths at configuration 505
Top left: $l_{eff} = 0.46$
Top right: $l_{eff} = 0.48$
Bottom left: $l_{eff} = 0.51$
Bottom right: $l_{eff} = 0.53$

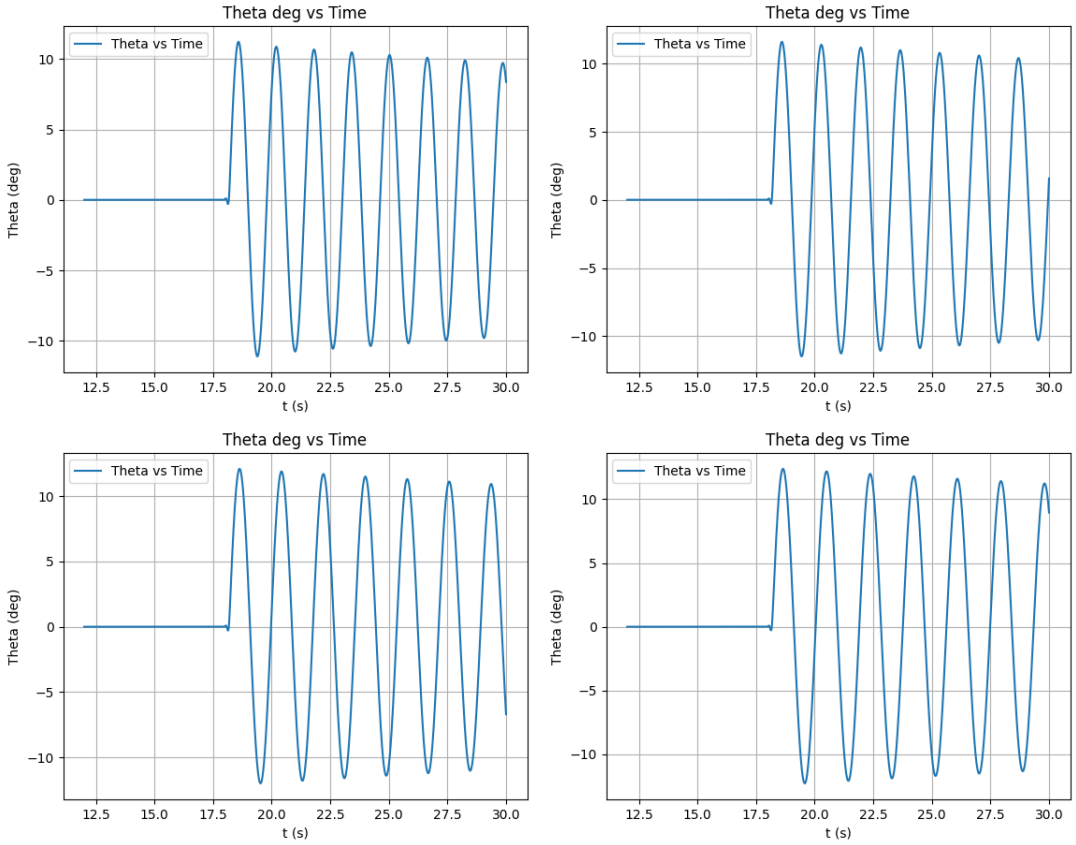

Figure 5.4: Deflections of pendulums with different effective lengths at configuration 515.
Top left:$l_{\text{eff}} = 0.46$ m
Top right:$l_{\text{eff}} = 0.48$ m
Bottom left:$l_{\text{eff}} = 0.51$ m
Bottom right:$l_{\text{eff}} = 0.53$ m

Table 5.2: Maximum deflection and kinetic energy for each pendulum, configuration 505

Configuration	Effective length pendulum (m)	Natural freq. (s^{-1})	Max. deflection (°)	Max Kinetic Energy (J)
505	0.46	4.62	10.9	2.5828
505	0.48	4.52	11.3	2.5086
505	0.51	4.38	11.8	2.4026
505	0.53	4.30	12.1	2.3310

Table 5.3: Maximum deflection and kinetic energy for each pendulum, configuration 515

Configuration	Effective length pendulum (m)	Natural freq. (s^{-1})	Max. deflection (°)	Max Kinetic Energy (J)
515	0.46	4.62	11.2	2.6850
515	0.48	4.52	11.6	2.6066
515	0.51	4.38	12.1	2.4887
515	0.53	4.30	12.4	2.4186

5.1.3. Configuration 605

In figure 5.5, the deflections of the pendulums with different effective lengths are shown. This time, they undergo the wave impact at configuration 605. The load on the pendulum over time is plotted in figure 5.2c. In table 5.4, the maximum deflections and kinetic energy of the pendulum are listed.

Table 5.4: Maximum deflection and kinetic energy for each pendulum, configuration 605

Configuration	Effective length pendulum (m)	Natural freq. (s^{-1})	Max. deflection (°)	Max Kinetic Energy (J)
605	0.46	4.62	10.8	2.3479
605	0.48	4.52	11.1	2.2672
605	0.51	4.38	11.5	2.1514
605	0.53	4.30	11.7	2.0773

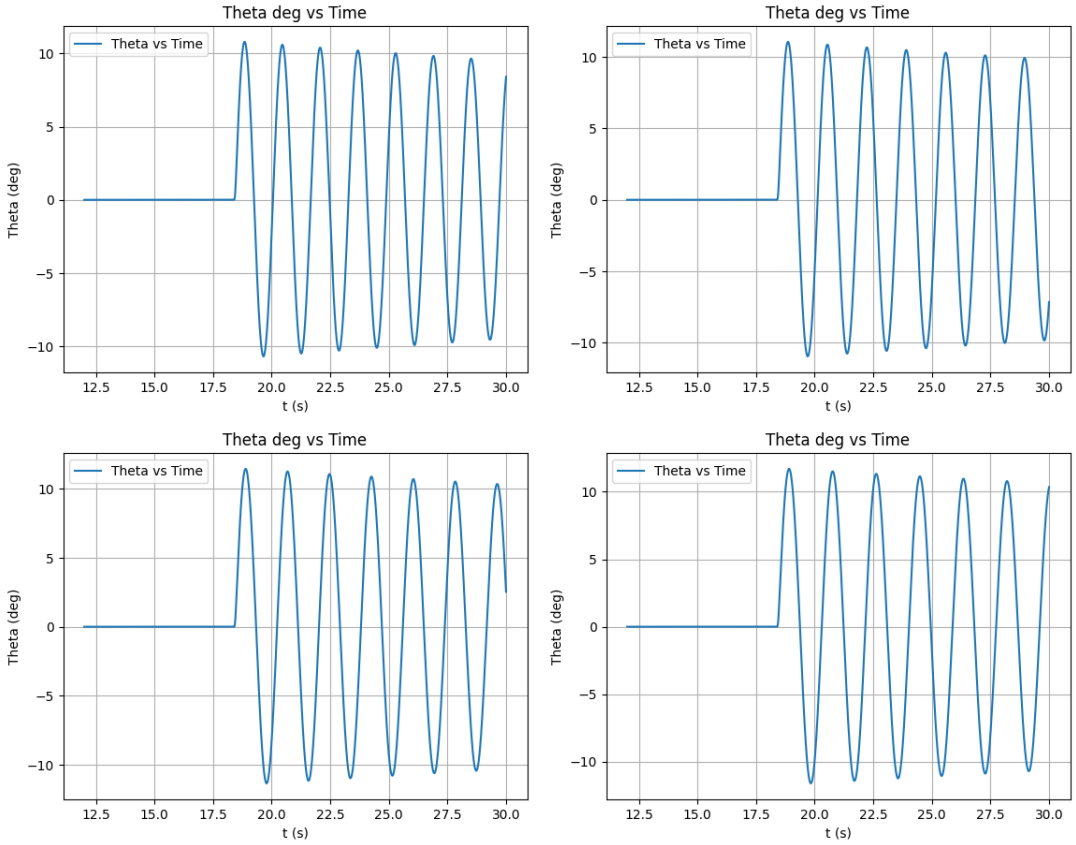

Figure 5.5: Deflections of pendulums with different effective lengths at configuration 605
Top left: l_{eff} = 0.46 m
Top right: l_{eff} = 0.48 m
Bottom left: l_{eff} = 0.51 m
Bottom right: l_{eff} = 0.53 m

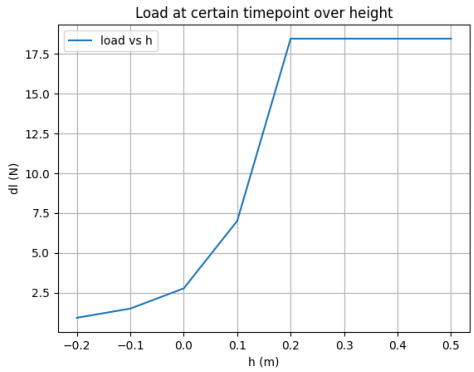

Figure 5.6: Distributed load that the wave would exert at a certain time point, configuration 505 $0 = h0$

5.2. Beam model

The model of the beam is also used for an experiment. This time the natural frequencies of the beam are varied. This is done by varying the effective length of the beam. In this case the effective length means the length used to calculate the response motions of the beam. The real length of the beam is kept constant. This means that the location of interaction with the wave stays the same. The impact location of force from the wave at beam also stays constant. In table 5.5 the effective lengths and corresponding natural frequencies are listed. These are the natural frequencies of the first mode of the beam. This will be the mode that is dominant in the motion of the beam.

For now, the beam is chosen with a length of 0.4 m and a width of 0.4 m. The thickness is 0.5 mm. The value of E is based on the average E value of stainless steel, E=1600000000000. For now there is only looked into the influence of the effective length, not into the actual deflections of a realistic beam. The model still shows a bit of instability. This will be improved later in the study.

Table 5.5: Natural frequencies plate

Test	Effective length (m)	1^{st} Natural frequency plate (s^{-1})
1	0.4	17.9
2	0.45	15.0
3	0.5	12.8
4	0.55	11.12

5.2.1. Distributed load

Figure 5.6 shows the load that is exerted by the wave on to the beam when the beam is placed in configuration 505. In this figure the load is shown over the theoretical height of the wave, where 0 is the mean surface $h0$. This load represents the load that the wave would exert at a certain theoretical height. Note that the beam will only interfere with the wave at $h = 0.05$ or $h = 0.1$ to $h = h_{wave}$. This wave model is based on the equations described in 2.4.2. In figure 5.7, the magnitude of the load at the bottom point of the plate is shown over time. This is also at configuration 505.

5.2.2. Configuration 505

The first configuration that is tested is 505. The effective lengths from table 5.5 are tested. The deflections of the beam over time are plotted in figure 5.8. These deflections are the deflections at the free end of the beam. In figure 5.9, the deflections over the length of the beam are plotted.

5.2.3. Configuration 515

The next configuration that is tested is 515. The l=effective lengths from table 5.5 are tested. The deflections of the beam over time are plotted in figure 5.10. In figure 5.11, the deflections over the length of the beam are plotted.

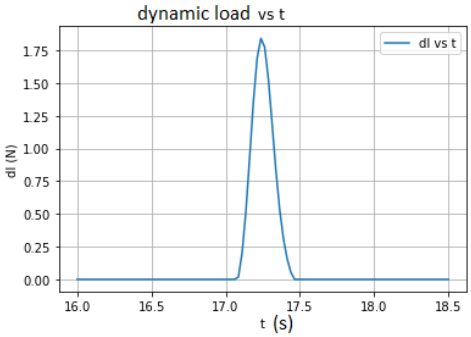

Figure 5.7: Load at lowest point of the plate over time 505

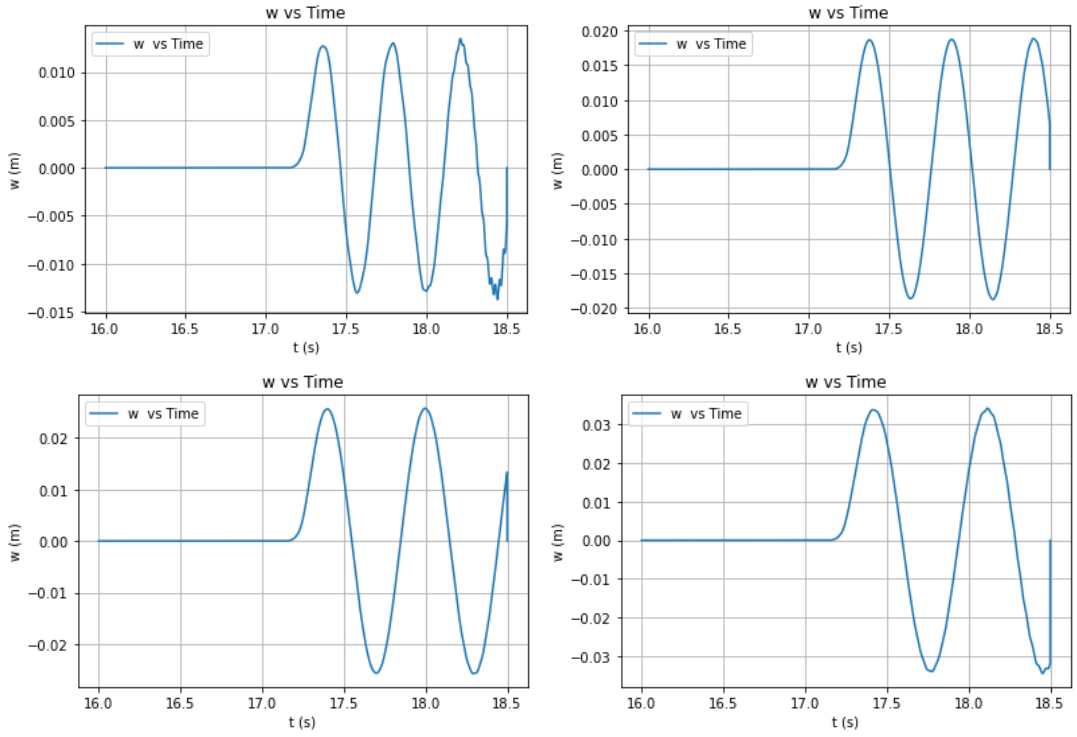

Figure 5.8: Deflection of the beam at the free end over time.
Top left: l_{eff} = 0.40 m
Top right: l_{eff} = 0.45 m
Bottom left: l_{eff} = 0.50 m
Bottom right: l_{eff} = 0.55 m

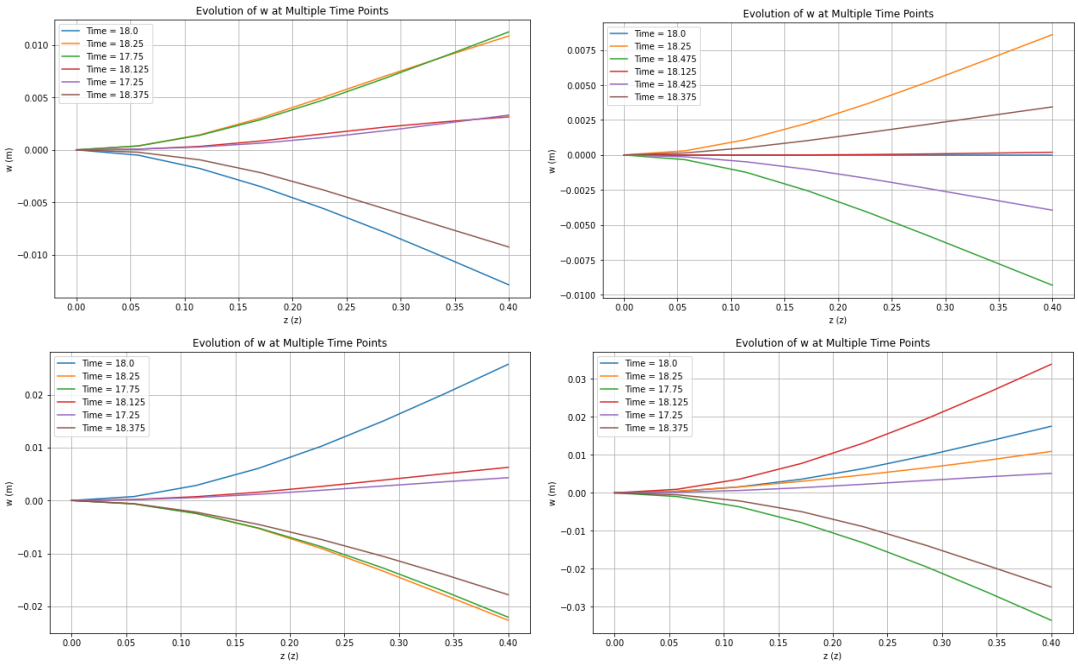

Figure 5.9: Deflection of the beam over its length at multiple time steps.
Top left: l_{eff} = 0.40 m
Top right: l_{eff} = 0.45 m
Bottom left: l_{eff} = 0.50 m
Bottom right: l_{eff} = 0.55 m

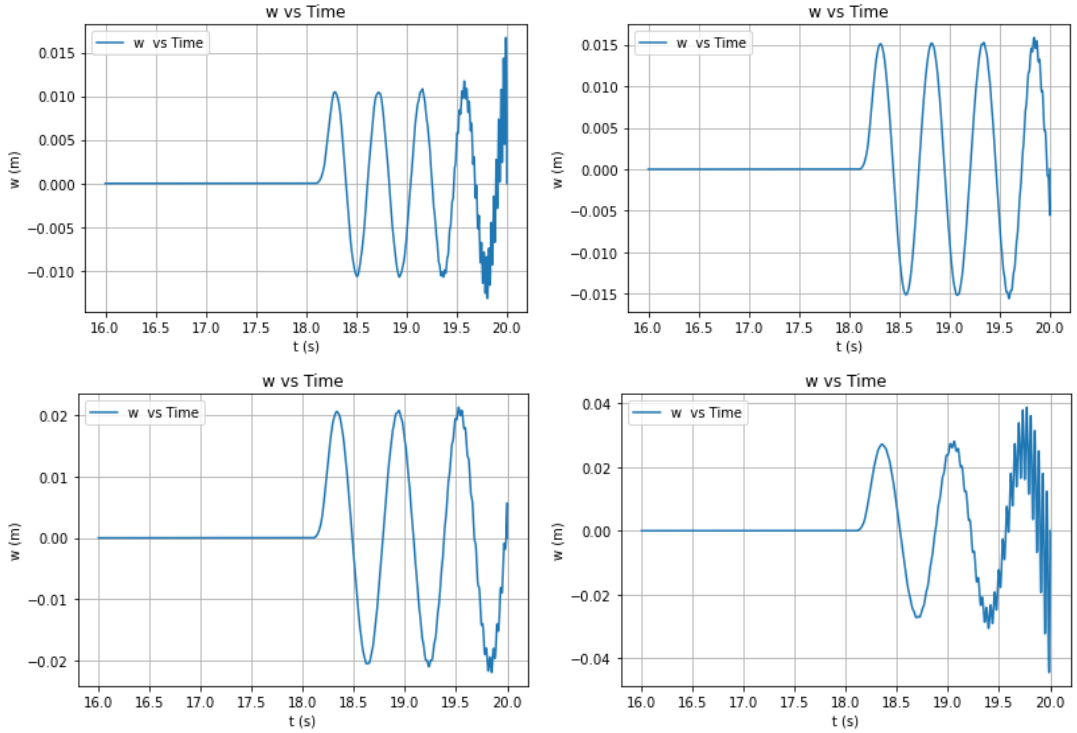

Figure 5.10: Deflection of the beam at the free end over time.
Top left: l_{eff} = 0.40 m
Top right: l_{eff} = 0.45 m
Bottom left: l_{eff} = 0.50 m
Bottom right: l_{eff} = 0.55 m

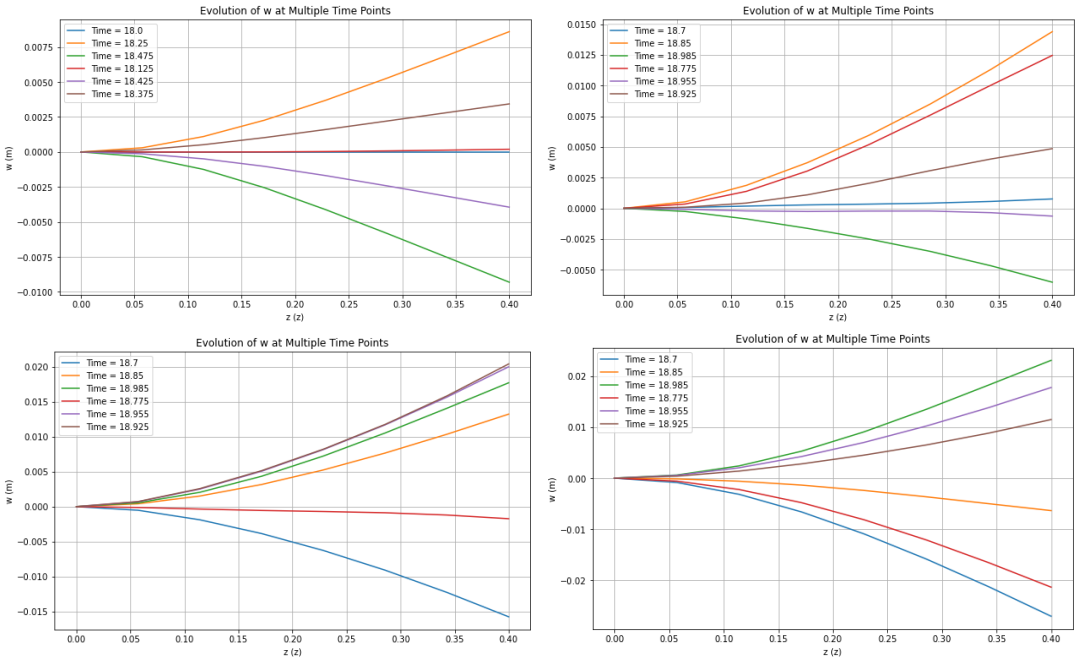

Figure 5.11: Deflection of the beam over its length at certain time points.
Top left: l_{eff} = 0.40 m
Top right: l_{eff} = 0.45 m
Bottom left: l_{eff} = 0.50 m
Bottom right: l_{eff} = 0.55 m

6

Predictions Sloshing tank experiment

In this chapter, the motion of the plate for the situation in the sloshing tank is modelled. From this prediction, the plate dimensions are decided. The chosen dimensions are listed in table 6.1. The mass of stainless steel is assumed as 7500 kg/m^3. E is assumed as 195 000 MPa.

Table 6.1: Dimensions plates experiments

Plate	length (mm)	width (mm)	thickness (mm)
1	300	199	0.4
2	300	199	0.5
3	300	199	0.6
4	300	199	0.7

To predict the outcomes in the tank, each beam is modelled at each configuration. In figure 6.1 to 6.4, the motion of the bottom point of the beam is plotted over time for configuration 000. This is predicted using the beam model for each beam separately. The rest of the configurations are given in appendix A.

In table 6.2, a summary of the maximum deflections at the bottom of the plate are given. The natural frequencies are also calculated for each beam and given in table 6.3.

Table 6.2: Deflections plates experiments

Plate	Configuration	Max. deflection (mm)
1	105	6
1	000	18
1	005	45
1	010	78
2	105	4
2	000	12
2	005	28
2	010	45
3	105	3
3	000	7.5
3	005	18
3	010	30
4	105	2
4	000	5
4	005	14
4	010	20

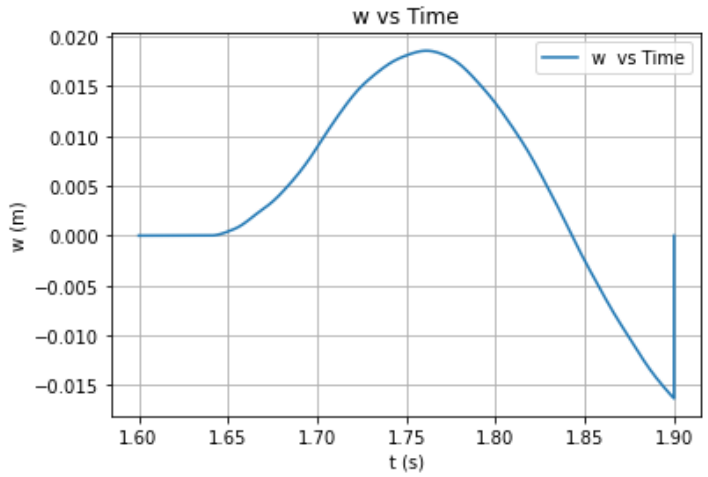

Figure 6.1: Motion bottom point of 0.4mm beam over time

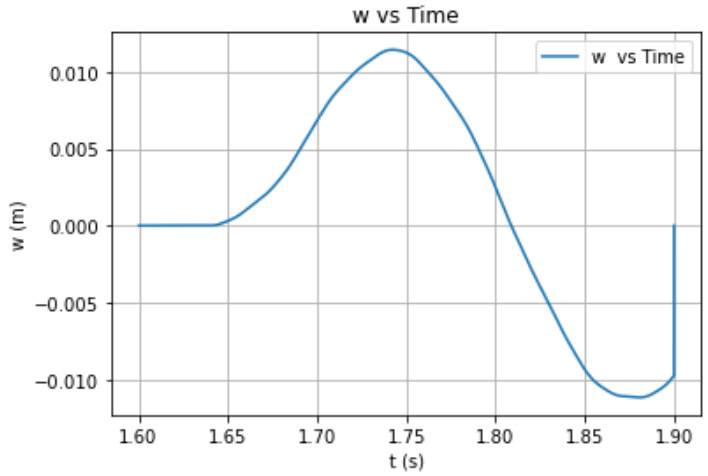

Figure 6.2: Motion bottom point of 0.5mm beam over time

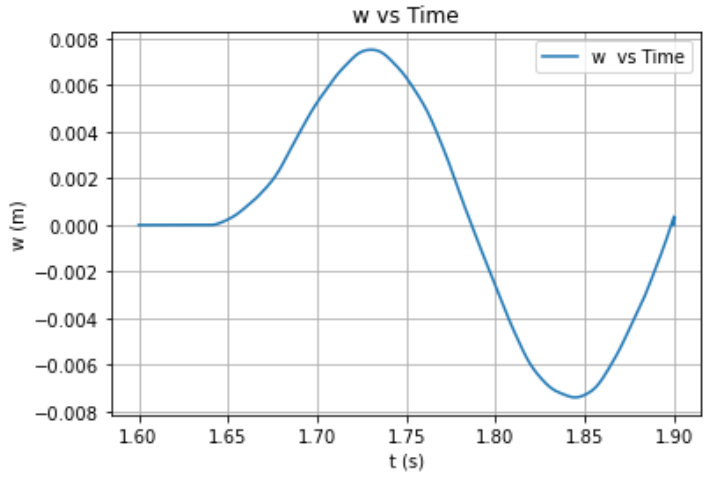

Figure 6.3: Motion bottom point of 0.6mm beam over time

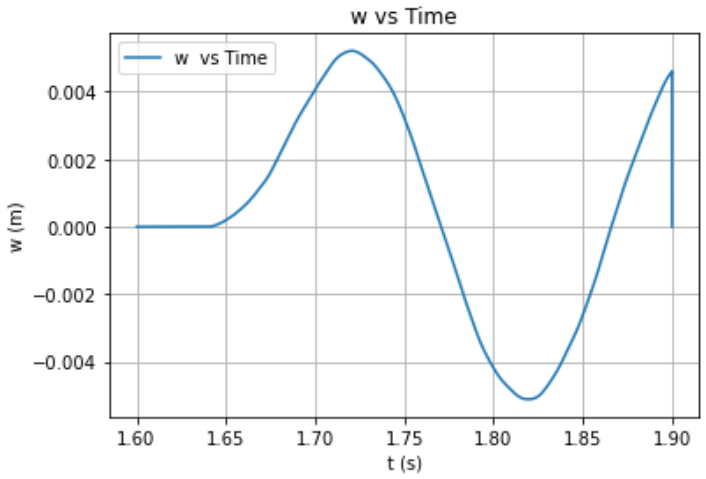

Figure 6.4: Motion bottom point of 0.7mm beam over time

Table 6.3: Natural frequencies plates experiments

Plate	Natural frequency (Hz)
1	5.26
2	5.88
3	7.14
4	8.33

7

Results sloshing tank experiment

In this chapter the experiments in the sloshing tank are discussed. In section 7.1, the final setup of the sloshing rig is shown. In section 7.2, the calibrations of the camera and the sensors is explained. In section 7.3, the outcome data of the measurements is shown.

During testing with a closed tank, the air pressure became high at the side of the tank where the wave was traveling to. It caused the plate to move in the opposite direction. This caught the attention and adjustments had to be made. After that, the experiments are conducted using a tank partially open at the top. This caused that only the configurations 00, 105 turned out to be possible to measure. Configuration 010 is also measured, using the wave that hit the side of the tank, and returned back the other direction, and then hit the construction. This is why the impact is not comparable with the ComFLOW results. The new ComFLOW prediction of configuration 000 can be found is chapter 8.

7.1. Set up experiment

In figure 7.1 the total set up of the rig is shown. In figure 7.2 The wave height meters and camera placement can be seen. In this image, the adjustment regarding the openings on the top of the tank are visible. The configurations that were possible to conduct after the alterations are shown schematically in figure **??**. Lastly the setup of the force sensors and the attachment system for the plate can be seen more clearly in figure 7.4.

7.2. Calibrations

Before starting the experiments, all sensors are calibrated. It is important to know how accurate the sensors are. The force sensors show 0.035 % deviation in the calibration. The wave height sensors show 0.36 % deviation. Working with the wave height meters was not ideal. Due to difficulties starting up, the calibration of the sensors took place a week before starting the actual measurements. After the calibration, the sensors continue to corrode as they are staying in the tank. This causes the sensors to give slightly different results over time. This can be seen in the results. However, the focus of the wave height meters is to measure the repeatability of the wave. When analysing the repeatability, the runs of the same day are used to compare to each other. The water height in the tank was measured each testing day manually, to make sure it was still at 145 mm.

7.2.1. Calibration camera

The camera is set up as seen in figure 7.2. The camera is meant to measure the deflection of the beam. The camera covers an area of 8 cm wide and 5.5 cm height. To make a reference of the position of the camera view, there are placed three dots in the view of each camera. This is to see if the camera has not rotated or vibrates during operation. This reference frames are shown in figure 7.5.

To calibrate the camera, images are made using a ruler. Using this images, the real life distance of a

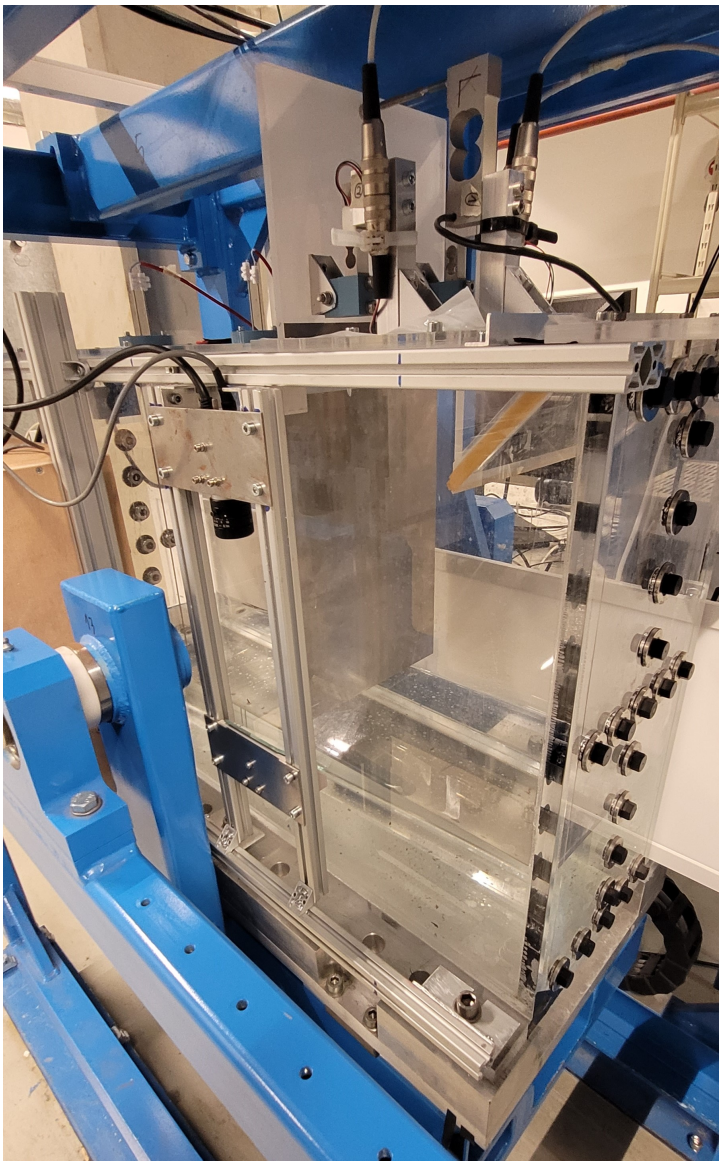

Figure 7.1: Overall view of the Sloshing rig

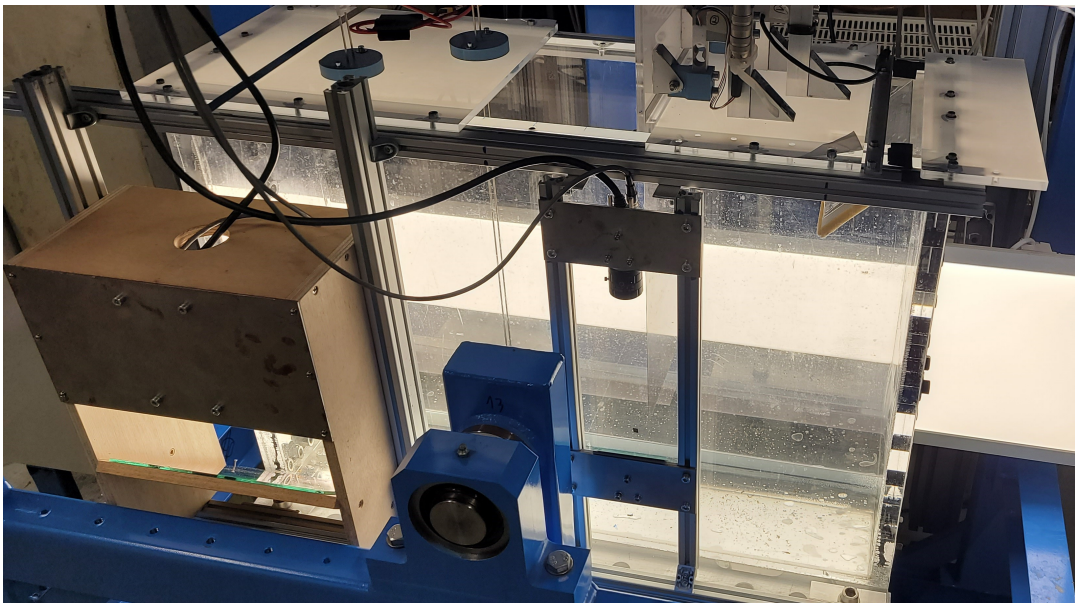

Figure 7.2: Setup of the wave height meters and camera placement.

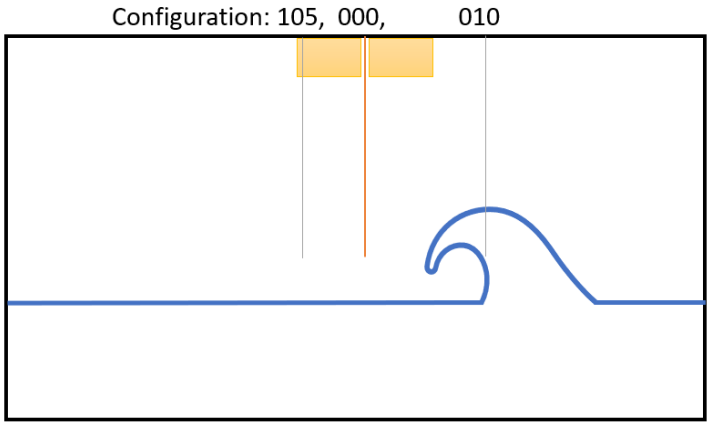

Figure 7.3: Schematic of conducted configurations of the plate positions.

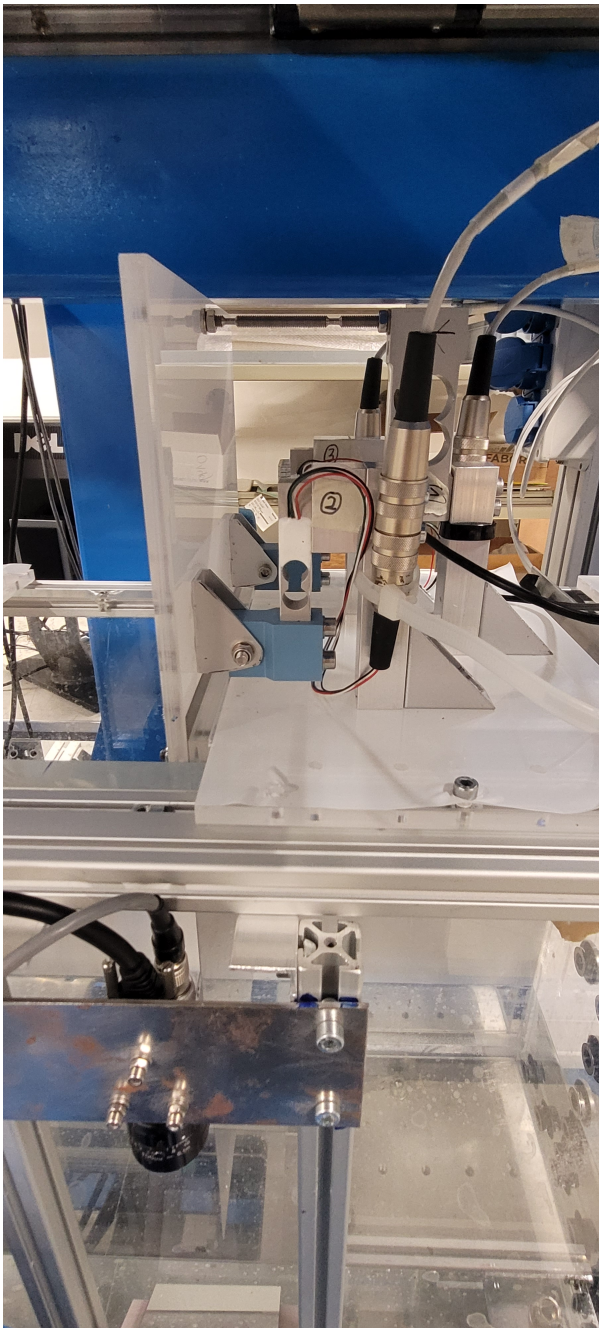

Figure 7.4: Setup of the force sensors

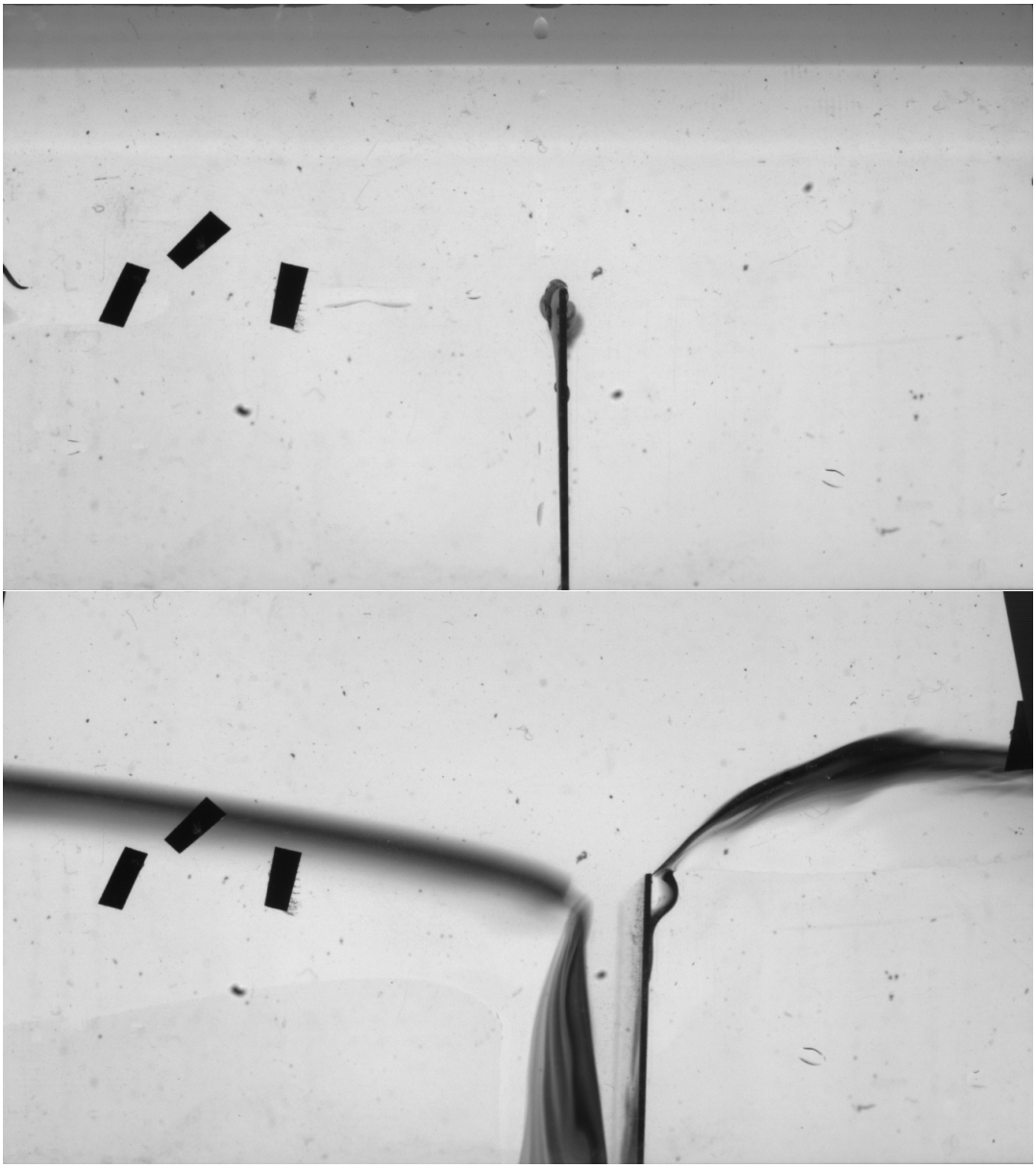

Figure 7.5: Example of a camera image. This is plate 0.6. The reference squares are visible.

pixel is determined. Due to the fishbowl effect, the distance at the sides of an image can differ from the distances in the middle of the frame. In table 7.1 an overview is given of the calibrated camera. The deviation of the measured distance on the sides of the image will be 1.14 % at maximum. However, when measuring a deflection in a corner, the distance is measured from the middle of the frame to the side. So on average the deviation will be less.

7.3. Measurements

In this section, the results of the measurements are presented. In section 7.3.1, the repeatability of the waves is discussed. In section 7.3.2, the results of the camera and force sensors are discussed.

7.3.1. Wave

In this section we will verify to what extend the wave is the same in each measurement. In this study, the wave impact for different types of structures is researched. To make a valuable comparison between the wave impact on the different plates, the wave must be as equal as possible at each run.

Table 7.1: Camera calibration. Deviations at sides of the frames.

Position	Distance (cm)	Distance/pixel (cm)	Deviation from center (cm)	Deviation (%)
Overall	7	0.004830		
Left side of the image	1	0.004868	-0.00005505	-1.144
Center of the image	1	0.004813		
Right side of the image	1	0.004823	-0.00001025	-0.213

In this experiments the wave is measured by two wave height sensors, named whm 6 and whm 7. These show the height of the wave over time. In figure 7.6 and 7.7, a plot of the wave height is given over time. In this figures, 9 wave measurements on one day are plotted in one figure. Here, the repeatability of the wave can be judged. The impact of the wave takes place at around 2.3 seconds for configuration 000 and 005 , for configuration 010, the impact takes place at around 2.9 seconds, this will be further explained in section 7.3.2.

In table 7.2 and 7.3, the peaks of the wave heights are listed for each measurement. From this data, we can conclude that the wave heights have a mean deviation of 0.76% at the third peak. This peak is the impact moment of the wave on the plate. After the third peak, the deviation become larger, as seen on the plot. This is due to the non linearity's in breaking waves. This causes small differences in the waves to lead to bigger effects.

Table 7.2: Wave peaks from 5 different measurements of the wave whm 6

Peaks	1	2	3
Wave 1 height(cm)	16.40	11.01	21.94
Wave 2 height(cm)	16.43	11.01	22.20
Wave 3 height(cm)	16.46	10.98	22.37
Wave 4 height(cm)	16.50	10.95	22.41
Wave 5 height(cm)	16.53	10.92	22.46
Average deviation (cm)	0.0404	0.0319	0.1649
Average deviation (%)	0.25%	0.29%	0.74%

Table 7.3: Wave peaks from 5 different measurements of the wave whm 7

Peaks	1	2	3
Wave 1 height(cm)	15.86	12.20	19.99
Wave 2 height(cm)	15.89	12.18	20.14
Wave 3 height(cm)	15.90	12.16	20.20
Wave 4 height(cm)	15.91	12.15	20.27
Wave 5 height(cm)	15.94	12.13	20.37
Average deviation	0.0218	0.0205	0.1038
Average deviation (%)	0.14%	0.17%	0.51%

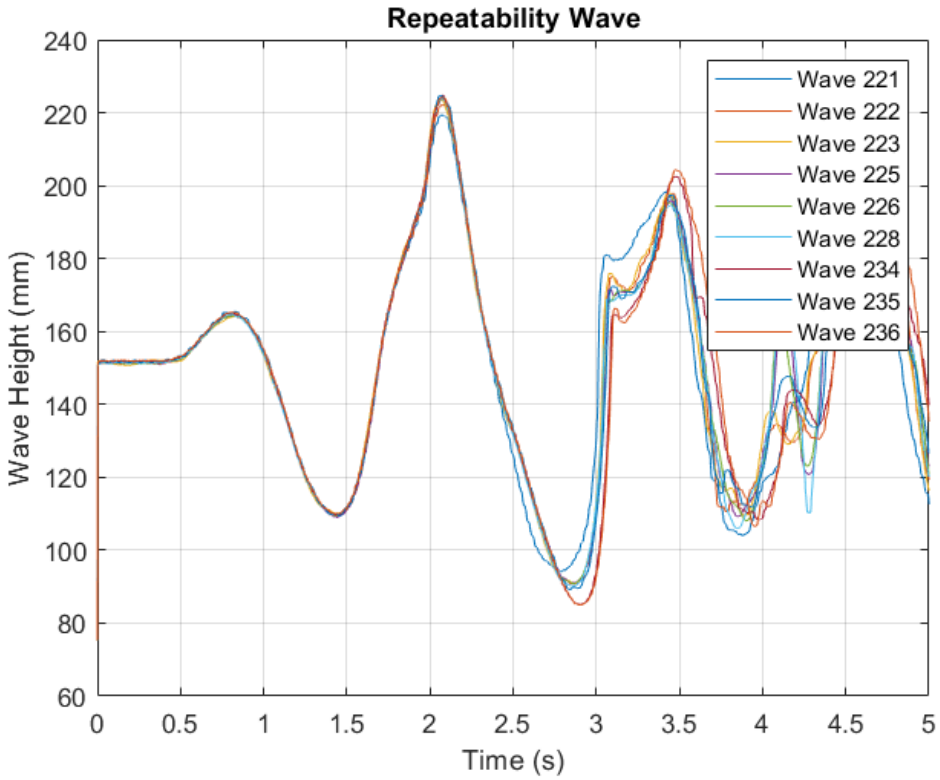

Figure 7.6: Different measurements of the wave in the sloshing rig on day one of testing whm 6

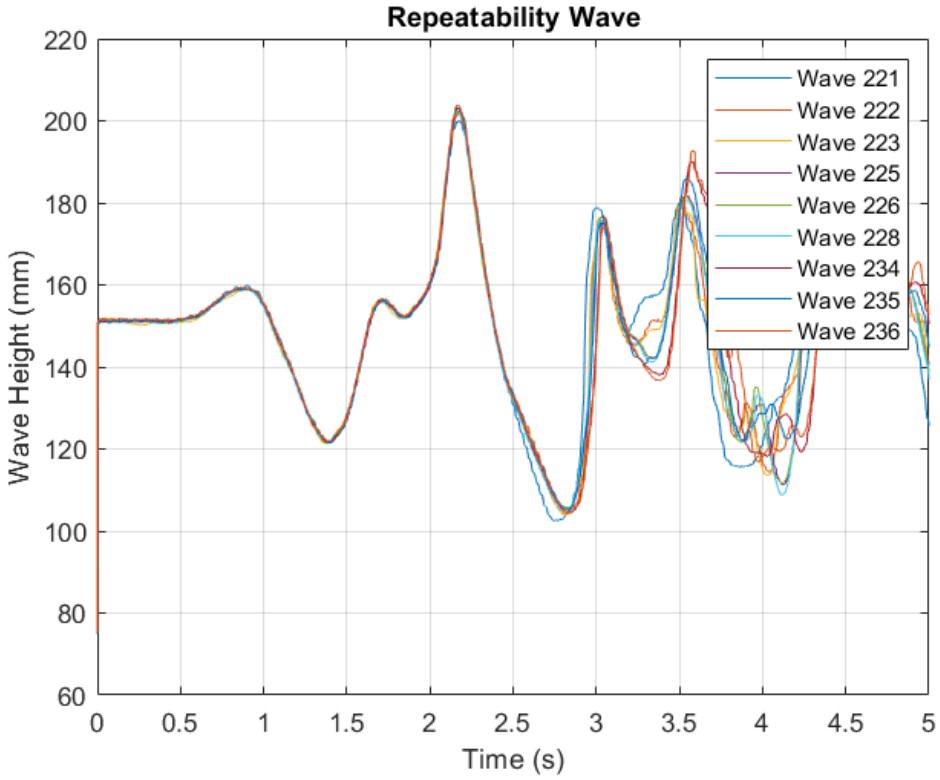

Figure 7.7: Different measurements of the wave in the sloshing rig on day one of testing, whm 7

7.3.2. Wave impact

In this section the measurements of the impact of the wave are given. During the tests, it turned out that the closed tank was not possible to work with. The traveling wave influenced the local air pressures on the two sides of the plates, due to the air not being able to escape easily trough the sides of the plate. This is logical because the plate only had a millimeter free on the sides. One of the tank plates had to stay open on both sides at the top of the tank.

This is why for configuration 010, the wave that traveled backwards, after hitting the side of the tank, is used for this measurement. This includes a bigger wave impact than expected. This does add a wider range of measurement points for the data.

Before testing the impacts on the plate, the natural frequency of each plate is measured. This is done because the prediction of the natural frequency can be different than in real life. The plate could have a slightly different type of stainless steel and the construction of the plate hanging on its force sensors, could influence its natural frequency as well. In table 7.4, an overview is given.

Plate	Nat. Freq. (Hz)
0.4	3,64
0.5	4,40
0.6	5,26
0.7	5,50

Table 7.4: Measured natural frequencies of the four different plates

Force sensors

In figure 7.8 to 7.10, the total horizontal force, measured by force sensors 2 and 3, is plotted over time for the four different plates in configuration 000, 005 and 010. In each figure, the three runs of the same situation are plotted. Force sensor 1 measures the moment that the total force exerts on the plate, this is not taken into account for now.

In table 7.5, the maximum values of the forces are summarized. These are the average values of three runs.

Plate	Configuration	Max Force average (N)
0.4	000	-3.37
	105	-2.77
	010	3.74
0.5	000	-4.07
	105	-2.29
	010	6.81
0.6	000	-5.74
	105	-3.67
	010	8.48
0.7	000	-6.38
	105	-3.84
	010	10.62

Table 7.5: Maximum horizontal force exerted on the plate

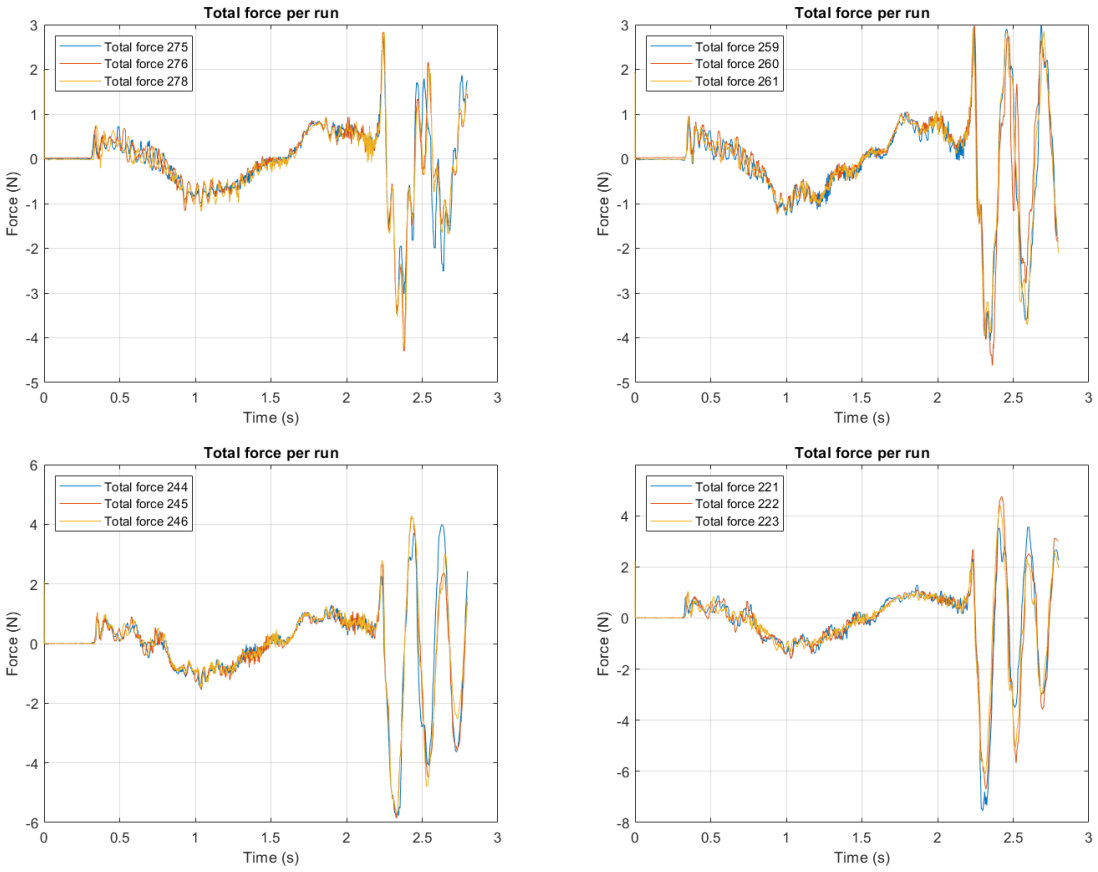

Figure 7.8: Total horizontal force on plates with thickness 0.4 mm, 0.5 mm, 0.6 mm and 0.7 mm. Configuration 000.
Top left: $th = 0.4mm$
Top right: $th = 0.5mm$
Bottom left: $th = 0.6mm$
Bottom right: $th = 0.7mm$

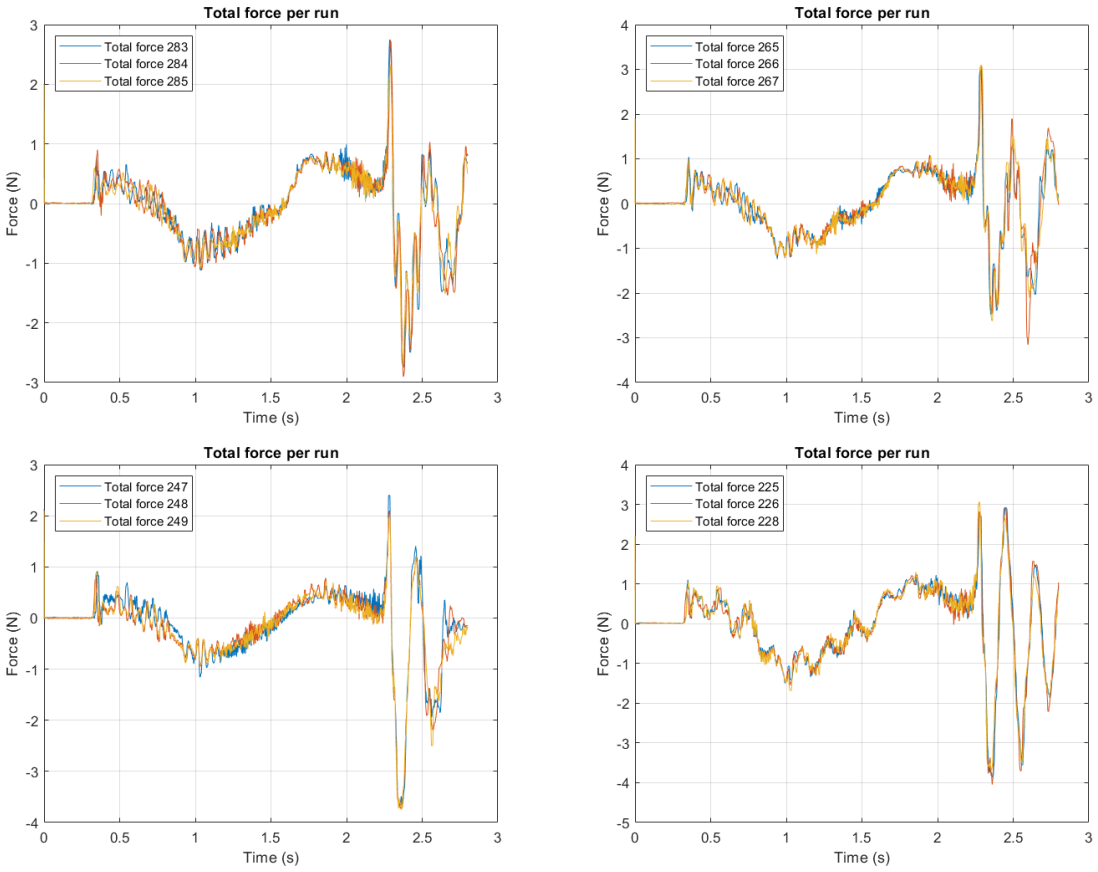

Figure 7.9: Total horizontal force on plates with thickness 0.4 mm, 0.5 mm, 0.6 mm and 0.7 mm. Configuration 105.
Top left: $th = 0.4mm$
Top right: $th = 0.5mm$
Bottom left: $th = 0.6mm$
Bottom right: $th = 0.7mm$

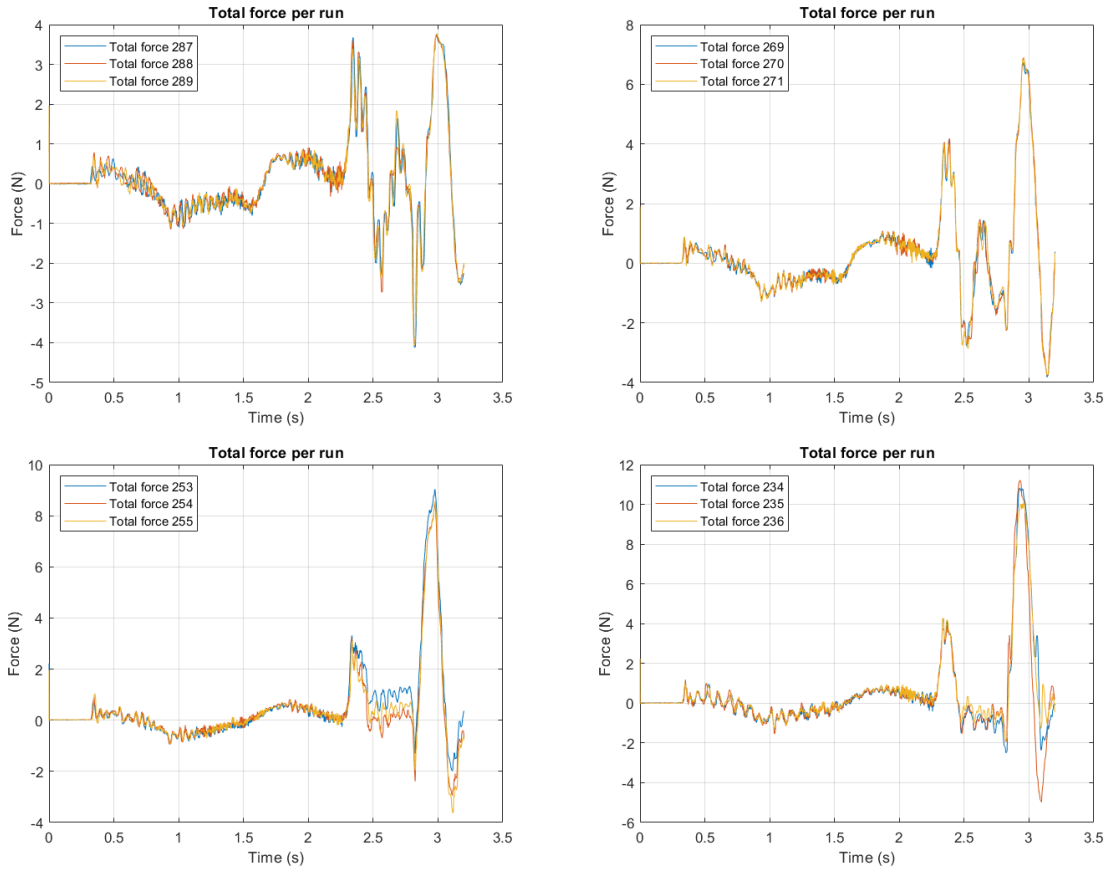

Figure 7.10: Total horizontal force on plates with thickness 0.4 mm, 0.5 mm, 0.6 mm and 0.7 mm. Configuration 010.
Top left: $th = 0.4mm$
Top right: $th = 0.5mm$
Bottom left: $th = 0.6mm$
Bottom right: $th = 0.7mm$

Deflection

The deflection of the plate is measured for each different run. In table 7.7 all the measured deflections are listed. Using the data, the standard deviations are calculated for each configuration. They are also listed in the table.

A table of the average maximum deflections for the plates is given in table 7.6. These values are the average over three runs per configuration.

Plate	Configuration	Max Deflection (cm)
0.4	000	2,18
	105	1,44
	010	4,44
0.5	000	1,67
	105	0,87
	010	3,75
0.6	000	1,43
	105	0,82
	010	2,64
0.7	000	1,31
	105	0,72
	010	2,48

Table 7.6: Max. deflection of bottom point of the plate

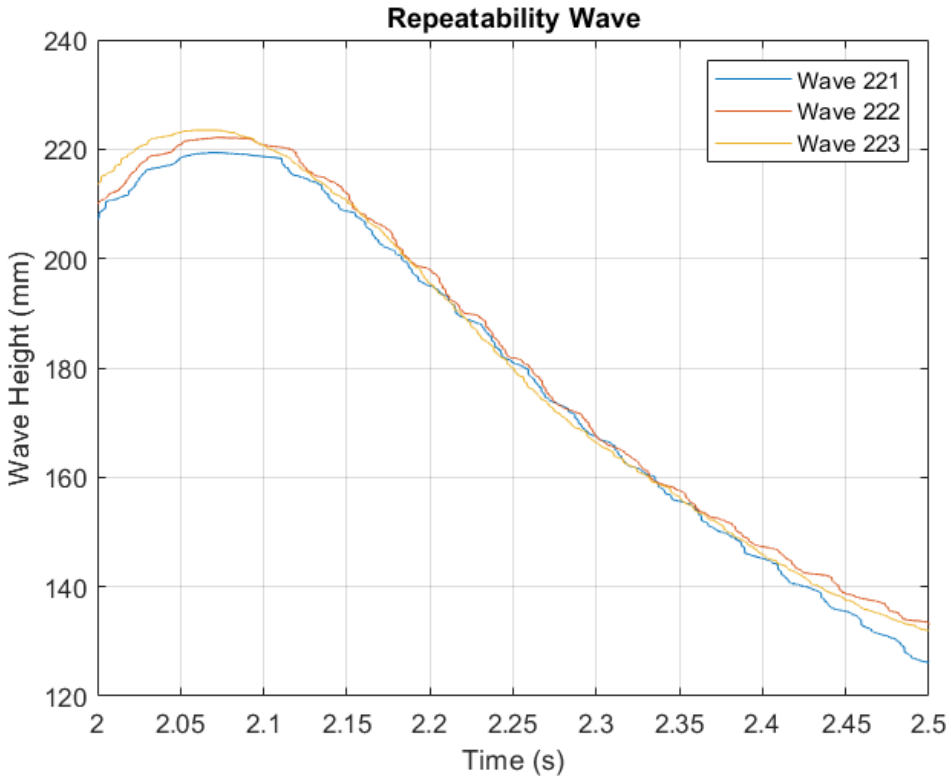

Figure 7.11: Variation in wave height measurement. Plate 0.7, configuration 000.

7.3.3. Variability

Breaking waves include wave effects that are nonlinear. This means that a small difference in the wave can lead to relatively big differences in the measured forces. In figure 7.11 and fig 7.12, the runs for plate 0.7, configuration 000 are shown. In the figure showing the wave height, small differences can be seen. In the figure showing the forces, the different runs show relatively more variation in force measurements. In table 7.8 the standard deviations are listed for all plates and configurations. As expected, the standard deviations are around a factor 10 bigger for the force sensors as they are for the wave height meter sensors. However, there are some exceptions on this. Due to the limited amount of data, one deviant run can influence the results majorly.

In table 7.9, the values of the forces are listed, including the maximum value of the confidence interval and the minimum value of the confidence interval. In table 7.10, the same is done for the deflections.

7.3.4. Comparison values

In figure 7.13, both the maximum deflections and the maximum forces on the plate are plotted for each configuration against the natural frequency of the plate. In this plot the force on the plate is given in absolute values.

For all sets of data, the confidence interval is determined for p=0.05. The average values are plotted with their confidence interval. In figure 7.14 the average of the measured values of the force and deflection are plotted with their confidence intervals.

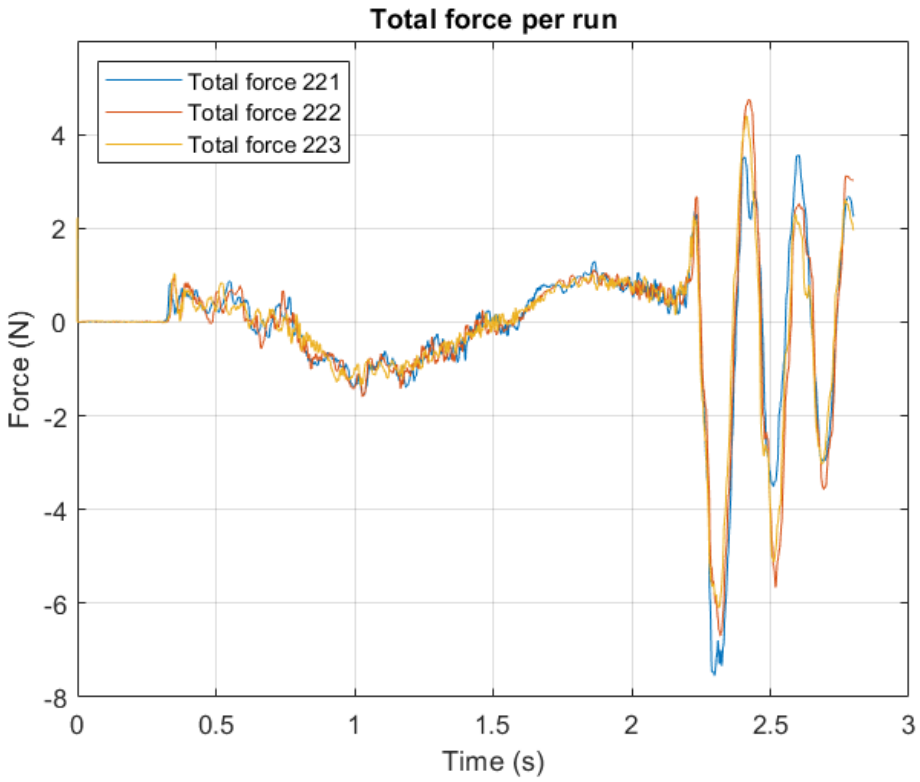

Figure 7.12: Variation in force measurement. Plate 0.7, configuration 000.

Table 7.7: Deflection measurements for different plate configurations, including the standard deviations.

Plate	Configuration	Deflection (cm)
0.4	000	2.17
		2.17
		2.18
St Dev		0.0058
	105	1.43
		1.41
		1.47
St Dev		0.0306
	010	4.45
		4.43
		4.44
St Dev		0.0100
0.5	000	1.68
		1.70
		1.63
St Dev		0.0361
	105	0.92
		0.82
		0.85
St Dev		0.0513
	010	3.71
		3.77
		3.76
St Dev		0.0321
0.6	000	1.40
		1.44
		1.44
St Dev		0.0231
	105	0.84
		0.80
		0.82
St Dev		0.0200
	010	2.66
		2.62
		2.65
St Dev		0.0208
0.7	000	1.38
		1.23
		-
St Dev		0.1060
	105	0.70
		0.74
		-
St Dev		0.0283
	010	2.55
		2.36
		2.64
St Dev		0.1430

Table 7.8: Measured values and standard deviations of all wave height meter and force sensor data

Plate	Configuration	Whm 6 (cm)	Whm 7 (cm)	Force (N)
0.4	000	16.59	16.87	-3.46
	000	16.57	16.88	-3.25
	000	16.62	16.96	-3.41
St. dev	000	0.022	0.051	0.108
0.4	105	15.66	15.82	-2.75
	105	15.75	15.86	-2.90
	105	15.68	15.68	-2.68
St. dev	005	0.047	0.096	0.114
0.4	010	11.27	16.66	3.74
	010	11.52	17.14	3.71
	010	11.43	16.81	3.76
St. dev	010	0.129	0.243	0.025
0.5	000	16.20	16.44	-4.08
	000	16.32	16.53	-4.26
	000	16.06	16.36	-3.88
St. dev	000	0.133	0.085	0.192
0.5	105	15.70	15.83	-2.48
	105	15.79	15.96	-2.15
	105	15.91	16.12	-2.25
St. dev	005	0.108	0.147	0.171
0.5	010	9.72	13.03	6.73
	010	9.70	12.96	6.86
	010	9.85	13.09	6.83
St. dev	010	0.082	0.061	0.069
0.6	000	16.25	16.56	-5.85
	000	16.41	16.72	-5.73
	000	16.40	16.74	-5.65
St. dev	000	0.086	0.102	0.102
0.6	105	15.95	16.16	-3.72
	105	15.90	16.11	-3.56
	105	15.97	16.17	-3.72
St. dev	005	0.037	0.034	0.091
0.6	010	10.43	14.84	8.49
	010	10.52	15.18	8.36
	010	10.56	15.19	9,04
St. dev	010	0.066	0.198	0.36
0.7	000	16.20	16.60	-7.55
	000	16.39	16.78	-5.82
	000	16.21	16.43	-5.78
St. dev	000	0.102	0.174	1.009
0.7	105	15.73	15.90	-3.86
	105	15.67	15.82	-4.05
	105	15.57	15.78	-3.61
St. dev	005	0.080	0.061	0.217
0.7	010	85.48	11.52	10.82
	010	92.52	12.23	11.21
	010	85.50	11.29	9.82
St. dev	010	4.061	0.491	0.715

Table 7.9: Forces, overview of confidence interval

Plate		000	105	010
0.4	average force (N)	3.37	2.77	3.74
0.4	min force (N)	3.25	2.65	3.71
0.4	max force (N)	3.50	2.90	3.77
0.5	average force (N)	4.07	2.29	6.81
0.5	min force (N)	3.85	2.10	6.73
0.5	max force (N)	4.29	2.49	6.88
0.6	average force (N)	5.74	3.67	8.63
0.6	min force (N)	5.63	3.57	8.60
0.6	max force (N)	5.86	3.77	8.67
0.7	average force (N)	6.38	3.84	10.62
0.7	min force (N)	5.24	3.59	9.81
0.7	max force (N)	7.53	4.08	11.43

Table 7.10: Deflections, overview of confidence interval

Plate		000	105	010
0.4	average deflection (cm)	2.18	1.44	4.44
0.4	min deflection (cm)	2.17	1.40	4.43
0.4	max deflection (cm)	2.18	1.48	4.45
0.5	average deflection (cm)	1.67	0.87	3.75
0.5	min deflection (cm)	1.64	0.81	3.71
0.5	max deflection (cm)	1.70	0.93	3.78
0.6	average deflection (cm)	1.43	0.82	2.64
0.6	min deflection (cm)	1.40	0.80	2.62
0.6	max deflection (cm)	1.45	0.84	2.67
0.7	average deflection (cm)	1.31	0.72	2.52
0.7	min deflection (cm)	1.18	0.69	2.35
0.7	max deflection (cm)	1.43	0.75	2.68

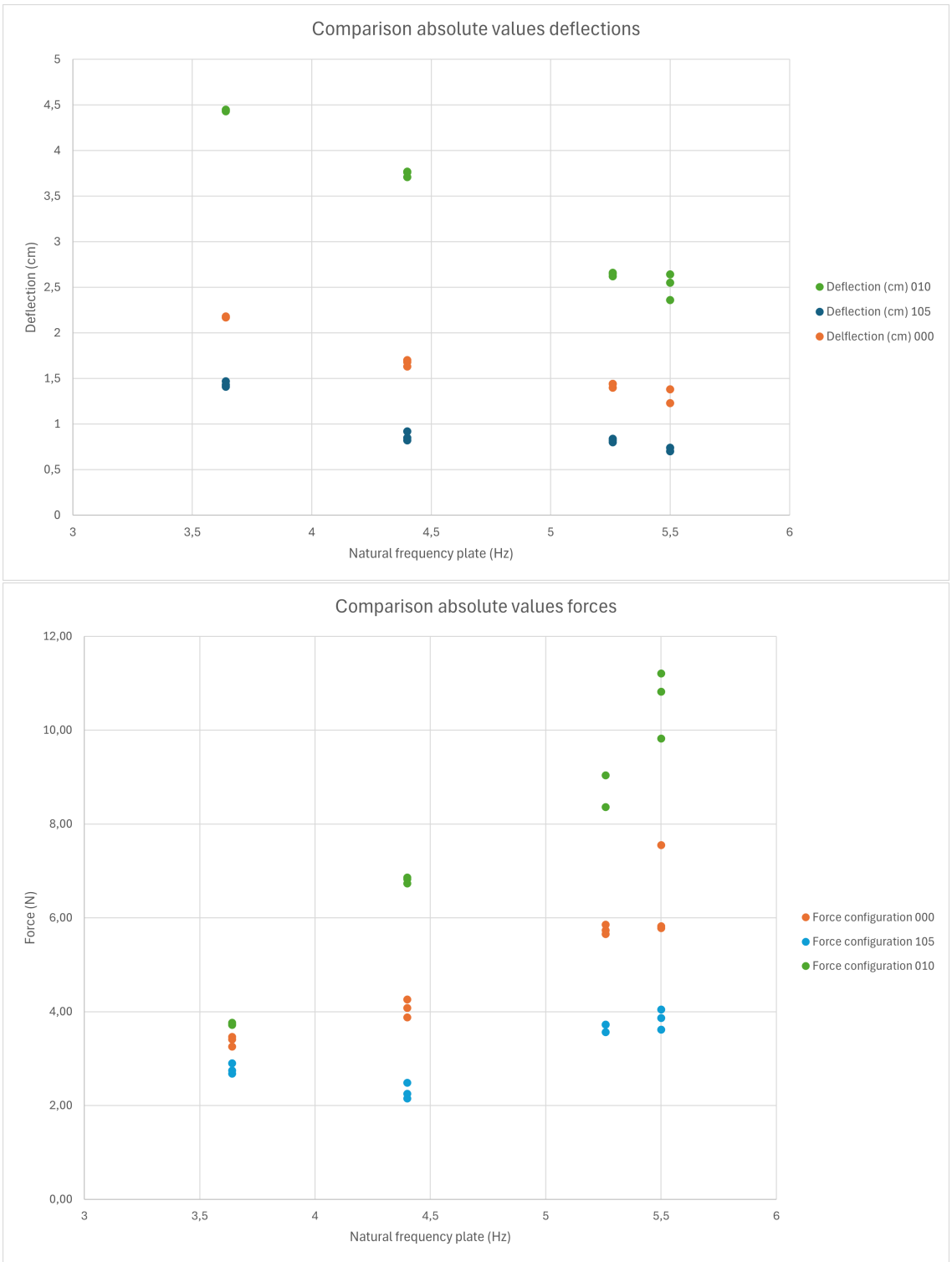

Figure 7.13: For each configuration, the measured values of the deflection (cm) (top) and the force (N) (bottom) are plotted against the natural frequency of the plate.

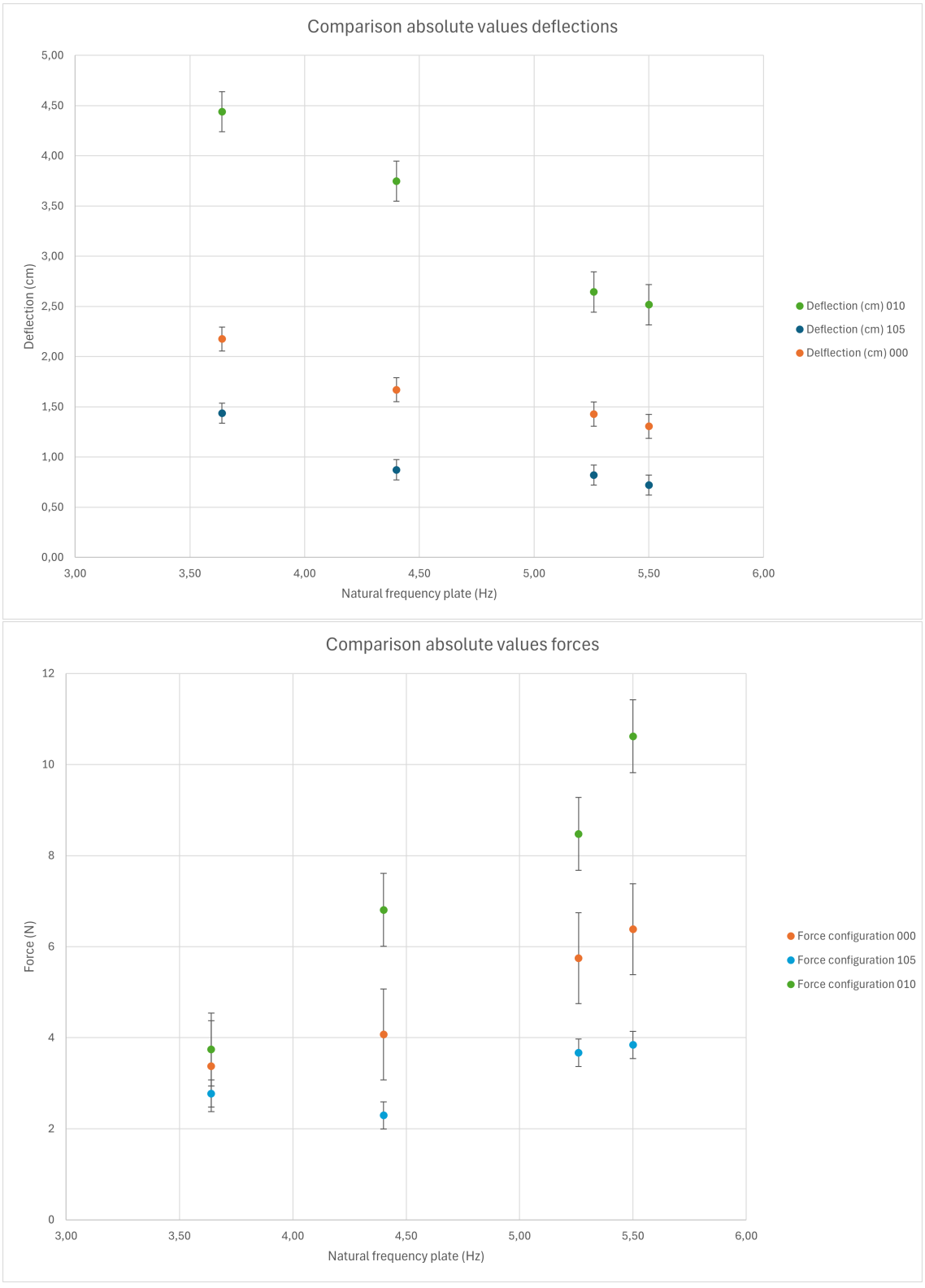

Figure 7.14: For each configuration, the average measured values of the deflection (cm) (top) and the force (N) (bottom) are plotted against the natural frequency of the plate. The confidence intervals are also visible in the plot.

8

Validation beam model and comparison outcomes

In this chapter, the findings of the model of the beam are validated using the results of the experiment. This is done by comparing the outcomes of the beam model with the outcomes of the experiment.

8.1. Properties material

Firstly, the material used in the experiments differ slightly from the used properties in the model. In table 8.1 the natural frequencies of the plates as predicted are given again. In table 8.2 the natural frequencies as measured in the experiments are given. The difference can be explained by a few things. The thickness and length of the plate is never perfectly at the desired value. This can vary around a percent. The construction that connects the plate to the tank is not perfectly rigid. This causes extra mass to vibrate with the plate. Lastly, the prediction relies on a assumption of the E value and the density. These values can be slightly different for the used material in the experiment. The material used in the experiment have lower natural frequencies than calculated in the model. This indicates that the material is less rigid than expected.

Table 8.1: Natural frequencies plates as calculated in the model

Plate	Natural frequency (Hz)
0.4	5.26
0.5	5.88
0.6	7.14
0.7	8.33

Table 8.2: Measured natural frequencies of the four different plates in the experiment

Plate	Natural Frequency (Hz)
0.4	3.64
0.5	4.40
0.6	5.26
0.7	5.50

8.2. Prediction configuration 010

In figure 8.1, the total force exerted on the plate is shown. This is a new prediction, taking into account the change of the situation as in the experiments. This prediction is made using the same ComFLOW simulation as in chapter 3. The prediction of the motion of the plate can be found in appendix A

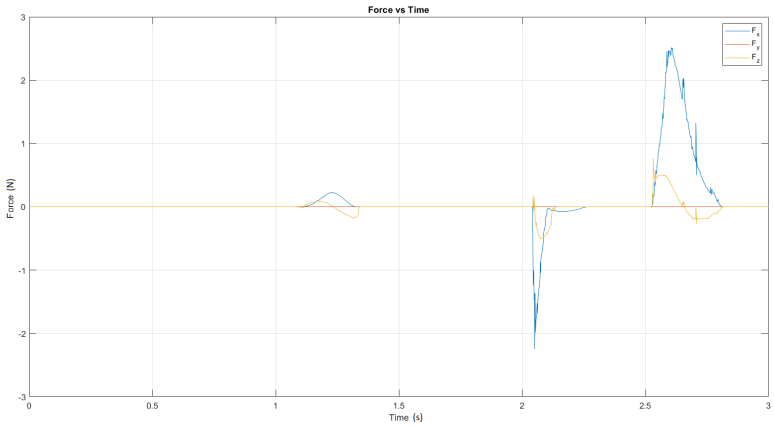

Figure 8.1: Prediction of the total force on the plate at configuration 010

8.3. Comparison model and experiment

There are some fundamental differences between the model and the experiment. In real life, there are many phenomena that influence the behaviour of the motions of the plate. In a model it is not possible to account for everything. The model accounts for the pressure of the water due to its velocity and diffraction. This pressure distribution is applied to the beam in the beam model. From this distribution, the motion of the beam is calculated. The model has a no-slip condition on the beam, meaning that shear stresses on the beam are taken into account. In the motion of the beam in the beam model, damping is not accounted for.

The model does not account for the influence of the motion of the beam on the flow of the water. As seen in equation 2.17, the Morison force is influenced by the relative velocity and accelerations of the beam and the water. The velocity term of the Morison equation calculates the drag over a structure exerted by a flow. The acceleration term captures the force contribution of the relative inertia. These components are not accounted for in ComFLOW or in the beam model. In real life, when water interferes with a structure, the flow does not only influence the structure, but the structure also influences the flow of the fluid. The structure has a certain location, velocity and acceleration. When in motion, the structure vibrates and stretches. This influences the location of the structure, as well as its velocity and its acceleration. As seen before, this influences the Morison force component of the impact force of the water on the structure.

8.3.1. Forces

In table 8.3, the forces found in the experiments are compared to the forces found in the ComFLOW model. The results show some differences. This can be explained partially by the numerical errors in the model. However they do not explain this significant difference.

The prediction of the ComFLOW model is done using a rigid beam. During the interaction with the water, the beam will not deform at all. Without taking into account the bending of the beam, it is logical that this will lead to bigger predicted forces due to two effects. Firstly, the interaction of water with a flexible beam leads to, on average, a more deformed beam during the interaction with the water. This causes the beam to reach with less depth into the water. It also causes the velocity of the water change direction less rapidly, due to the angle of the beam, causing a smaller diffraction component. This effect is illustrated in figure 8.2.

Concluding, it would be logical that the predicted forces from the ComFLOW model are higher than the forces measured in the experiment. However, when looking at the ratio between the measured forces and the predicted forces, the trend changes from smaller to larger. For the more rigid plates 0.6 and 0.7, the measured forces are up to 50% larger than the predicted forces at configuration 000 and 105. This is caused by the effects of the fluid- structure interactions captured by the Morison forces. As discussed before, the relative velocities and accelerations of the plate influence the Morison

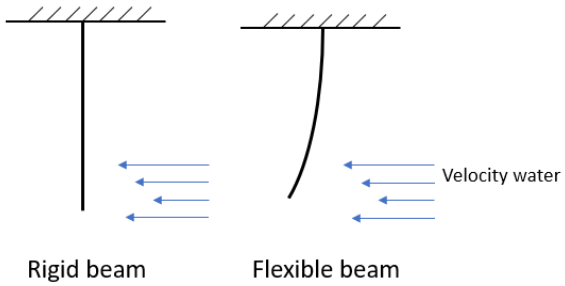

Figure 8.2: Comparison between situation of a rigid beam and a flexible beam.

component of the force. As seen in the results, the Morison force components are of different influence on the different plates, due to different natural frequencies of the structures.

For configuration 010, the predictions are more off than for the other configurations. This might be caused by the larger nonlinear effect of the wave. The wave has reached the wall and is reflected again at this point. This causes more variability and the wave is less predictable. This also follows from analysing the data of the wave height meters. It is interesting to see that the data follows the same trend, but the ratios change more rapidly. For this configuration, the predictions of ComFLOW might be inaccurate, due to the strong non linearity of the wave. However, the differences between the measured forces in the experiment are still taken into account.

We have established that the forces exerted on the plate in the experiment differ significantly. These differences can be explained by the properties of the material. Firstly the velocities of the material differ for each natural frequency. Once the plate starts the move, the velocity of the plate will at some point become contrary to the direction of the velocity of the water. This will cause a higher relative velocity and acceleration, and therefore a higher impact of the Morison force component. In addition, a breaking wave as used in the experiment, consists of a sum of many wave components. These components all have their own frequency. Similar to the wave, the motion of the plate is also a sum of motion components that correspond to all modes shapes. This is illustrated in figure 8.3. When a wave is exerted on a structure, these components all impact the structure. This means that all the wave components interfere with the structure in its own way. A wave that has certain components present that match the natural frequency of the structure, causes a resonance, and therefore higher relative velocities and accelerations, leading to larger forces. The biggest wave impact used in this experiment, 010, is also the most variable wave. It means that these is a large variety of components. This also means that the wave will have a bigger change of containing components that resonate with the structure. This could explain why the difference in impacts is the largest for this wave impact.

Table 8.3: Comparison of Prediction by ComFLOW and Measured Maximum Horizontal Force Exerted on the Plate

Plate	Configuration	Predicted max force (N)	Measured max force av. (N)	Ratio measured / predicted
0.4	000	4.2	3.37	0.80
	105	3.5	2.77	0.79
	010	2.5	3.74	1.50
0.5	000	4.2	4.07	0.97
	105	3.5	2.29	0.65
	010	2.5	6.81	2.72
0.6	000	4.2	5.74	1.37
	105	3.5	3.67	1.05
	010	2.5	8.48	3.39
0.7	000	4.2	6.38	1.52
	105	3.5	3.84	1.10
	010	2.5	10.62	4.25

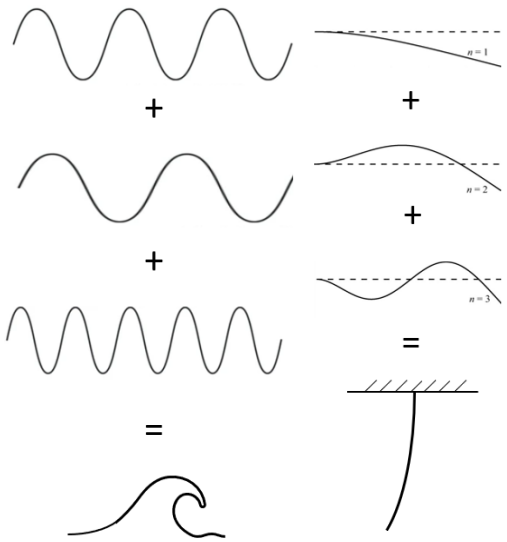

Figure 8.3: a:Components of a breaking wave. b: Components of the beam motion.

8.3.2. Deflections

The model of the beam uses the pressure distributions on the beam over time, generated by ComFLOW. These loads include diffraction, but not the fluid- structure interaction resulting from the motion of the beam. The loads from ComFLOW are applied on the beam in the beam model. In the beam model, the motions over the length of the beam are calculated. The wet area of the beam is calculated using the wave height and the still beam. This makes the wet area similar to the the wet area of the ComFLOW model.

The beam model does not take into account the fluid- structure interactions of the wave and the moving beam. As seen in section 8.3.1, this interaction causes more force on the plate, which is now not accounted for in the beam model. Logically, the beam model uses less force on the beam, resulting in less deformation than measured in the experiment. However, the difference between the forces from ComFLOW and the beam model are also large, this is not as expected. This might rely on an error. The plots of the force ion the beam are shown in figure 8.4. The force on the plate during the impact of the wave according to the beam model and the ComFLOW model, are compared in table 8.4.

Table 8.4: Comparison of Forces between ComFLOW and Beammodel

Configuration	Force ComFLOW (N)	Force Beammodel (N)
Config 105	3.5	1.6
Config 000	4.2	2.0
Config 010	2.5	2.10

In table 8.5 the deflections as predicted by the beam model and the actual deflections are listed. The measured deflections are higher for configuration 105 and 000. This is as expected, taking into account the limitations of the beam model. It is logical that the predicted deflections are too low, considering the forces on the plate predicted by the model are also lower. Being able to accurately predict the impulse of a wave, is still complicated. In addition, as discussed in section 8.1, the material used in the experiments is slightly less rigid than expected. When looking at the ratio between predicted and measured values in the table, the same trend is seen as for the forces. The structures with higher natural frequencies turn out with relatively higher values.

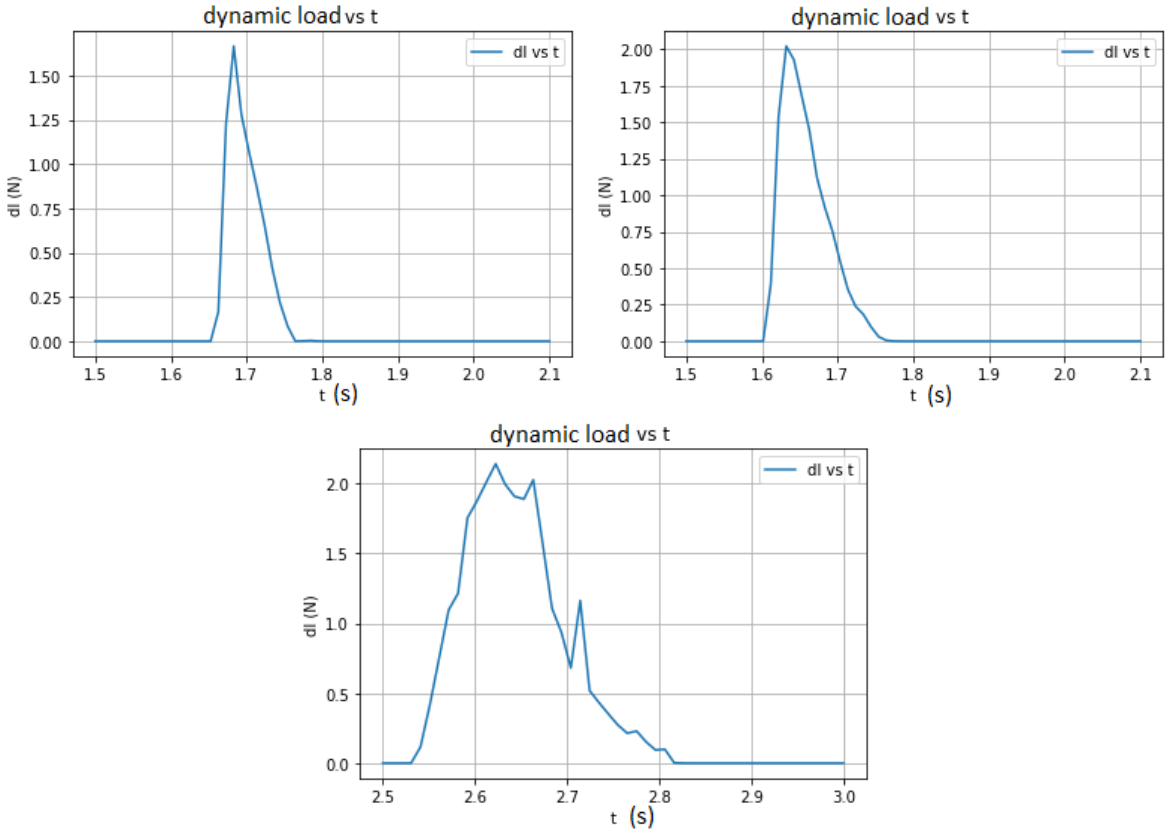

Figure 8.4: Force on the plate, calculated by the beam model
Top left: configuration 105
Top right: configuration 000
Bottom: configuration 010

Table 8.5: Comparison of predicted deflection by the beam model and measured deflections of plates

Plate	Configuration	Deflection predicted (mm)	Deflection measured (mm)	Ratio measured / predicted
0.4	105	6	14.4	2.4
0.4	000	18	21.8	1.21
0.4	010	41	44.4	1.08
0.5	105	4	8.7	2.18
0.5	000	12	16.7	1.39
0.5	010	23	37.5	1.63
0.6	105	3	8.2	2.73
0.6	000	7.5	14.3	1.91
0.6	010	18	26.4	1.47
0.7	105	2	7.2	3.6
0.7	000	5	13.1	2.62
0.7	010	7	24.8	3.54

9

Conclusion

In this study, the effect of dynamic properties of the structure on the magnitude of breaking wave loads is investigated. Firstly, an existing study using a pendulum to represent a moving structure is repeated and extended. Secondly, a model representing a 2D beam is made. This beam undergoes an impact of a breaking wave. The beam model is used to simulate and design the experiment and to compare the experimental outcomes with the numerical outcomes. Lastly the experiment is conducted.

When looking into the results of the pendulum model experiments, some points are interesting regarding the natural frequencies and the motions of the pendulum. In section 5.1, we look back at table 5.2 to 5.4. The response angles of the pendulum increase when the natural frequency decreases. However, shorter pendulums reach higher response angles with the same impulse as a longer pendulum. This is why the kinetic energy of the pendulum is taken into account as well. The pendulums with a higher natural frequency, have a larger resultant kinetic energy, when undergoing the same wave impact. This can be explained when looking into the relative speed of the pendulum and the water. When looking at the Morrison equation 2.17, the relative speed between the structure and the water determines the force that the water exerts on the structure. The relative speed will be higher when the pendulum has a faster natural motion of itself.

Now, we are looking back at the results of the experiment. The plot that compares the findings of the horizontal forces on the plate, measured during the experiment shows interesting differences. This plot is shown in figure 7.14. As seen in the figure, the impact forces differ over the different plates. This difference indicates that the impact of a wave differs, when being received by structures with different natural frequencies. For structures with a higher natural frequency, the impact forces are higher. Taking into account the confidence intervals of the data points, the trend is significant for configuration 010 and 000. At configuration 005, the trend is not very clear.

When looking at table 8.3, the measured forces in the experiment for the plates 0.4 and 0.5 are lower than the predicted forces in the ComFLOW model. This is as expected due to bending of the plate in the experiment, as the plate in ComFLOW is completely rigid. However, the forces measured on plate 0.6 and 0.7 are higher than predicted in ComFLOW. Without taking into account the fluid- structure interactions, it was expected that these values would turn out lower as well. The difference between the measured and predicted forces indicates that the fluid- structure interaction of these plates leads to this difference. Meaning that the natural frequency of the plate does have a significant effect. For plates with higher natural frequencies, the impact force is higher. This can be explained by the different fluid- structure interaction for different plates. If velocities of the plates with higher natural frequencies are higher, the Morison component of the impact force becomes larger. Therefore these impacts can become higher than for other structures. If the breaking wave contains components with frequencies that match those of the plate, a resonant effect occurs. This enhances the impacts and the differences will become even bigger. The differences of the impact can be up to 50% for two plates with the same wave impulse, but different natural frequencies.

In table 8.5, the predictions and the measurements of the deflections are given. The predictions deviate from the values from the experiment. This was as expected due to limitations of the model. The model dose not take into account the influence of the motions of the beam on the water. The motions of the plate influences the Morison component of the impact force, leading to significant influence on the force. The differences between the predictions and the outcome of the experiment, show the same trend as for the forces. As the natural frequency of the plate increases, the results show relatively higher measured deflections.

Overall, when answering the research question: How is the fluid structure-interaction of a structure in focused breaking waves related to the natural frequencies and mode shapes of a structure? It is concluded that structures with higher natural frequencies can undergo a bigger load form the same wave impact as structures with a low natural frequency. More research is needed to establish in what extend and in what type of relation the two phenomena are related.

10

Recommendations

In this chapter, recommendations will be made for further research. After conducting this research, some aspects turn out to be interesting for further research. Furthermore, some aspects of the research itself can be improved upon the enhance the conclusions.

In the first part of this research, a model is used to calculate the motions of a pendulum and of a beam. The model describing the motion of the beam could be improved by taking into account the bending of the beam, damping and improving the accuracy of the impact forces. By improving the model further, more accurate conclusions can be drawn regarding the influence of the natural frequency of the plate on the impact. If the predictions of the deflection are closer to the real outcomes, a more valuable comparison can be made. When all other phenomena are modelled very accurately, the exact influence of the Morison component of the force will become visible. This can lead to a stronger conclusion about the differences between the values and a stronger conclusion about what causes the differences between the values.

Regrading the experiments, some additions could be done to further improve the outcomes. Firstly, the experiments were started using a closed tank. This caused the plate to move in a direction opposite to the wave direction. This effect disappeared when the tank was opened at both sides. This indicates that the effect of air is significant. Often in experiment the air contribution is overlooked or neglected. The findings of the early runs of my experiment show that this effects should be considered.
It would be of additional value to do measurements of the wave impacts on a rigid plate. In a physical model, it is of course not possible to test a perfectly rigid plate. However one could be very close to rigid. The results of this plate could give more insight into the accuracy of the predicted forces by the ComFLOW model. This results could support the conclusion regarding the higher forces on the plates with a high natural frequency.
Prior to the experiments, the intention was to film the whole tank using a video measurement system. However, the cameras used for this types of measurements systems have a limited with of the frame that it can record. In order to film the whole tank, the camera must have a relatively large distance from the tank. The construction of the rig itself caused difficulties to attach the cameras safely to the tank, at a distance. This problem was partially solved using mirrors, but the range of the width of the frames was still limited.
During the experiments the wave height meters slightly changed their measurement values over time. This is an effect that was expected due to their working principle. However the use of the wave height meters is not ideal.
Due to the nonlinear nature of the breaking waves, repeating the wave is difficult. In further research, this effect cannot be completely avoided. To obtain more accurate measurements, one could however conduct a greater amount of repetitions. This will lead to a more certain distribution of the wave height and the measured forces. This could improve the certainty of the conclusions. In addition, more different configurations of the constructions can be investigated. This will lead to more sets of different force distributions on the construction. Having conclusions for all these different situations could strengthen the conclusions. This study concludes that the impacts of breaking waves on a structure is influenced

by the natural frequencies of the structures. In further research, it will be interesting to find how big this influence exactly is. It would be ideal to find a type of relation between the two phenomena.

References

[1] O. A. Bauchau and J. I. Craig. *Structural Analysis: With Applications to Aerospace Structures*. Solid Mechanics and Its Applications. Springer Dordrecht, 2009. DOI: 10.1007/978-90-481-2516-6.

[2] Alexei Bereznitski. “Local hydroelastic response of ship structures under impact loads from water (slamming)”. Doctoral dissertation. PhD thesis. Delft, Netherlands: Delft University of Technology, 2003. URL: http://resolver.tudelft.nl/uuid:41110849-1de4-4603-9515-fb02b04f0f1c.

[3] H. Bogaert et al. “Hydro-structural behaviour of LNG membrane containment systems under breaking wave impacts: findings from the Sloshel project”. In: *ISOPE International Ocean and Polar Engineering Conference*. ISOPE. June 2010, ISOPE–I.

[4] R. W. Bos. *Models for Fluid-Structure Interaction in Liquefied Natural Gas Sloshing*. Available at: https://doi.org/10.4233/uuid:683c061b-056d-41bd-811a-69d061add709. 2022. URL: https://doi.org/10.4233/uuid:683c061b-056d-41bd-811a-69d061add709.

[5] R. W. Bos and P. R. Wellens. “Fluid structure interaction between a pendulum and focused breaking waves”. In: *Physics of Fluids* 33 (6 2021), p. 062118. DOI: 10.1063/5.0054426.

[6] R. W. Bos and P. R. Wellens. “Fluid–structure interaction between a pendulum and monochromatic waves”. In: *Journal of Fluids and Structures* 100.Issue Number (2021), p. 103191. DOI: https://doi.org/10.1016/j.jfluidstructs.2020.103191.

[7] Benjamin Bouscasse et al. “Mechanical energy dissipation induced by sloshing and wave breaking in a fully coupled angular motion system. Part II: Experimental Investigation”. In: *arXiv preprint arXiv:1307.6063* (2014). Dated: January 13, 2014.

[8] Mark J. Cooker and D. H. Peregrine. “Pressure-impulse theory for liquid impact problems”. In: *Journal of Fluid Mechanics* 292 (1995), pp. 1–26. DOI: 10.1017/S0022112095001761.

[9] Francesca De Serio and Michele Mossa. “Experimental Study on the Hydrodynamics of Regular Breaking Waves”. In: *Coastal Engineering* 32 (2005), pp. 255–287.

[10] Rodney Eatock Taylor. “Hydroelastic analysis of plates and some approximations”. In: *Journal of Engineering Mathematics* 58 (2007), pp. 267–278. DOI: 10.1007/s10665-006-9121-7.

[11] O. M. Faltinsen. “The effect of hydroelasticity on ship slamming”. In: *Philosophical Transactions of the Royal Society of London. Series A: Mathematical, Physical and Engineering Sciences* 355.1724 (1997), pp. 575–591.

[12] Odd M. Faltinsen. “Hydroelastic Slamming”. In: *Journal of Marine Science and Technology* 5 (2000), pp. 49–65.

[13] R. C. Hibbeler. *Mechanics of Materials*. Pearson Education Limited, Aug. 2023.

[14] B. Hofland, M. L. Kaminski, and G. Wolters. “Large scale wave impacts on a vertical wall”. In: *Coastal Engineering Proceedings* 32 (2010).

[15] J. M. J. Journée and W. W. Massie. *Offshore Hydromechanics*. Second. Delft University of Technology, 2008.

[16] A. Kamath et al. “Breaking wave interaction with a vertical cylinder and the effect of breaker location”. In: *Ocean Engineering* 128 (2016), pp. 105–115. DOI: 10.1016/j.oceaneng.2016.10.025. URL: https://doi.org/10.1016/j.oceaneng.2016.10.025.

[17] O. Kimmoun, S. Malenica, and Y.M. Scolan. “Fluid Structure Interactions Occurring at a Flexible Vertical Wall Impacted by a Breaking Wave”. In: *Proceedings of the Nineteenth International Offshore and Polar Engineering Conference*. Copyright © 2009 by ISOPE, ISBN 978-1-880653-53-1 (Set); ISSN 1098-6111. The International Society of Offshore and Polar Engineers (ISOPE). Osaka, Japan, June 2009.

[18] M. Salih Kirkgoz, A. Kamil Tanrikulu, and Cengiz Dundar. “Dynamic Analysis of a Vertical Plate Exposed to Breaking Wave Impact”. In: *Ocean Engineering* 31.12 (2004), pp. 1623–1635. DOI: https://doi.org/10.1016/j.oceaneng.2004.02.003.

[19] J. Kvalsvold and O. M. Faltinsen. “Hydroelastic modeling of wet deck slamming on multihull vessels”. In: *Journal of Ship Research* 39.03 (1995), pp. 225–239.

[20] C. Lugni, M. Brocchini, and O. M. Faltinsen. “Wave impact loads: The role of the flip-through”. In: *Physics of Fluids* 18 (2006), p. 122101. DOI: 10.1063/1.2399077.

[21] D. H. Peregrine. “Water-Wave Impact on Walls”. In: *Annual Review of Fluid Mechanics* 35 (2003), pp. 23–43. DOI: 10.1146/annurev.fluid.35.101101.161153.

[22] Hao Qin et al. “Numerical study on structural response of anti-sloshing baffles of different configurations in a sloshing tank considering hydroelasticity”. In: *Ocean Engineering* 188 (2019), p. 106290.

[23] Singiresu S. Rao. *Mechanical Vibrations*. University of Miami: Pearson Education, Inc., 2004. ISBN: 978-0-13-212819-3.

[24] M. Rezaee and V. Maleki. “An analytical solution for vibration analysis of carbon nanotube conveying viscose fluid embedded in visco-elastic medium”. In: *Proceedings of the Institution of Mechanical Engineers Part C Journal of Mechanical Engineering Science* 229.4 (2014), pp. 644–650. DOI: 10.1177/0954406214538011.

[25] C. Vuik et al. *Numerical Methods for Ordinary Differential Equations*. Delft Academic Press, 2014.

[26] Shupeng Wang et al. “Fourier Series Approach for the Vibration of Euler–Bernoulli Beam under Moving Distributed Force: Application to Train Gust”. In: *Shock and Vibration* 2019 (2019), p. 21.

[27] Mi-An Xue et al. “Experimental study on vertical baffles of different configurations in suppressing sloshing pressure”. In: *Ocean Engineering* 136 (May 2017), pp. 178–189.

[28] Mohammad Zannon. “Free vibration of thin film cantilever beam”. In: *International Journal of Engineering and Technical Research (IJETR)* 2.11 (2014). ISSN: 2321-0869.

A

Predictions tank experiments

A.1. Configuration 005

In figure A.1 to A.4, the predicted motions of the bottom point of the beams are plotted for configuration 005.

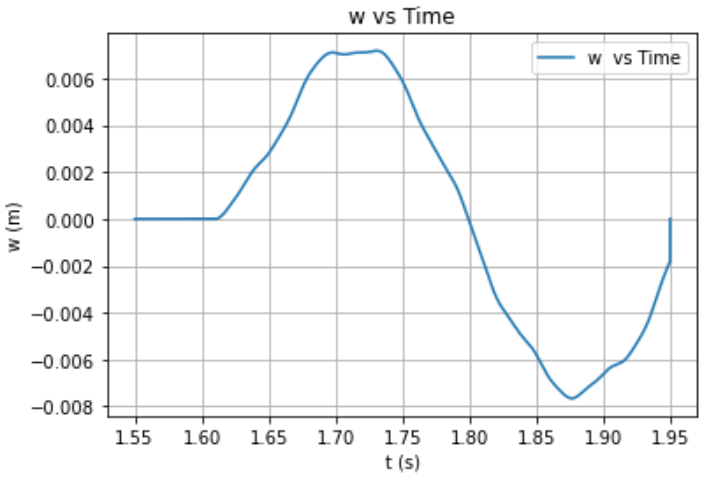

Figure A.1: Motion bottom point of 0.4mm beam over time

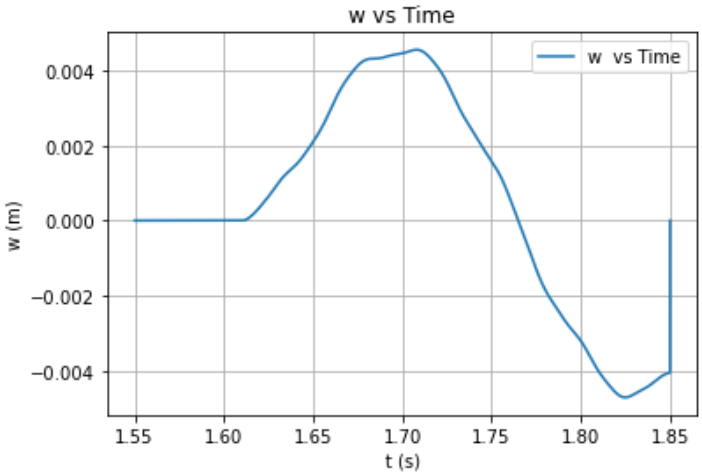

Figure A.2: Motion bottom point of 0.5mm beam over time

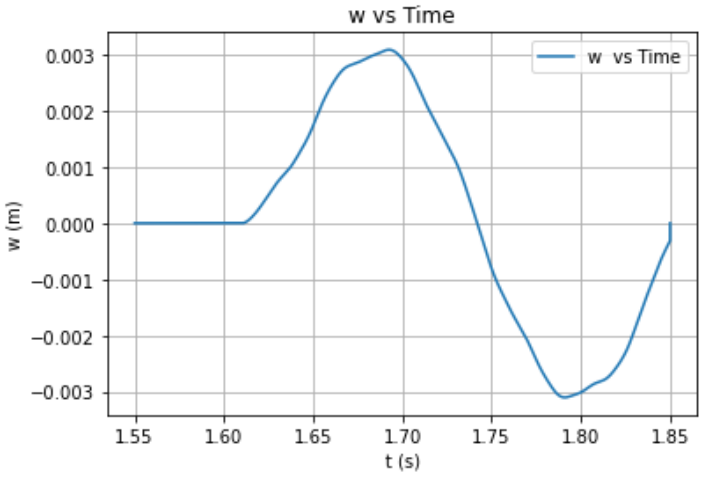

Figure A.3: Motion bottom point of 0.6mm beam over time

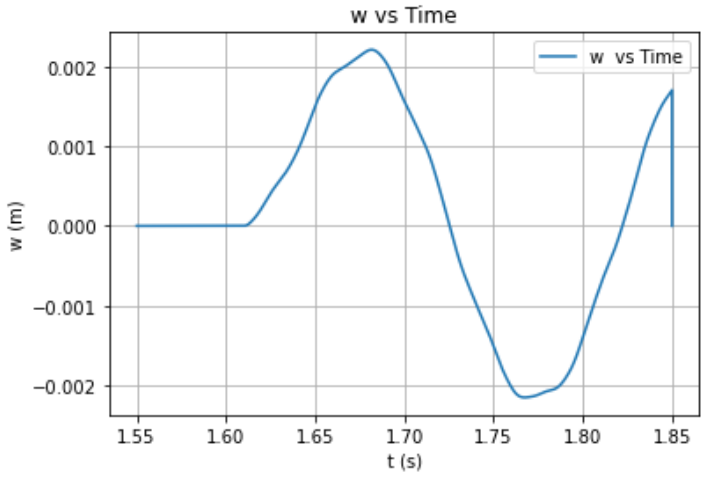

Figure A.4: Motion bottom point of 0.7mm beam over time

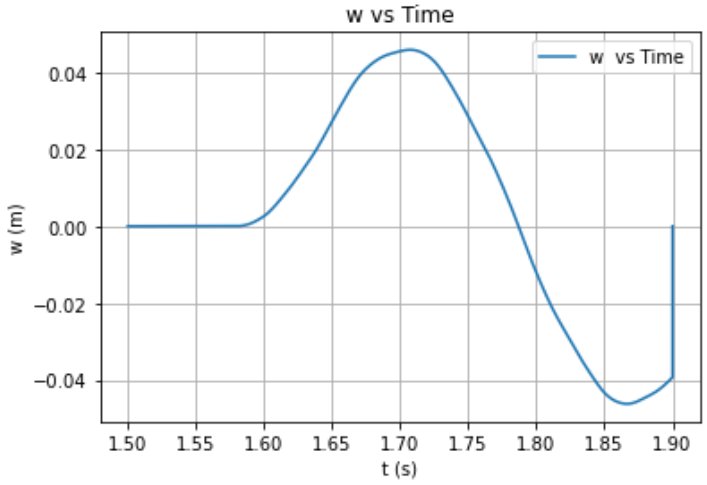

Figure A.5: Motion bottom point of 0.4mm beam over time

A.2. Configuration 105

In figure A.5 to A.8, the predicted motions of the bottom point of the beams are plotted for configuration 105.

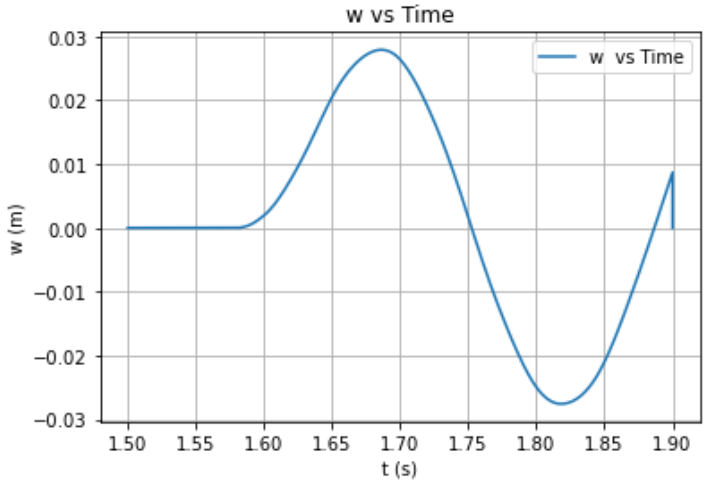

Figure A.6: Motion bottom point of 0.5mm beam over time

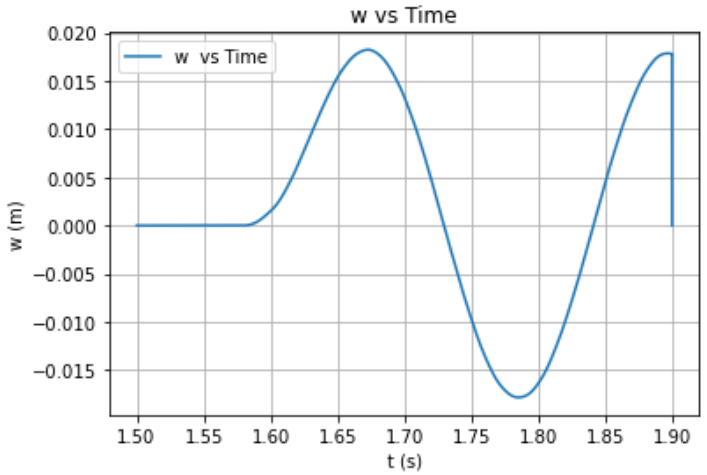

Figure A.7: Motion bottom point of 0.6mm beam over time

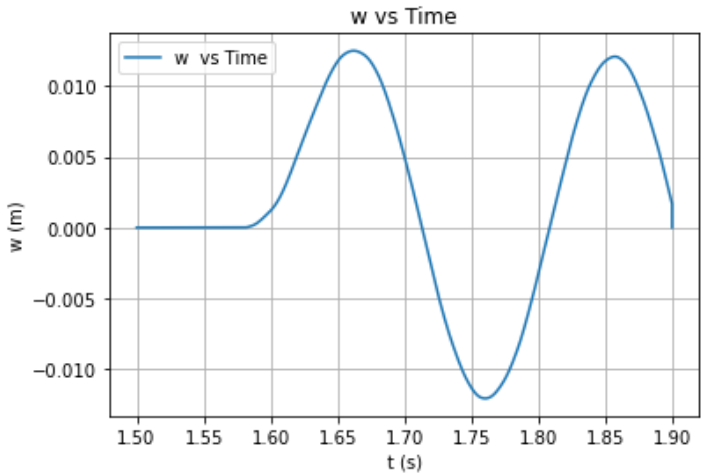

Figure A.8: Motion bottom point of 0.7mm beam over time

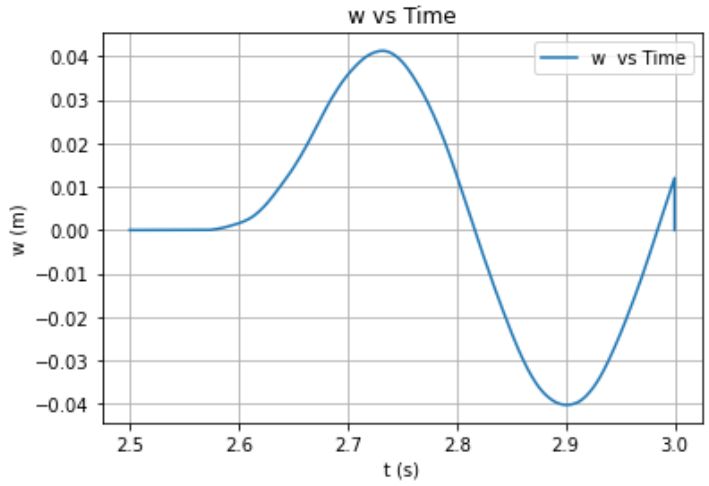

Figure A.9: Motion bottom point of 0.4mm beam over time

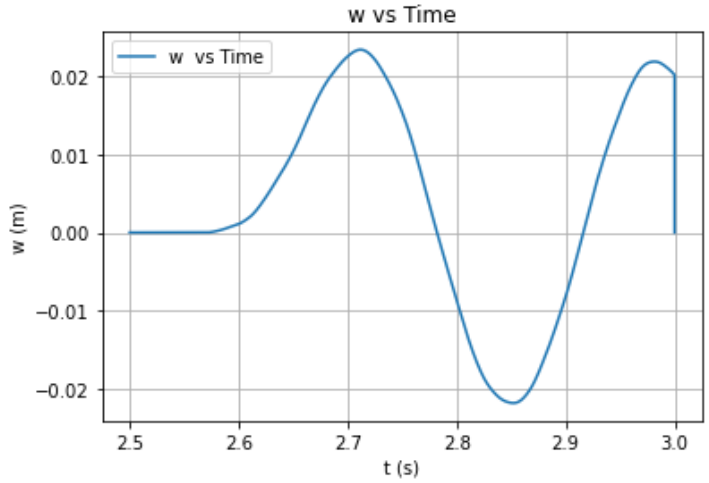

Figure A.10: Motion bottom point of 0.5mm beam over time

A.3. Configuration 010

In figure A.9 to A.12, the predicted motions of the bottom point of the beams are plotted for configuration 010.

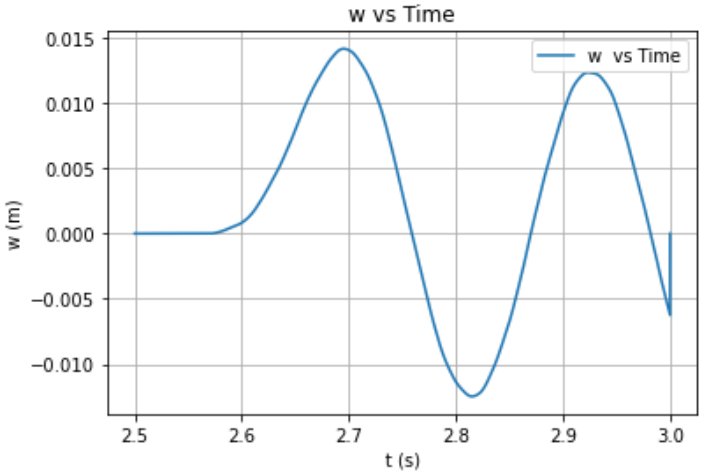

Figure A.11: Motion bottom point of 0.6mm beam over time

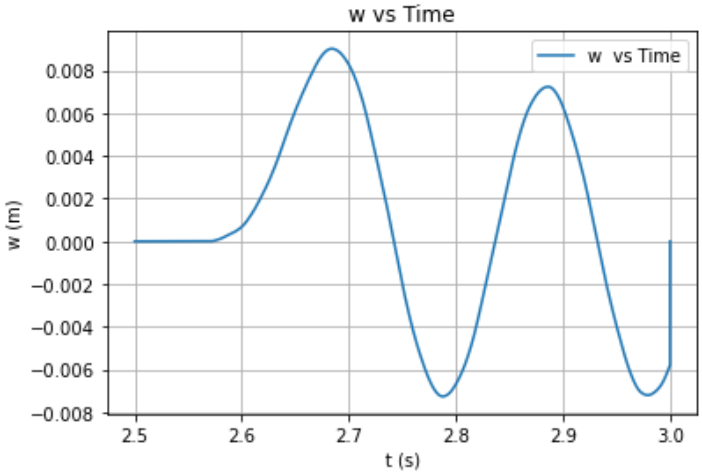

Figure A.12: Motion bottom point of 0.7mm beam over time

B

Data experiments

B.1. Wave height meter results

During the experiments, three runs are done for each configuration. Here all the plots of the wave height meter 6 are shown. Per plot, three runs are shown that are used for the same configuration. The plots are shown in figure B.1 to B.12.

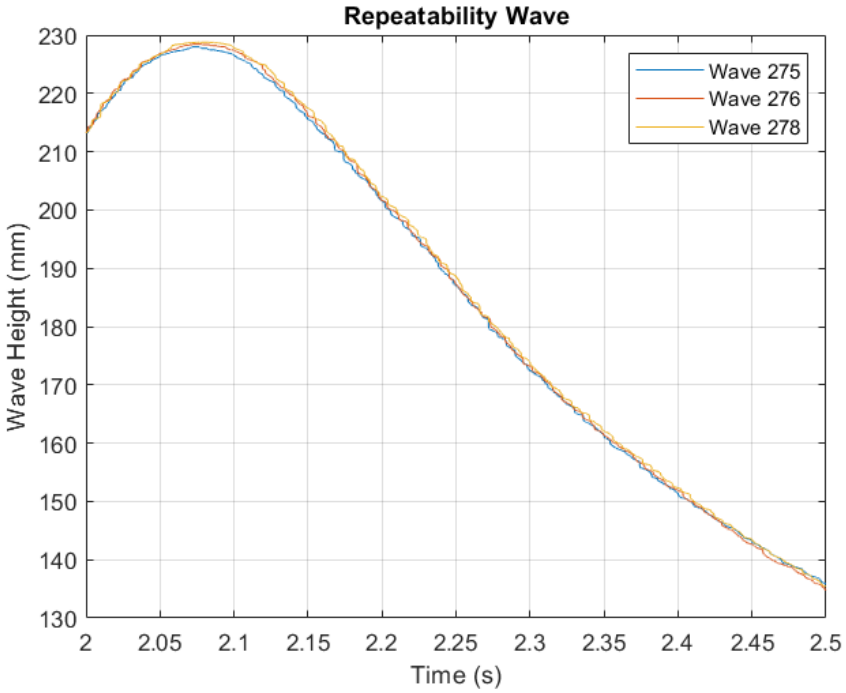

Figure B.1: Wave height meter results of whm6, plate 0.4, configuration 000

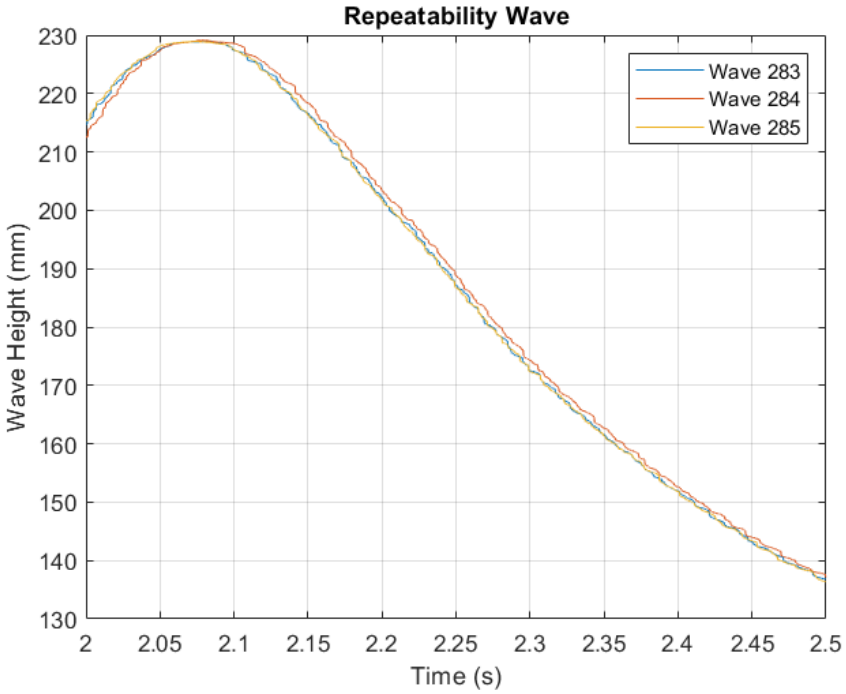

Figure B.2: Wave height meter results of whm6, plate 0.4, configuration 005

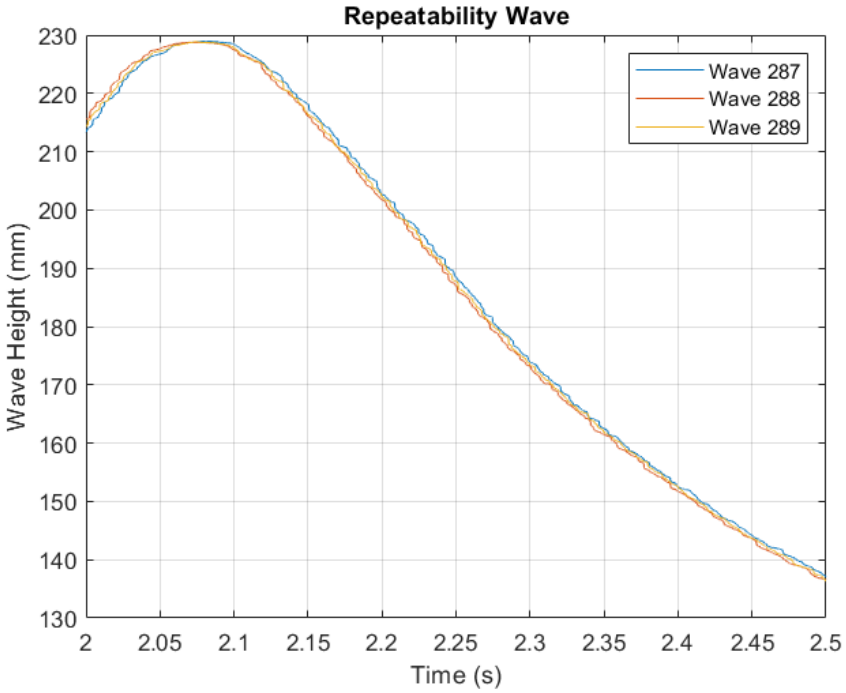

Figure B.3: Wave height meter results of whm6, plate 0.4, configuration 010

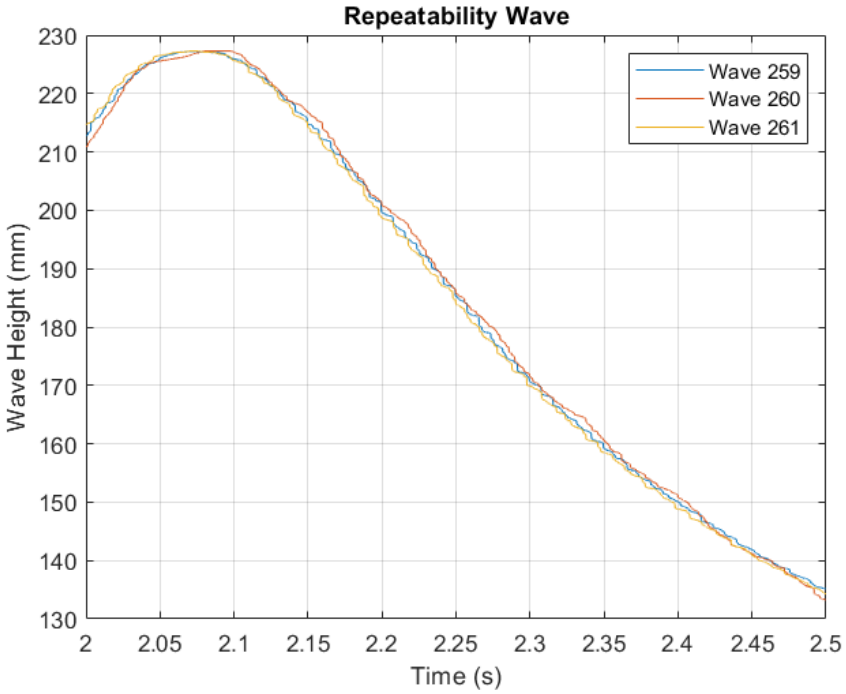

Figure B.4: Wave height meter results of whm6, plate 0.5, configuration 000

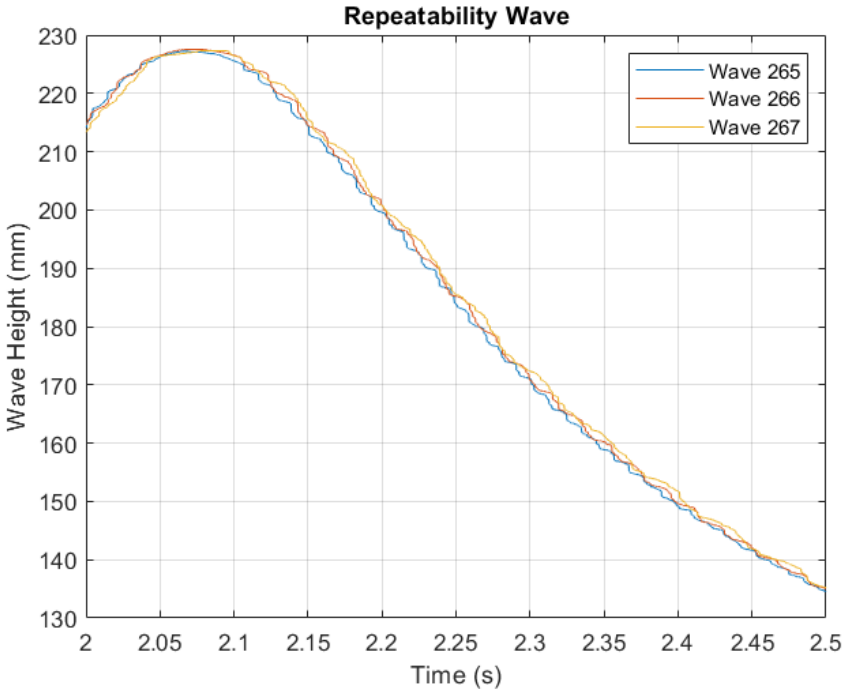

Figure B.5: Wave height meter results of whm6, plate 0.5, configuration 005

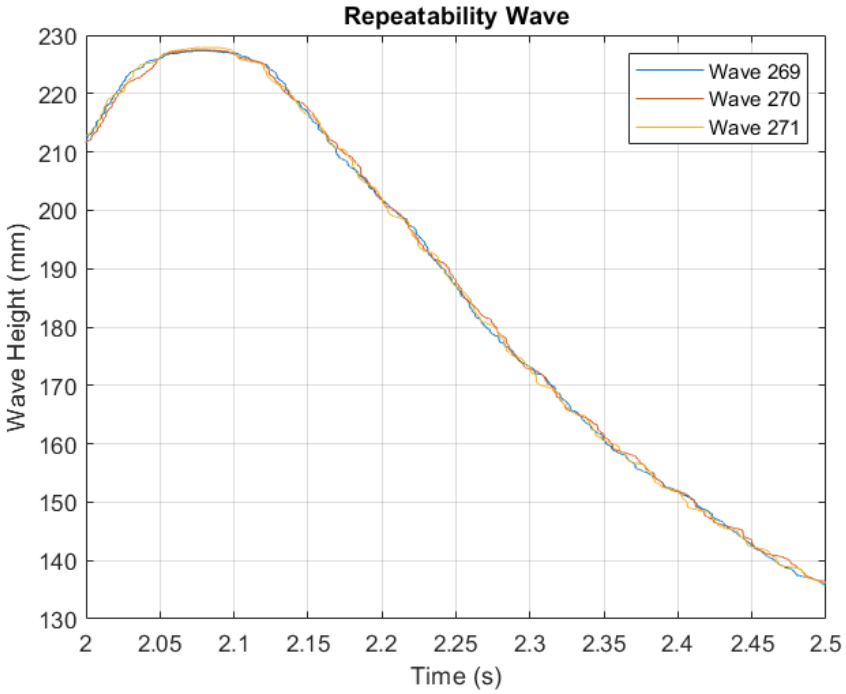

Figure B.6: Wave height meter results of whm6, plate 0.5, configuration 010

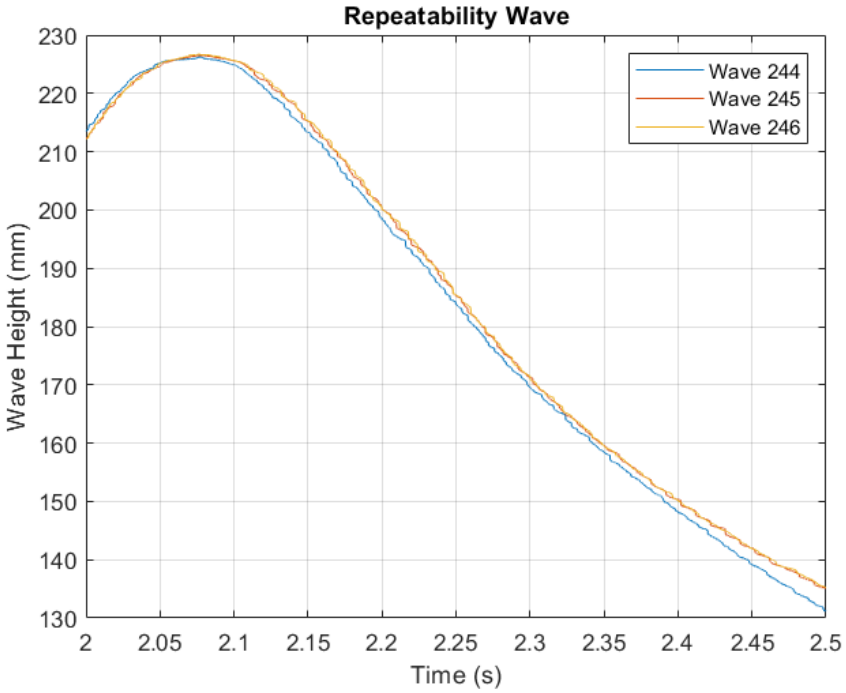

Figure B.7: Wave height meter results of whm6, plate 0.6, configuration 000

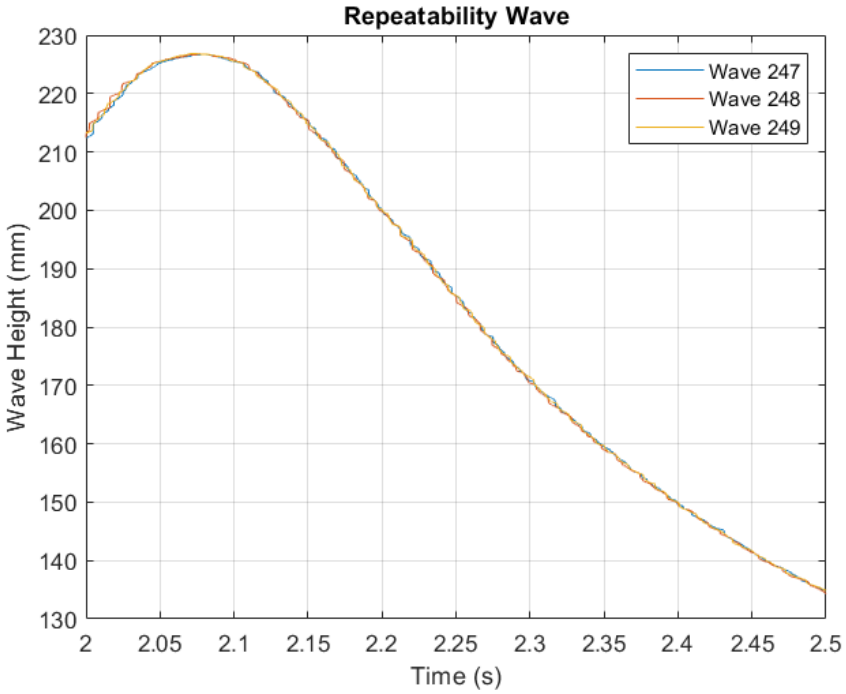

Figure B.8: Wave height meter results of whm6, plate 0.6, configuration 005

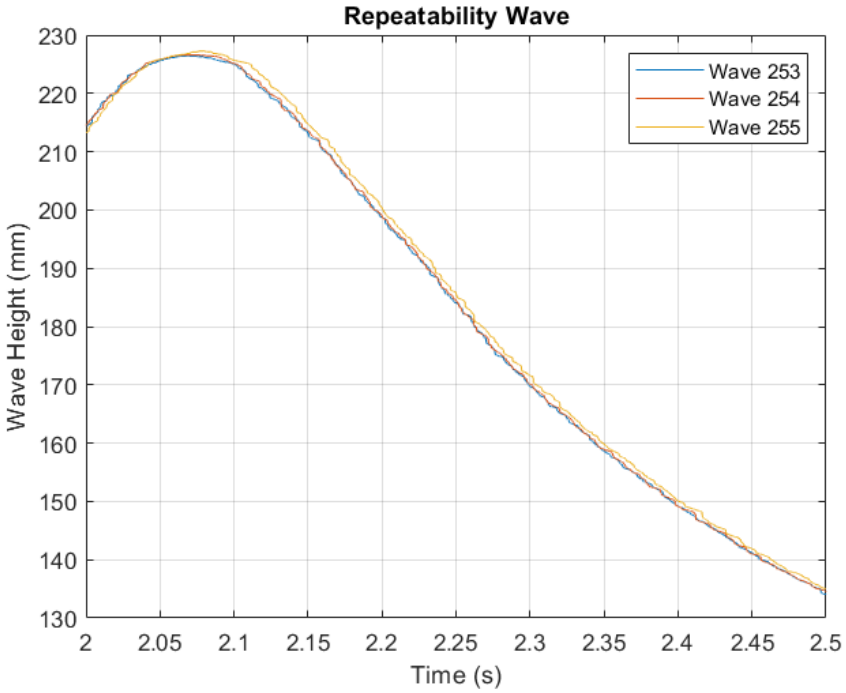

Figure B.9: Wave height meter results of whm6, plate 0.6, configuration 010

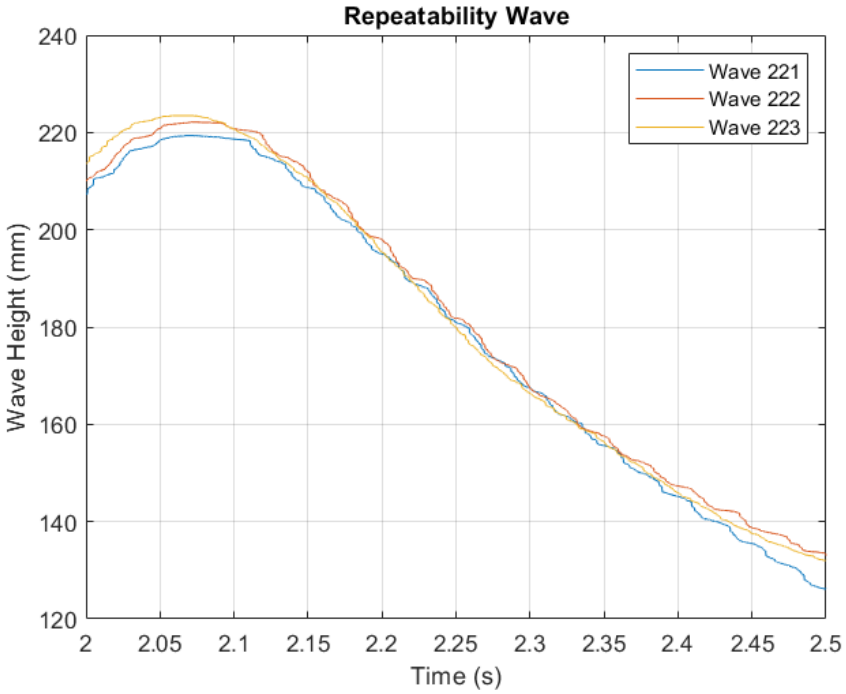

Figure B.10: Wave height meter results of whm6, plate 0.7, configuration 000

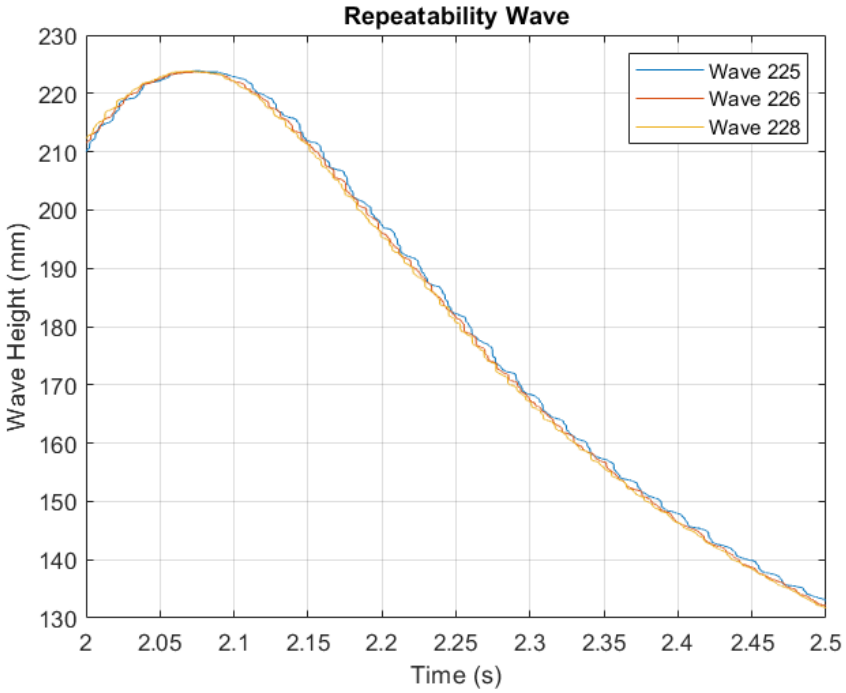

Figure B.11: Wave height meter results of whm6, plate 0.7, configuration 005

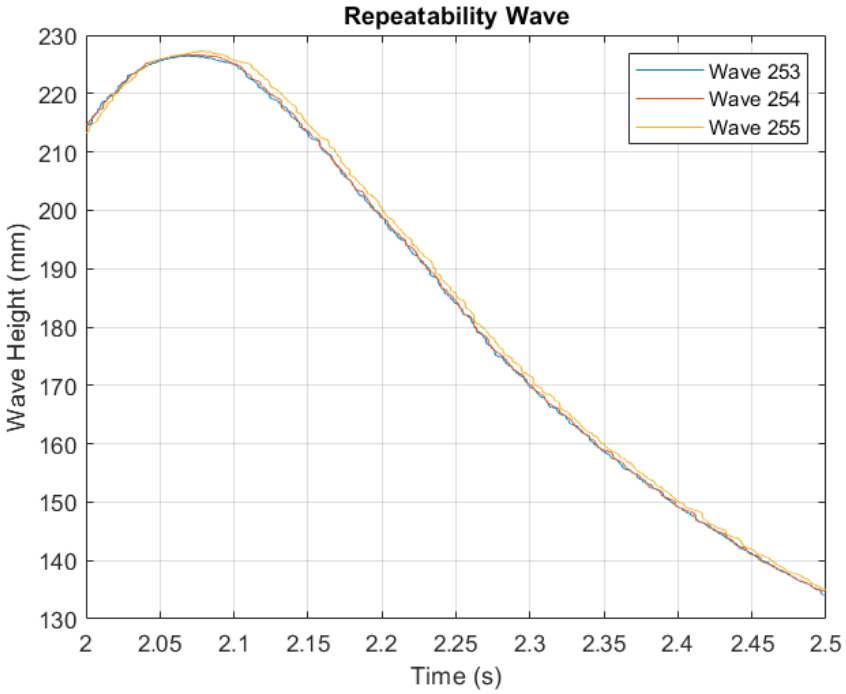

Figure B.12: Wave height meter results of whm6, plate 0.7, configuration 010